FACILE SYNTHESIS OF GRAPHITE- AND GRAPHENE-BASED HYBRID ADDITIVES BY SILANIZATION AND EFFECTS OF THESE ADDITIVES ON THE THERMAL CONDUCTIVITY OF CEMENTITIOUS GROUTS USED IN SHALLOW GEOTHERMAL SYSTEMS

by

İlayda Berktaş

Submitted to the Graduate School of Engineering and Natural Sciences
in partial fulfillment of the requirements for the degree of
Master of Science

SABANCI UNIVERSITY

DECEMBER 2020

FACILE SYNTHESIS OF GRAPHITE- AND GRAPHENE-BASED HYBRID ADDITIVES BY SILANIZATION AND EFFECTS OF THESE ADDITIVES ON THE THERMAL CONDUCTIVITY OF CEMENTITIOUS GROUTS USED IN SHALLOW GEOTHERMAL SYSTEMS

APPROVED BY:

DATE OF APPROVAL: 22/12/2020

To loved ones and those who will be loved in the future.

ABSTRACT

FACILE SYNTHESIS OF GRAPHITE- AND GRAPHENE-BASED HYBRID ADDITIVES BY SILANIZATION AND EFFECTS OF THESE ADDITIVES ON THE THERMAL CONDUCTIVITY OF CEMENTITIOUS GROUTS USED IN SHALLOW GEOTHERMAL SYSTEMS

İlayda BERKTAŞ

Materials Science and Nanoengineering, MSc. Thesis, 2020

Thesis Supervisor: Assoc. Prof. Dr. Burcu Saner Okan

Keywords: Graphene nanoplatelet, expanded graphite, recycled materials, silanization, thermal conductivity, cement-based composites; ground source heat exchangers

The thermal conductivity of grout backfilling boreholes and pipes has been considered as an important issue for the improvement of the efficiency of shallow geothermal systems. Especially preserving the heat through the boreholes in the ground without temperature difference is achieved by formulating grout composition having high thermal conductivity. In this thesis, the main objective is to develop hybrid silica-carbon additives to enhance the thermal conductivity of the grout and thus increase the effectiveness of the heat transmission and prevent the aggregation of treated hybrid additives in grout mixture. Three main materials, graphene from waste tire, expanded graphite and rice husk ash, were hybridized by using silane coupling agents and building chemical bridges with silica particles in grout composites. This functionalization provided to enhance the dispersion and solubility of carbon materials and adjust their water uptake during grout mixing since there is a close relation between water demand and thermal conductivity. According to optimization study on the formulation development of grout mixtures, as the amount of graphene-based hybrid additive increased from 3 to 5 wt%, water uptake increased from 660 to 725 g resulting in the reduction of thermal conductivity by 20.6%. Furthermore, the highest thermal conductivity of 2.656 W/mK was achieved by adding 5 wt% expanded graphite-based hybrid additive compared to reference grout having thermal conductivity of 2.373 W/mK. Consequently, this study shows noticeable potential of hybrid additives produced from virgin and recycled sources to be used in the grouts of geothermal heat-exchange boreholes. This research will be more discernible since renewable energy sources come into prominence by ever-increasing energy-demand and global pollution.

ÖZET

GRAFİT VE GRAFEN ESASLI HİBRİT KATKI MADDELERİNİN SİLANİZASYON YOLUYLA SENTEZİ VE BU KATKI MADDELERİNİN SIĞ JEOTERMAL SİSTEMLERDE KULLANILAN ÇİMENTOLU HARÇLARIN ISIL İLETKENLİĞİ ÜZERİNDEKİ ETKİLERİ.

İlayda BERKTAŞ

Malzeme Bilimi ve Nanomühendisliği, Master Tezi, 2020

Tez Danışmanı: Assoc. Prof. Dr. Burcu Saner Okan

Anahtar kelimeler: Grafen nanoplakalar, genişletilmiş grafit, geri dönüştürülmüş malzemeler, silanizasyon, termal iletkenlik, çimento bazlı kompozitler, toprak kaynaklı ısı eşanjörleri

Sondaj deliklerinin ve boruların etrafında saran dolgu malzemesini, sığ jeotermal sistemlerin verimliliğinin artırılması için önemli bir olgu olarak kabul edilmiştir. Özellikle, sondaj deliği ve yer arasında ki geçişte ısının sıcaklık farkı olmaksızın korunması, yüksek ısı iletkenliğine sahip harç bileşiminin formüle edilmesi ile sağlanmaktadır. Bu tezin asıl amacı, hibrit silika-karbon katkı maddeleri geliştirerek harcın ısıl iletkenliğini artırmak ve böylece ısı iletiminin etkinliğini artırmak ve işlem görmüş hibrit katkı maddelerinin harç karışımında birikmesini/ çökmesini önlemektir. Atık lastikten üretilmiş grafen, genişletilmiş grafit ve pirinç kabuğu külü olmak üzere üç ana malzeme, silan bağlama maddeleri kullanılarak ve harç kompozitlerinde silika parçacıklarıyla kimyasal köprüler inşa edilerek hibritlendi. Bu işlevselleştirme, karbon malzemelerin dağılımını ve çözünürlüğünü arttırmak ve su talebi ile ısıl iletkenlik arasında yakın bir ilişki olduğundan, harç karıştırma sırasında su alımını ayarlamak için sağlanmıştır. Harç karışımlarının formülasyon geliştirme ile ilgili optimizasyon çalışmasına göre, grafen bazlı hibrit katkı maddesi miktarı ağırlıkça% 3'ten% 5'e yükseldikçe, su alımı 660'dan 725 g'a çıkarak ısıl iletkenliğin% 20.6 oranında azalmasına neden oldu. Ayrıca, 2,373 W/mK termal iletkenliğe sahip referans harca kıyasla 2,656 W/mK ile en yüksek ısıl iletkenlik, ağırlıkça % 5 genişletilmiş grafit bazlı hibrit katkı maddesi eklenerek elde edilmiştir. Sonuç olarak, bu çalışma, jeotermal ısı değişim kuyularının derzlerinde kullanılmak üzere saf ve geri dönüştürülmüş kaynaklardan üretilen hibrit katkı maddelerinin dikkat çekici potansiyelini göstermektedir. Sürekli artan enerji talebi ve küresel kirlilik ile yenilenebilir enerji kaynakları ön plana çıktığı için bu araştırma daha fark edilebilir olacaktır.

ACKNOWLEDGEMENTS

First and foremost, I would like to thank my supervisor, Assoc. Prof. Dr. Burcu Saner Okan for her dedicated support and guidance.

I would like to express my gratitude and appreciation to Prof. Dr. Yusuf Menceloglu for his encouragement and his valuable comments and suggestions.

Furthermore, I would like to thank the rest of the BSO's graduate research team for their collaborative support during this journey.

I am also very thankful to the SU-IMC and Fens faculty and all its member's staff for all the considerate guidance.

Very special thanks go out to Leila Haghighi Poudeh, Murat Tansan and Serbay Polat for their friendship, helps and efforts. They always cheered me up and kept me motivated.

Most importantly, my sincere appreciation goes to my family and my friends for their unconditional support and encouragement throughout the process.

Finally, I would like to express my sincere gratitude to European Union's Horizon 2020 research and innovation programme under grant agreement Nº 727583 for financial support , to project partners, for giving me the opportunity of becoming a part of this study and to Scientific and Technical Research Council of Turkey (TUBITAK) with the project numbers of 218M709.

TABLE OF CONTENT

LIST OF FIGURES

LIST OF TABLES

LIST OF ABBREVATIONS

APTES	(3-Aminopropyl)triethoxysilane
C_3A	$Ca_3Al_2O_6$
C_3S	Ca_3SiO_5
CBMs	Carbon-based Materials
CNT	Carbon Nanotubes
Cr	Cristobalite
C-S-H	Calcium Silicate Hydrates
DLS	Dynamic Light Scattering
EDX	Energy-dispersive X-ray
EG	Expanded Graphite
f-RHA	Functionalized Rice Husk Ash
FTIR	Fourier Transform Infrared Spectroscopy
GNP	Near Prime Graphene Nanoplatelet
GO	Graphene Oxide
GQD	Graphene Quantum Dot
H-EG-1, fSi:EG=1:1	Functionalized Silica Grafted EG at the Ratio of 1:1
H-EG-2, fSi:EG=1:5	Functionalized Silica Grafted EG at the Ratio of 1:5
MWCNT	Multi-walled Carbon Nanotubes
Q	Quartz
RAMAN	Renishaw inVia Reflex Raman Microscopy System
RHA	Rice Husk Ash
SEM	Scanning Electron Microscope
SGES	Shallow Geothermal Energy System
Si:GNP=1:10	Functionalized Silica Grafted GNP at the Ratio of 1:10
Si:GNP=1:5	Functionalized Silica Grafted GNP at the Ratio of 1:5
SP	Superplasticizer
TEM	High Resolution Transmission Electron Microscope
TEOS	Tetra-ethoxysilane
TGA	Thermogravimetric Analysis
THF	Tetrahydrofuran
W/C	Water to cement ratio

WRHA	White Rice Husk Ash
XPS	X-ray Photoelectron Spectroscopy
XRD	X-ray Diffraction

CHAPTER 1: STATE-OF-THE-ART

Economic growth and rise in the population emerged more energy demand all around the world. Nonrenewable energy sources such as coal, crude oil, natural gas become insufficient and are available in limited supplies. Besides, they are environmentally harmful since sources like fossil fuel emit large amount of carbon monoxide gas through the environment for the production of electric power [1]. Because of the environmental threats, the importance of energy produced from renewable energy sources which are solar, wind, hydro, biomass, and geothermal has been taken great attention. Also, these sources are much more accessible and environmentally friendly. However, they are dependent on the outer sources such that, wind power is intermittent with regard of the weather condition. Similarly, solar irradiance and hydro sources are periodically variable. Geothermal energy, which uses the heat energy reserved at the shallow of Earth's surface to provide heating or cooling to the buildings, provides green, low-combustion energy, with abundant reserves, economically viable and massive potential for application [2]. In addition, the heat of Earth is not weather dependent like solar or wind power, they use of the earth as a source rather than the ambient air [3].

Among them, Shallow Geothermal Energy System (SGES), which is one of the main types of Renewable Energy Systems, can be utilized as a substitute for the energy obtained from traditional fossil-fuel [4]. They can be built up even in the smallest lands since loop system can be settled both horizontal and vertical depending on the size of the field. In general, as shown in Figure 1, the boreholes are dipped into a certain depth of ground. Inside the borehole, U shaped pipes, two outcoming and incoming pipes, carry the fluid which circulates inside the pipes. The space between the borehole and the pipes is surrounded with the grout composition which is responsible for the heat transfer. Therefore, the efficiency of SGES highly depends on the thermal properties of the grout composition. High thermal conductivity is needed to successfully transfer the heat of the ground through the boreholes to the fluid circulating inside the pipes without heat loss [5]. If the heat during injection or extraction is lost, the performance/efficiency of the system can be reduced, thus the thermal conductivity of the grout is highly important in SGES.

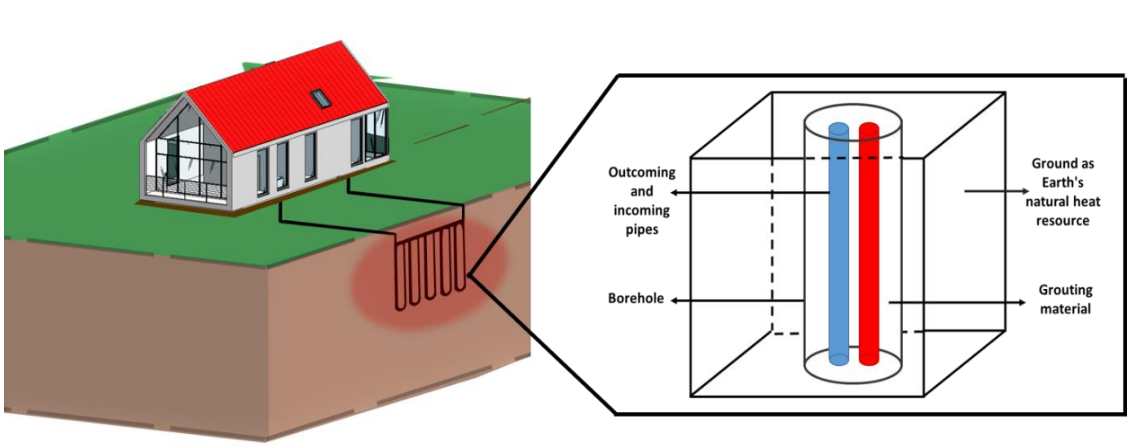

Figure 1. Cross sectional image of the mechanism of SGES.

To sum up, the performance of geothermal energy system is highly sensitive and correlated the thermal properties which are thermal conductivity, thermal diffusivity, specific heat capacity as well as other factors like number and configuration of energy loops, pile length and diameter which can also be regulated since grout with higher thermal conductivity decreases the required length of the boreholes and the cost of the construction eventually [6]. In other words, improving the thermal conductivity of the grout backfilling the boreholes as heat exchangers of the pumps, which enables heat transfer between ground and the pipes located in borehole, can enhance the efficiency of the SGES.

Although SGES has a lot of advantages as aforementioned, there are still some obstacles which can be overcome by reducing the installation costs and increasing system efficiency [7]. Accordingly, in this study, we found an efficient approach to improve the properties of grout compositions by synthesizing three different carbon-based hybrid additives by using virgin and recycled sources. Carbon-based materials (CBMs) were selected to be used in hybridization with silica and silane coupling agent to enhance thermal conductivity of grout. Each carbon materials were selected from different properties such as particle size, cost, the production source different budget value ranges in order to monitor the differences in thermal conductivity in grout mixture. The presence of silica in hybrid structure carries a high significance since it is compatible with the structure of cement, thus improves the dispersion and prevents the agglomeration of carbon based hybrid additives in cementitious grout composite. In order to gather silica and CBMs in one material, (3-Aminopropyl)triethoxysilane (APTES) as silane coupling

agent was selected. Figure 2 represents the reaction mechanism of APTES functionalized silica grafted CBMs schematically. Three hydrolyzed OH groups of APTES condensed to the surface of silica. In further step, amine functional groups of the silane on the surface of silica linked to the functional groups on carbon surface. With these developed hybrid structures, it is aimed to prevent the aggregation problems of CBMs used in grouts and control water demand.

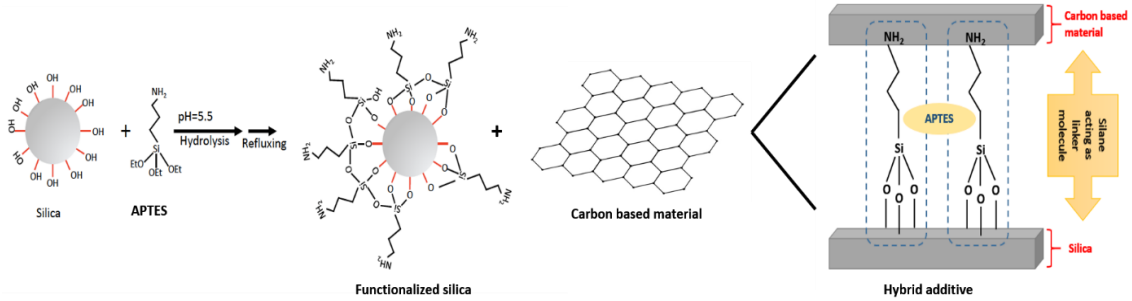

Figure 2. Schematic representation of step-wise production for functionalized silica-carbon hybrid additive.

In the current thesis, hybrid additives by using carbon-by-products were developed in order to reduce the installation costs in geothermal applications. In the first part of study, near prime graphene nanoplatelets (GNP), which is produced from recycled carbon obtained by pyrolysis of waste tire, was selected for the development of hybrid structure from recycled sources. In the second part, expanded graphite (EG) was selected due to the high capability of increasing the thermal conductivity with high carbon content and also compared to the thermal conductivity of GNP based grouts. In the last part, besides GNP based hybrid additive, rice husk ash (RHA), which is also a recycled source, was functionalized with APTES (silica was not grafted on the surface of RHA since it consists mostly of amorphous silica in the structure) used in grout formulations to monitor the effect of cement hydration. The effect of aforementioned hybrid additives in the cementitious grout were investigated from material selection to processing optimization.

Material from this dissertation has been published in the two following forms and the third paper is under review process:

Berktas I, Ghafar AN, Fontana P, et al (2020) Facile synthesis of graphene from waste tire/silica hybrid additives and optimization study for the fabrication of thermally enhanced cement grouts. Molecules 25:. https://doi.org/10.3390/molecules25040886 [8]

Berktas I, Ghafar AN, Fontana P, et al (2020) Synergistic effect of expanded graphite-silane functionalized silica as a hybrid additive in improving the thermal conductivity of cementitious grouts with controllable water uptake. Energies 13: https://doi.org/10.3390/en13143561 [9]

Berktas I, Chaudhari O, Ghafar AN, Menceloglu Y, Saner Okan B, Controlling the surface chemistry of SiO_2 decorated carbon nanosheets from waste rice husk ash by silanization and its effect on heat flow and hydration of cement-bentonite based grouts (Submitted)

CHAPTER 2. Facile synthesis of graphene from waste tire/silica hybrid additives and optimization study for the fabrication of thermally enhanced cement grouts

This work evaluates the effects of newly designed graphene/silica hybrid additives on the properties of cementitious grout. In the hybrid structure, graphene nanoplatelet (GNP) obtained from waste tire was used to improve the thermal conductivity and reduce the cost and environmental impacts by using recyclable sources. Additionally, functionalized silica nanoparticles were utilized to enhance the dispersion and solubility of carbon material and thus the hydrolyzable groups of silane coupling agent were attached to silica surface. Then, hybridization of GNP and functionalized silica was conducted to make proper bridges and develop hybrid structures by tailoring carbon/silica ratios. Afterwards, special grout formulations were studied by incorporating these hybrid additives at different loadings. As the amount of hybrid additive incorporated into grout suspension increased from 3 to 5 wt%, water uptake increased from 660 g to 725 g resulting in the reduction of thermal conductivity by 20.6%. On the other hand, as the concentration of GNP in hybrid structure increased, water demand was reduced and thus the enhancement in thermal conductivity was improved by approximately 29% at the same loading ratios of hybrids in the prepared grout mixes. Therefore, these developed hybrid additives showed noticeable potential as a thermal enhancement material in cement-based grouts.

2.1. Introduction

In geothermal energy systems, the thermal conductivity of the grout used for backfilling the heat exchange boreholes and the pipes used in the loops for circulating the heat carrier fluid has been considered as an important issue for the improvement of the efficiency of the system. That is because the media influencing the heat exchange between the heat carrier fluid (in the loops) and the surrounding formations (i.e. soil or rock) include the pipe's wall and the backfill materials in the borehole [10, 11]. The poor thermal conductivity of neat cementitious grout not only decreases the efficiency of the system performance but also influences on thermal cracking of the used backfill grout due to the high temperature gradient between the pipe and the surrounding ground during the heat injection or extraction process [12]. Therefore, it is crucial to provide grouting materials with sufficiently improved thermal conductivity, while ensuring the other important properties such as the rheological properties, permeability, bleeding and workability are

in the accepted ranges. Accordingly, graphene is a promising candidate to incorporate into the grouting materials due to its high thermal conductivity property.

The porosity and the rate of hydration can be reduced with the integration of graphene based materials in cement paste resulting in the development of stronger and more durable products [13]. In one of the recent studies, 0.01 wt% of graphene oxide (GO) nanosheets was mixed with cementitious materials consisting of ordinary Portland cement, silica fume, and ground granulated blast-furnace slag and increased the compressive strength of cement as about 7.82% after 28 days of curing [14]. Furthermore, Shang *et al*. demonstrated that using GO encapsulated silica fume, one can provide better rheological properties and increase the compressive strength of cement paste by 15.1% only by addition of 0.04 wt% of GO [15]. Accordingly, previous studies are mostly focused on enhancement of mechanical and rheological properties of cement by low loading graphene. However, there is limited work done on introduction of graphene in cement-based materials to improve the thermal conductivity. For instance, Sedaghat *et al*. demonstrated that addition of 1% graphene did not have any significant effect on thermal diffusivity of the mixture but incorporation of 5% graphene enhanced the thermal diffusivity by 25% at 25°C and about 30% at 400°C compared to that using the neat cement paste [13]. In another work, Ramakrishnan *et al*. incorporated 0.5 wt% of graphite, carbon nanotubes and GNP into form-stable Phase Change Material based composites and observed that using those additives led to the enhancement of thermal conductivity by 45%, 30% and 49%, respectively [16].

One of the main factors that affects the thermal conductivity in cement paste/mortar is water/cement ratio, since increasing the water content reduces the density, increases the porosity that finally decreases the thermal conductivity [17, 18]. Jobmann and Buntebarth showed that the water uptake decreased from 8.4 to 0.1% between 5 and 95% graphite and increased the thermal conductivity up to 3.67 W/mK with the composition of 10% graphite and 90% bentonite at 20°C [19]. Herein, it is significant to adjust the water content between water-bearing bentonite and water-free graphite to attain high thermal conductivity and thus surface chemistry of selected additives becomes a crucial factor in mixing of cementitious materials.

Silanization has taken on special attention in the surface functionalization and the adjustment of hydrophilicity to control the penetration of water in cement structure [11,12]. Silane coupling agents have a significant influence on the dispersion of matrix and also affect the thermal, mechanical and physical properties of nanocomposites. There

are numerous attempts for the modification of silica by organosilanes to connect to organic groups and act as bridging component [21]. Especially silanol groups in silica have the ability to react with silane coupling agents and make the silica much more suitable for coupling reactions [22]. Among silane coupling agents, 3-aminopropyl triethoxysilane (APTES) was widely preferred as a binding agent in several applications such as composites, coatings and adhesives [23]. Wang *et al.* reported that silane modified GO polymerized with acrylic acid showed better distribution in saturated lime water than neat GO [24]. Zhao *et al.* stated that hybrid additive, which was produced by the impregnation of silica nanoparticles on GO modified by polycarboxylate superplasticizer, was added into cement matrix (1.5% SiO_2 and 0.02% GO by weight of cement) and increased the compressive strength as about 38.31%, 44.47% and 38.89% at 3^{th}, 7^{th} and 28^{th} days, respectively [25].

Although several studies have been performed to improve the different properties of cement pastes by using GO and modified GO sheets, there is still growing interest in the subject with the aim to reduce carbon footprint and develop sustainable and durable cement paste/ grout. Herein, carbon based materials obtained from waste sources such as gamma irradiated recycled plastic [26], carbon powder waste obtained from the cutting process of laminate carbon composite [27] and rice husk ash [28] can be good alternatives to GO produced by harsh acidic and toxic conditions [21,22,23] to be used as an additive in grout mixtures. Another important issue is to reduce the manufacturing costs by using carbon-by products or waste carbon materials. Therefore, a new methodology should be developed to address the issue related in thermal conductivity, aggregation, cost and environmental impact in grouting.

In the present study, the main objective is to develop hybrid silica-GNP additives to enhance the thermal conductivity of the grout and thus increase the efficiency of the heat transmission and prevent the aggregation of treated hybrid additives in grout mixture and also decrease the manufacturing costs by using waste sources. To the best of our knowledge, there is no work about the utilization of graphene nanoplatelets produced from recycled carbon black obtained from the pyrolysis of waste tire as an additive in the preparation of grout. In order to prevent agglomeration and reduce the water absorption, silica particles were functionalized by APTES to make a suitable bridge with the surface of GNP. Then, the developed hybrid additives were added into the grout mixture by changing additive and water ratios, and the flow behaviors and the thermal conductivity

property of the prepared grout mixtures were investigated in detail to monitor the effects of carbon addition on the performance of the grouts.

2.2. Materials and Methods

2.2.1. Materials

In this investigation, 3-Aminopropyl triethoxysilane (APTES, >98%, 0.946 g/ml) and acetic acid were purchased from Sigma- Aldrich, USA. Amorphous silica (SiO_2) was purchased from Merck, Germany. Graphene nanoplatelet (GNP) was obtained from pyrolyzed waste tire provided by NANOGRAFEN Co., Turkey. Two types of silica sands from Kumsan (30-35 AFS and 60-70 AFS), superplasticizer from Sika (SRMC-310S) and bentonite from Canbensan were used in the preparation of grout mixtures.

2.2.2. Method of Surface functionalization of silica

In silica functionalization, 1 g of silica was dispersed in 50 mL distilled water via Ultrasonic Homogenizer from Hielscher Ultrasonics at room temperature to provide homogeneous dispersion. Then, 1 mL APTES was added into the mixture by adjusting weight to weight ratio of silica and silane amounts and pH level of solution was adjusted to 5.5 by dropping acetic acid. In this process, APTES amount was approximately equal to silica amount. The as-prepared mixture was refluxed at 80°C for 24 h. At the end of reaction, filtration was performed by washing with water and ethanol twice. The filtrate was dried in oven at 70°C for 24 h. In order to get optimum functionalization degree, silica and APTES ratios were adjusted. Table 1 summarizes silica functionalization conditions with three different APTES ratios.

Table 1. The reaction conditions of silica functionalization with three different APTES ratios.

Sample	**Silica amount (g)**	**APTES amount (ml)**	**Reaction Time (h)**	**Reaction Medium**	**Reaction Temperature (°C)**
Si:APTES=1:1	1	1	24	Water	80
Si:APTES=1:2	1	2	24	Water	80
Si:APTES=1:3	1	3	24	Water	80

2.2.3. Hybridization of functionalized silica with GNP

Surface functionalized silica was used for the modification of the surface of GNP to attain better dispersion in grout mixture. In the hybridization step, 740 g GNP was dispersed in 7400 ml distilled water to prepare colloidal suspension under sonication process. Then, aqueous solution having Silica: APTES in the amount of 74:148 weight % was added slowly into the GNP suspension. The reaction was performed through refluxing at 80°C for 24 h. The resultant material was directly applied to filtration process and the material was easily separated from water. Then, the material was kept in vacuum oven at 70°C for 24 h. For grouting formulations, two different GNP based hybrid additives encoded as H-GNP-1 and H-GNP-2 were developed by changing silica and GNP ratios of 1:5 and 1:10, respectively.

2.2.4. Preparation of grouts by the addition of Si-GNP hybrid additives

In the preparation of grouts, water, superplasticizer (SP) and Si-GNP hybrid additives were mixed for 2 min at 2000 rpm using high share mixer (VMA- Getzmann). Then, bentonite, cement and two types of silica sands were added orderly into the mixture and mixed at 6000 rpm for 4 min. Several experiments including Marshcone test and Flow-table test were carried out to evaluate the developed grout flow properties. The developed grout was then molded in cylindrical molds (20 mm height and 60 mm diameter) and cured at 100% relative humidity and 20°C for evaluation or their thermal conductivity.

2.2.5. Characterization

The morphological studies of GNP and its hybrid additives were analyzed using a Leo Supra 35VP Field Emission Scanning Electron Microscope (SEM) and a JEOL JEM-ARM200CFEG UHR- Transmission electron microscopy (TEM). X-ray diffraction (XRD) measurements were carried out by using a Bruker D2 PHASER Desktop with a CuKα radiation source. Raman spectroscopy was employed to characterize the structural changes in GNP samples using a Renishaw inVia Reflex Raman Microscopy System with a laser wavelength of 532 nm in the range of 100-3500 cm^{-1}. Functional groups of functionalized silica samples were analyzed using a Thermo Scientific Fourier Transform Infrared Spectroscopy (FTIR). Surface composition of GNP and its hybrid additives were examined quantitively by Thermo Scientific K-Alpha X-ray Photoelectron Spectrometer System (XPS). Zetasizer Nano ZS, Malvern Dynamic Light Scattering (DLS) was used to measure the particle size of carbon and silica samples. Surface areas of the prepared

samples were measured by BET method by using Micromeritics 3Flex equipment. Thermogravimetric Analysis (TGA) was carried out using a Mettler Toledo thermal analyzer (TGA/DSC 3+) over the temperature range of 25 °C to 1000 °C at a heating rate of 10°C/min under nitrogen. Thermal conductivity analysis of GNP based grouts was conducted by Hot Disk Thermal Constants Analyser, TPS 2500 S. For the cementitious grouts casted as 60 mm x 20 mm, sensor with 6.394 radius was selected for thermal conductivity of the cementitious grout samples since in case of isotropic sample, the thickness should be at least equal to the radius of sensor and the diameter must be at least equal to two times the diameter of sensor. The main working principle of this instrument is to provide an electrical current by sensor through an isothermal sample which results in temperature increasement and to record the temperature increase that was reflected in resistance increases of the sensor. As shown in Figure 3a, the selected sensor was placed in a position which localizes to the center of the sample and fasten via clamp and screws. Figure 3b shows the position of the second identical sample placed on top of the sensor. After arranging the position of samples and the sensor, a square tablet of metal should be placed on the sample above with the help of a screw and the samples were clamped by screw for providing sufficient contact and prevent any possible air gap between samples and sensor.

(a) **(b)**

Figure 3. (a) and (b) Sensor position between grout samples.

2.3. Results and Discussion

2.3.1. Optimization study for surface functionalization of silica

Among silane coupling agents, 3-Aminopropyl triethoxysilane (APTES) is a widely used coupling agent. The chemical structure of APTES includes an amine functional group (-NH_2) and three hydrolyzable groups which can be attached to the surface of silica. Figure 4 represents the reaction mechanism of silica functionalization by APTES schematically. Hydrolyzable groups of $(-OCH_2CH)_3$ in the structure of APTES was converted into -OH groups during hydrolysis as shown in Figure 4a. After the condensation reaction occurred, pH was adjusted as 5.5 and then APTES was attached to the silica surface with different bridging modes as seen in Figure 4b. In this step, NH_2 groups of APTES remained available in the tails for the hybridization with GNP whereas hydrolyzable groups were linked to the -OH groups on the surface of silica particles. In other words, APTES acts as a bridge between silica surface and carbon. Optimization study was conducted using three different APTES ratios to get an ideal surface composition.

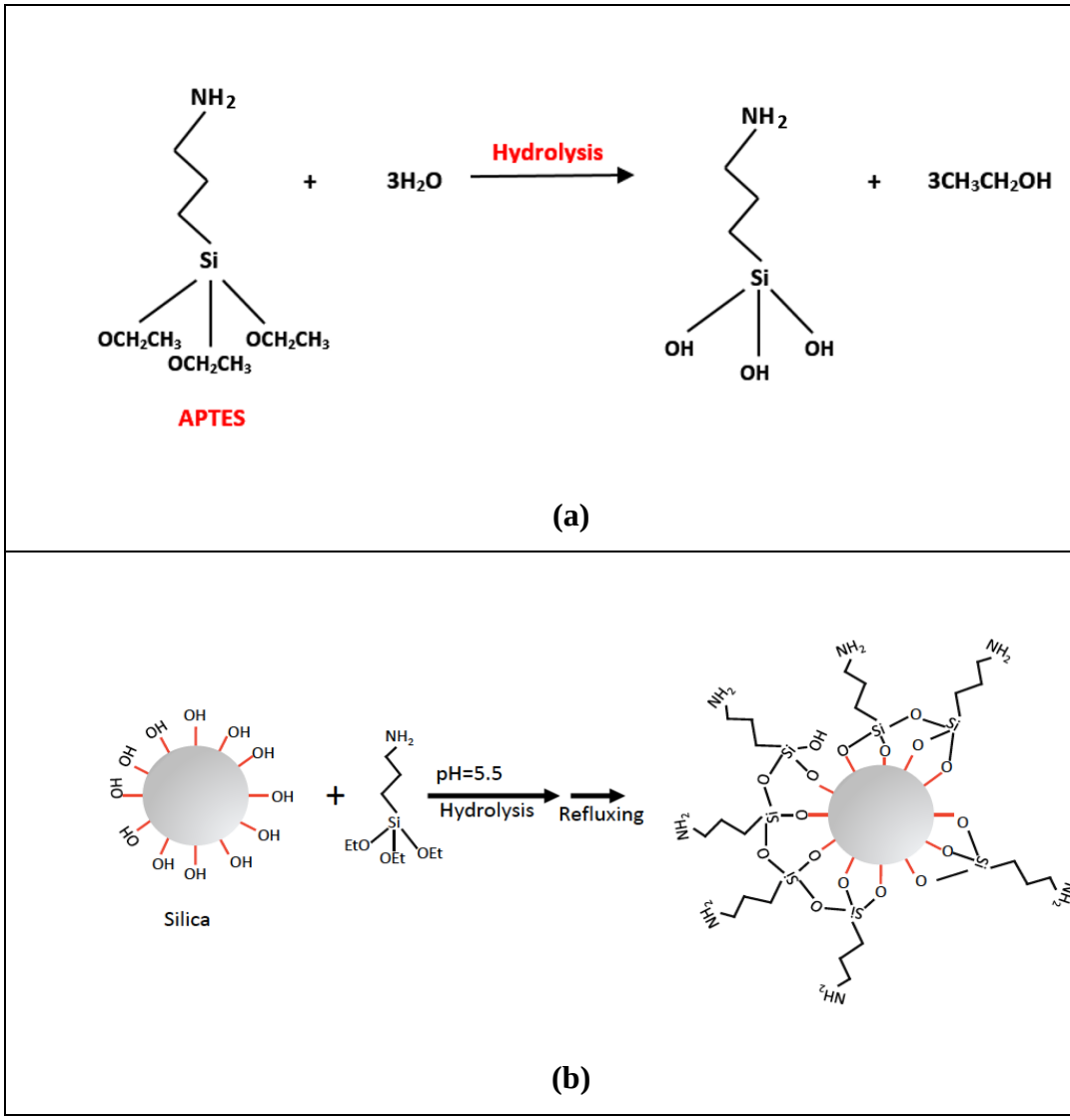

Figure 4. Schematic representation of the reaction of APTES functionalized silica particles in water: (a) hydrolysis and (b) condensation reactions.

First, amorphous silica having the surface area of 473.8 m^2/g with the particle size of 258 nm was selected and three different Si:APTES ratios were studied for APTES functionalization. FTIR characterization was then carried out to identify the functional groups and observe the effect of APTES amount on the surface of silica. Figure 5 shows the FTIR spectra of APTES, neat silica and APTES functionalized silica particles. Herein, the most prominent peaks for all spectra are located between 950 cm^{-1} and 1250 cm^{-1} attributed to Si-O-Si and Si-O-C modes [31] and -OH bending vibration appeared at 800 cm^{-1} [32]. Furthermore, CH_2 asymmetric and symmetric stretching modes that can be seen at around 2932 cm^{-1} and 2864 cm^{-1}, respectively, indicate the presence of the propyl chains of APTES [33]. The two labelled peaks appeared at around 1500 cm^{-1} and 1600 cm^{-1} belonging to the NH_2 scissor vibrations indicating the presence of the NH_2 terminal group of APTES [34]. These peaks become more prominent as APTES concentration increases. In addition, in the FTIR spectrum of APTES, the double peaks at 2803 cm^{-1} and 2970 cm^{-1} are attributed to stretching modes of CH_2 [35]. However, -NH peak was not appeared in the spectra of APTES functionalized silica particles since the peak belonging to Si is dominant and the intensity of amine groups coming from APTES functionalization is significantly low. On the other hand, the attachment of NH_3 on the surface of silica surface was confirmed by XPS characterization. Table 2 presents the XPS results of silica functionalized with APTES at different ratios. The results indicated that nitrogen content is comparably lower than the other elements of carbon, oxygen and silicon on silica surface and the highest nitrogen amount is attained by the ratio of Silica:APTES=1:2.

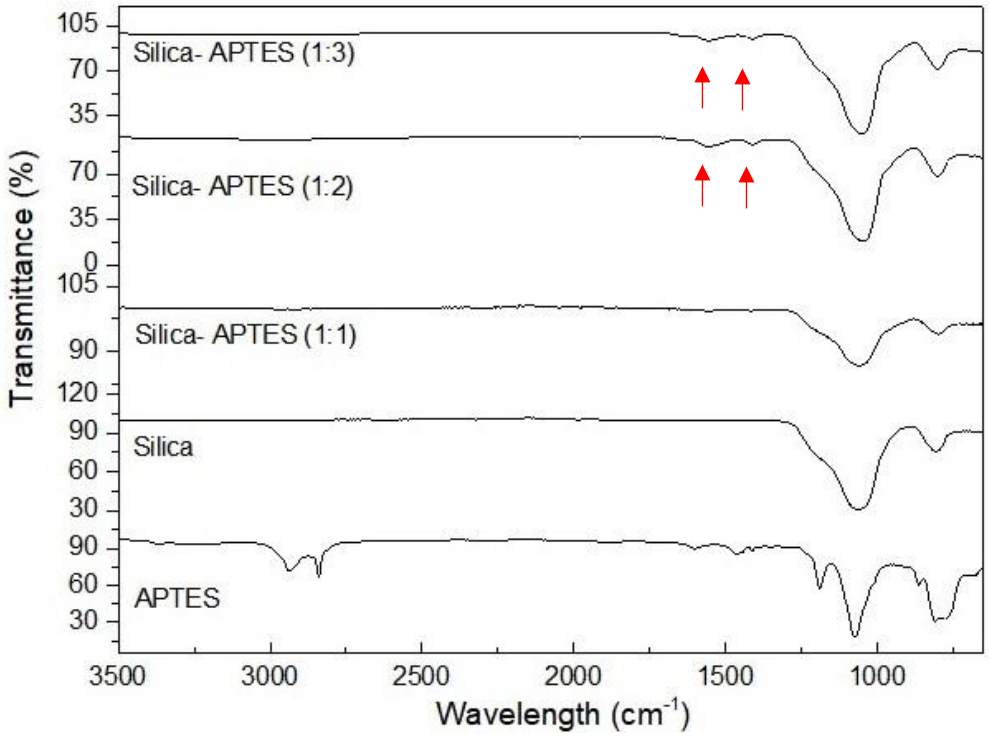

Figure 5. FTIR spectra of APTES, neat silica and APTES functionalized silica with three different ratios.

Table 2. XPS results of neat silica and silica functionalized with APTES at different ratios.

Sample name	**Carbon (at%)**	**Oxygen (at%)**	**Silicon (at%)**	**Nitrogen (at%)**
Silica	3.3	60	36.7	-
Silica:APTES=1:1	18	49	31	2
Silica:APTES=1:2	26	43	27	3.1
Silica:APTES=1:3	15	50	32	3

In order to monitor the degradation behavior of functionalized silica samples, TGA analysis was conducted under nitrogen atmosphere. Figure 6 represents TGA curves of three different APTES functionalized silica samples. Neat silica showed the most stable behavior with the weight loss of 1.73%. In functionalized silica samples, the first weight loss between 50-120°C comes from physically absorbed water molecules and the second weight loss is attributed to the removal of chemically absorbed water between 120-200°C [36]. Then, there is a significant weight loss between 200 and 600°C due to the removal

of organo-functional groups [37]. In addition, there are variations in the weight loss values of functionalized silica particles owing to the differences in functionalization degree. The characterization results confirmed the binding of silane groups on the silica surface.

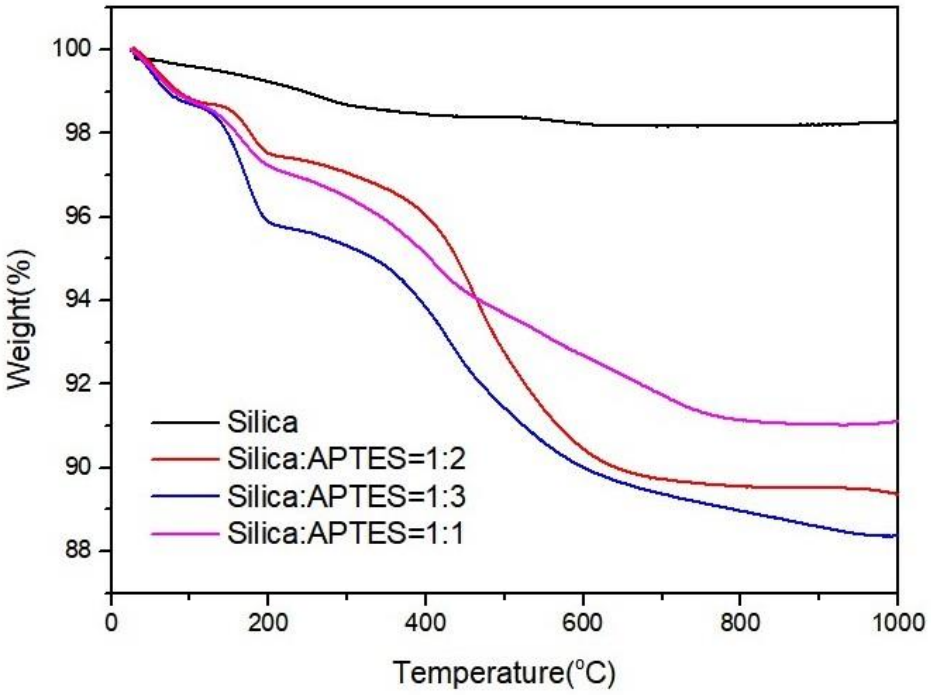

Figure 6. TGA curves of APTES functionalized silica particles with different Si:APTES ratios.

2.3.2. Morphological and structural properties of silica-GNP hybrid additive

The morphological properties of the produced GNP based hybrid additives were examined by using macroscopic techniques. Figure 7 represents SEM images of GNP, neat silica and Si:GNP=1:5 and Si:GNP=1:10 hybrid materials. As shown in Figure 7a, GNP has a layered structure. Figure 7c indicates that, after the introduction of silica nanoparticles on the surface of GNP, particles were distributed randomly and coated on the graphene plates. As Si ratio decreased, aggregation was diminished and more homogenous structure was observed as seen in Figure 7d. TEM image also supports the platelet structure with the average size of 50 nm observed in Figure 7a. Silica particles with the average size of 3 nm was observed in Figure 8b and 8c showing the homogenously distributed APTES functionalized silica particles on GNP.

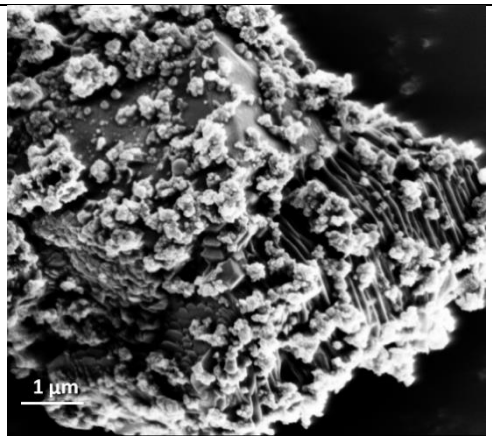

(a)

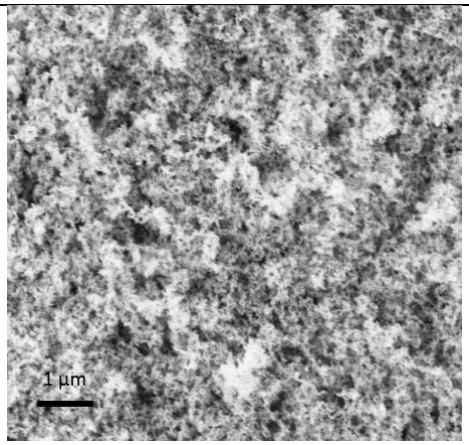

(b)

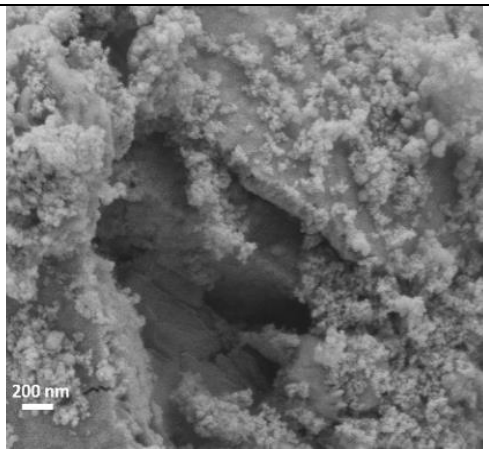

(c)

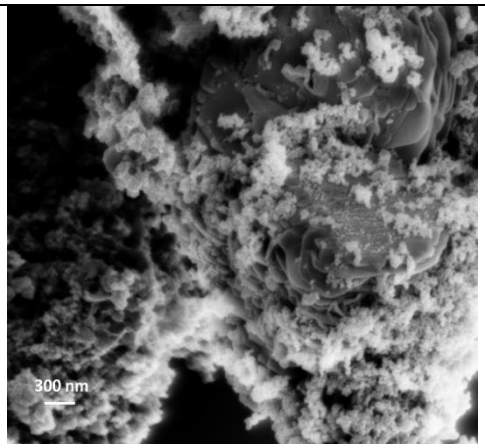

(d)

Figure 7. SEM images of (a) GNP, (b) neat silica, (c) Si:GNP=1:5 and (d) Si:GNP=1:10 hybrid additives.

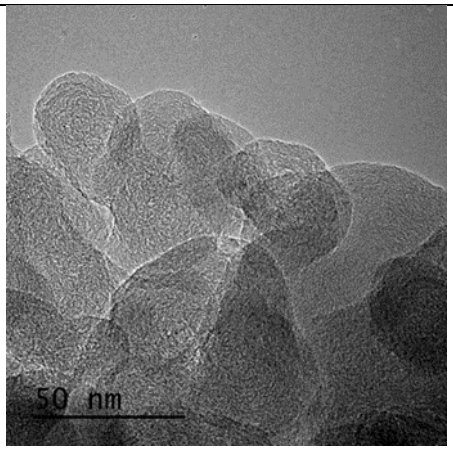

(a)

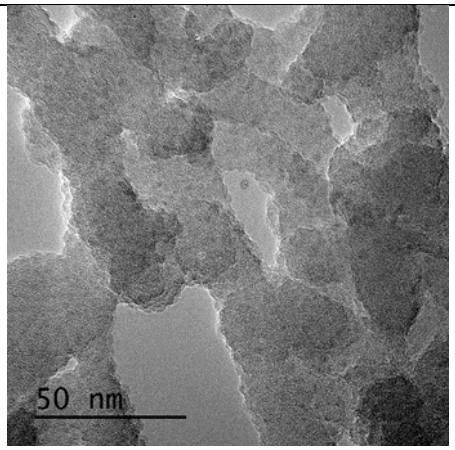

(b)

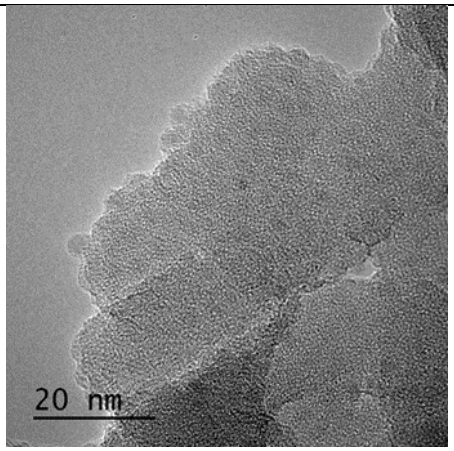

(c)

Figure 8. TEM images of (a) neat GNP, (b) and (c) its hybrid of Si:GNP=1:10.

XPS analysis was performed to investigate the surface chemical composition of the produced samples. Table 3 represents XPS characterization results of silica, Si: APTES=1:2, GNP, and hybrid additives of Si:GNP=1:5 and Si:GNP=1:10. GNP has a specific surface area of 131 m^2/g with a chemical composition of 87 at% carbon, 9.1 at% oxygen, 2 at% silicon, 0.5 at% iron and others (S and Zn). With the incorporation of APTES functionalized silica on GNP, carbon content increased and thus the concentrations of oxygen and nitrogen decreased in hybrid materials when compared to that in the Si:APTES=1:2 sample. In comparison of neat GNP, nitrogen based groups were appeared in the developed additives after the hybridization with functionalized silica and silica amounts were also increased. The XPS peaks of C1s, O1s, Si2p, and N1s for neat and hybrid samples are shown in the XPS survey scan spectra as seen in Figure 9a. After the functionalization of silica particles by APTES, N1s peak was appeared in the spectrum of Si:APTES=1:2 depicting the successful functionalization. After the hybridization of Si:APTES=1:2 with GNP, N1s peak was disappeared indicating the linkage of amino group with graphene during the reaction. Figure 9b indicates the changes in C1s peak intensities of neat and hybrid samples. The existence of C1s binding energy values of 284.28, 284.08 and 284.38 eV for GNP, Si:GNP=1:5, Si:GNP=1:10 denotes the presence of sp^2 hybridized C=C/C–C bonds [38]. Figure 9c indicates the changes in O1s peak intensities by showing the formation of the Si–O and C=O bond for the case of Si:GNP=1:5 and Si:GNP=1:10 is observed at the binding energy of 532 eV [30,31]. N1s spectra of Silica:APTES=1:2, Si:GNP=1:5 and Si:GNP=1:10 was shown in Figure 9d. The broad N1s peak of Silica:APTES=1:2 sample at 399 eV in belongs to NH_3 group

whereas the N1s binding energy of Si:GNP=1:5 and Si:GNP=1:10 shows a hydrogen bonded NH_2 group at 401.2 eV [40]. Furthermore, the C/O ratios of GNP and its hybrids of Si:GNP=1:5 and Si:GNP=1:10 were calculated as 2.5, 0.6, and 0.8, respectively, as shown in Table 4. These results demonstrated the adjustment of hybrid additive composition by systematic optimization of silica and graphene contents.

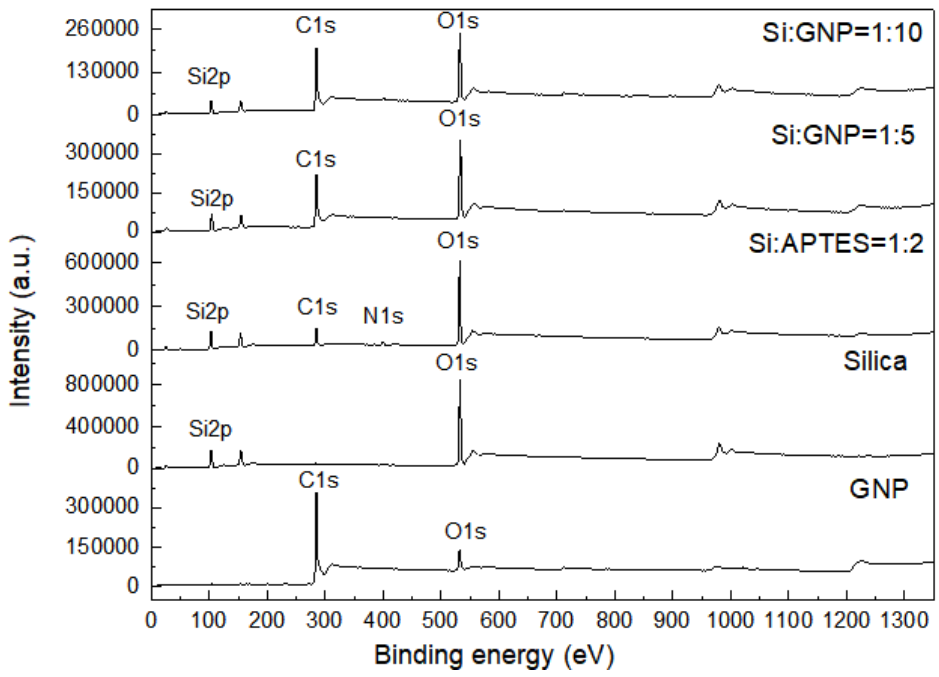

(a)

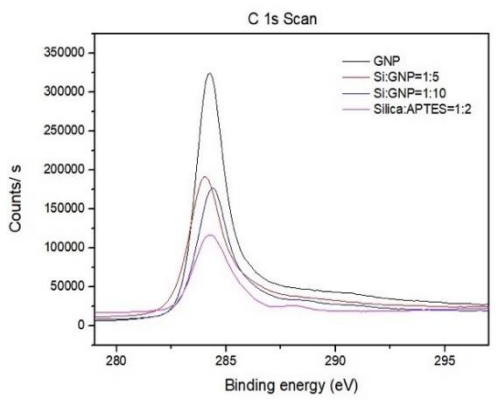

(b)

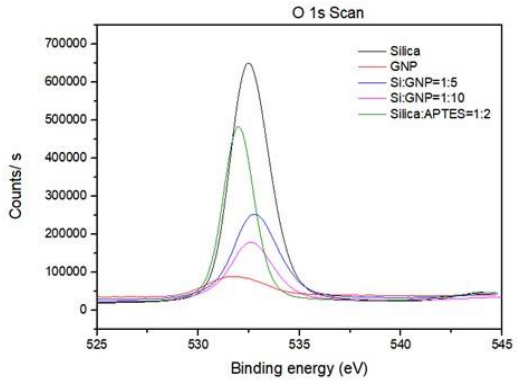

(c)

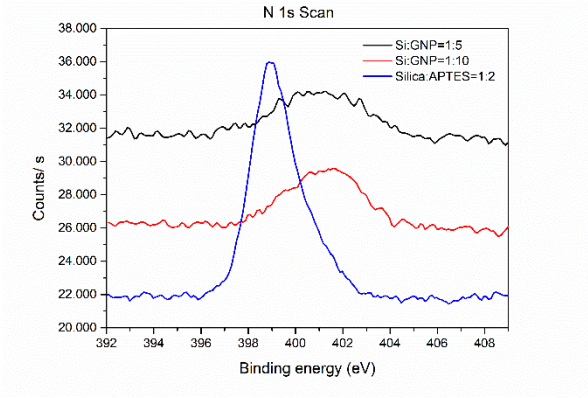

(d)

Figure 9. (a) XPS survey scan spectra, (b) C1s spectra, (c) O1s spectra and (d) N1s spectra of Silica, GNP, Si:GNP=1:5, Si:GNP=1:10 and Silica:APTES=1:2

Table 3. XPS results of GNP and its hybrids of Si:GNP=1:5 and Si:GNP=1:10.

Samples	**Carbon (at%)**	**Oxygen (at%)**	**Silicon (at%)**	**Nitrogen (at%)**	**Other (at%)**
Silica:APTES=1:2	26	43	27	3.1	-
GNP	87	9	2	-	2
Si:GNP=1:5	53	30	16	1	-
Si:GNP=1:10	60	25.1	12.7	1.5	0.7

Table 4. C/O ratios according to XPS results.

Samples	**Carbon (%)**	**Oxygen (%)**	**C/O ratio**
GNP	361644	144321	2.5
Si:GNP=1:5	220471	350888	0.6
Si:GNP=1:10	204405	249117	0.8

Figure 10 shows the TGA curves of silica, GNP and hybrid additives of Si:GNP=1:5 and Si:GNP=1:10. In this figure, weight loss of GNP as a function of temperature under nitrogen atmosphere was about 9 at% at 1000°C due to the removal of surface oxygen groups. Both hybrid materials lost weight slightly owing to the elimination of surface

functional groups. This weight loss was 6% at 1000°C for Si: GNP = 1: 5 and 8% for Si: GNP = 1: 10. Finally, the results show that as silica concentration was increased, the hybrid materials became more stable due to the highest thermal stability of silica.

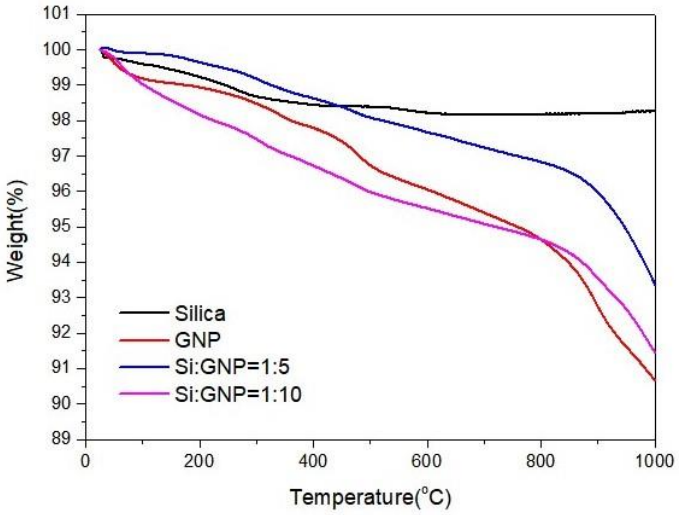

Figure 10. TGA curves of silica, GNP, Si:GNP=1:5 and Si:GNP=1:10 hybrid materials.

Figure 11a represents Raman spectra of silica, GNP and hybrid additives of Si:GNP=1:5 and Si:GNP=1:10. GNP has two main Raman peaks of D and G appeared at 1342 cm^{-1} and 1585 cm^{-1}, respectively. The first peak named as D peak is related to the disorderness degree of graphene samples, while the second one named as G peak attributes to the vibrational mode of sp^2 carbon in graphitic materials [41]. There was no detected Raman peak in the analysis conducted on the neat silica. The defect density and crystallinity were then estimated using the intensity ratio of D peak to G peak (I_D/I_G) [42],[43]. After hybridization, the I_D/I_G ratios of the hybrid materials were changed. The disorderness of Si:GNP=1:5 was slightly increased, whereas the increase in GNP content in Si:GNP=1:10 led to a decrease in I_D/I_G ratio indicating a more ordered structure. Table 5 summarizes the Raman peak intensities ratios (I_D/I_G) and the crystallinity index of GNP and the hybrid additives of Si:GNP=1:5 and Si:GNP=1:10. Figure 11b shows the XRD patterns of silica, GNP and the hybrid additives of Si:GNP=1:5 and Si:GNP=1:10. XRD analysis was conducted to monitor the changes in crystallinity. GNP has broad and less intense (002) peak at around at 2θ=25°. Furthermore, the peak at 2θ=35.8˚ belongs to the (311) reflection of Fe catalyst coming from the production process of graphene from waste tire. By addition of silica particles, the peak at around 2θ=25° becomes wider. However, there is no significant difference between the two hybrid additives, since GNP has a more prominent structure that suppresses the silica peak.

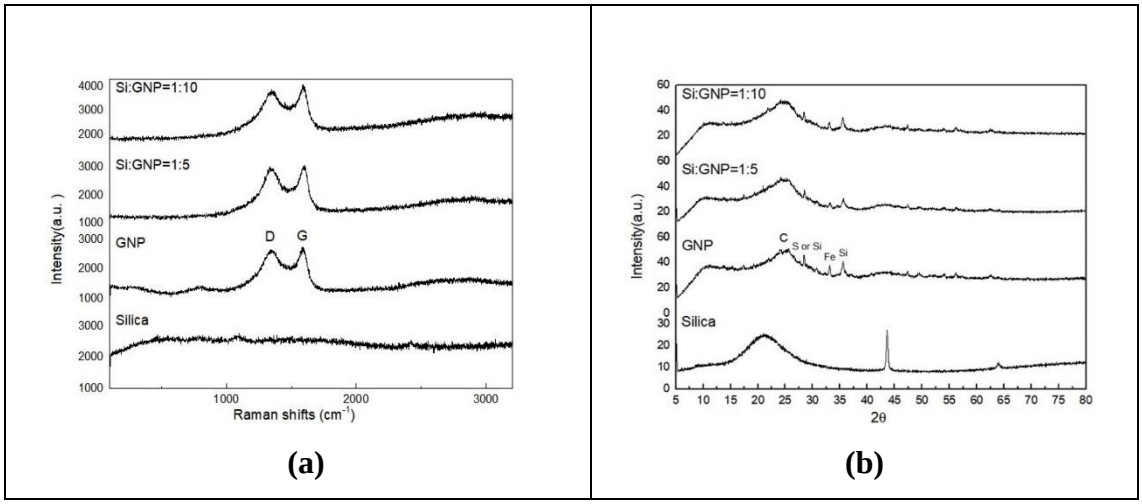

Figure 11. (a) Raman spectra and (b) XRD patterns of silica, GNP, and Si:GNP=1:5 and Si:GNP=1:10 hybrid additives.

Table 5. Raman peak intensities, I_D/I_G ratios and crystallinity index of GNP, Si-GNP=1:5 and Si:GNP=1:10 hybrid additives.

Samples	D peak intensity (a.u.)	G peak intensity (a.u.)	I_D/I_G	Crystallinity (%)
GNP	2670.6	2754.5	0.97	24.1
Si:GNP=1:5	3043.9	3100	0.98	27.8
Si:GNP=1:10	3894.2	4111.6	0.94	23.3

2.3.3. Grout formulations by GNP based hybrid additives and their characteristics

The rheological properties of the grout used to backfill the heat-exchange boreholes are essential for several reasons. A grout with good rheological properties can provide good pumpability, less entrapped air and consequently lower permeability, less sensitivity to freeze and thaw cycles and accordingly more durability and good thermal contact between the grout, the pipes and the surrounding underground formations that lead to higher thermal conductivity between the heat carrier fluid and the ground [44]. One of the most important parameter that affects the efficiency of geothermal energy system is the thermal resistance of the heat-exchange boreholes that in turn depend on the thermal properties of the backfill [11]. The thermal resistivity of the grout, R_g can be determined using the following equation (1), where S_b is the borehole shape factor and λ_g is the thermal conductivity of the backfill grout in terms of [W/mK] [45]:

$$R_g = \frac{1}{S_b.\lambda_g} \quad (1)$$

Since R_g and λ_g are reciprocals of one another, the minimum thermal resistance of the borehole means the maximum thermal conductivity in correlation with the shape factor enhancing the heat transfer rate between the heat carrier fluid and the Earth [46].

Table 6 summarizes the thermal conductivity results of the grout samples prepared by addition of Silica-GNP hybrid additives at different loadings. In the first trials, thermal conductivity of GNP based cement sample was measured at three curing conditions on 7^{th}, 14^{th} and 28^{th} days. As seen in Table 6, as carbon content is increased in both the hybrid structure and the grout mixture, water uptake is increased compared to the reference grout. The increase in the water demand in Si:GNP=1:5 samples (that occurred due to the higher loadings of 1-5 wt%) decreased the thermal conductivity values from 2.373 W/mK to 1.816 W/mK. As the content of GNP was doubled in the hybrid additive (from Si:GNP=1:5 to Si:GNP=1:10), water demand of the grout mix was decreased and thus the thermal conductivity of the grout sample was increased from 1.816 W/mK to 2.341 W/mK at 5 wt% loading which corresponds to 29% improvement. In addition to thermal conductivity, Table 6 shows a summary of the results obtained from the flowability tests (using a Marshcone and a Flow table), the bleeding tests (using glass cylinders) as well as the density measurements (using a Mud-balance). In this study, the target values for the Marshcone time and the Flow-table test were in the range of 80-120 sec and 20-30 cm, respectively. Similarly, the maximum accepted value for the bleeding and the minimum accepted value for the density were 2% and 1.3 g/cm^3, respectively. As seen in Table 5, all the test results obtained from the grout samples having Silica-GNP hybrid additives were in the accepted ranges.

Table 6. Thermal conductivity results and rheological properties of selected reference grout and samples having hybrid additives.

Test no	**Cement (g)**	**Silica Sand 30-35 AFS (g)**	**Silica Sand 60-70 AFS (g)**	**Bentonite (g)**	**Additive (g)**	**SP (g)**	**Water (g)**	**Marshcone (sec)**	**Flowtable (cm)**	**Bleeding (%)**	**Density (g/cm^3)**	**Thermal Conductivity (W/mK)**
1	930	900	900	10	0 Reference	18.6	650	77	26	0.49	2.1	2.373
2	930	900	900	10	9.3 (Si:GNP=1:5) (1 wt%)	18.6	650	90	28	<0.3	2.02	2.427
3	930	900	900	10	27.9 (Si:GNP=1:5) (3 wt%)	18.6	660	105	24	0.10	2.04	2.287
4	930	900	900	10	46.5 (Si:GNP=1:5) (5 wt%)	18.6	725	95	27	0.25	2.03	1.816
5	930	900	900	10	46.5 (Si:GNP=1:10) (5 wt%)	18.6	700	96	28	1.2	2.05	2.341

2.4. Conclusions

In the present study, silane functionalization routes were developed to treat silica surface and make compatible hybridization with GNP. Optimization study provided the proper amount of APTES (i.e. 1:2 of Silica to APTES (w/w)) to be used in the treatment of silica. This was verified by FTIR and TGA analyses. Then, GNP produced from the recycled carbon black obtained by the pyrolysis of waste tire was selected as a carbon source for the hybridization step. This type of graphene has also surface oxygen functional groups of 9 at% to make suitable bridges with amine groups on the surface of APTES functionalized silica. After the structural confirmation of hybrid additive, reference grout formulation was determined by adjusting the contents of cement, silica sands, bentonite, superplasticizer and water. The effects of GNP amount in hybrid structure and the concentration of hybrid additive on the thermal conductivity of the prepared grouts showed that as water content increased, thermal conductivity value decreased. On the other hand, increasing GNP amount in hybrid additive led to an increase in thermal conductivity by 29% by keeping the GNP loading ratio of 5 wt% in two different grouts. Consequently, the study finally shows noticeable potential of the hybrid additives produced from GNP to be used in the backfill grout formulations in the geothermal heat-exchange boreholes. This will be more discernible, since renewable energy sources come into prominence by ever-increasing energy-demand and global pollution.

CHAPTER 3: Synergistic Effect of Expanded Graphite-Silane Functionalized Silica as a Hybrid Additive in Improving Thermal Conductivity of Cementitious Grouts with Controllable Water Uptake

Recently, a growing demand on geothermal applications leads to the exploitation of energy efficiently by developing grouting materials in the borehole between the pipes and ground. Therefore, the current study develops newly formulated cementitious grouts by the integration of expanded graphite (EG) based hybrid additives synthesized by building chemical bridges between silica particles and EG in the presence of amino functional silane coupling agents. These produced hybrid additives with controlled EG and silica ratios were utilized in these grout mixtures used in borehole heat exchangers to enhance the thermal conductivity. According to optimization study on the formulation development of grout mixtures having bentonite, silica sands, cement, and superplasticizer by adding neat EG and EG based hybrids, the relationship between carbon amount and water demand has been found to have a significant impact on thermal conductivity. The highest thermal conductivity value of 2.656 W/mK was achieved by the incorporation of 5 wt% hybrid additive with the ratio silica/EG of 1:5 compared to the reference grout having the thermal conductivity of 2.373 W/mK. Therefore, the enhancement in thermal conductivity was dependent on the increase in EG content and also additive loading ratio resulting in slight increase in the water demand.

3.1. Introduction

New researches on renewable energy have been growing due to the increasing demand of energy all over the world. At this point, shallow geothermal energy systems have attracted enormous research interests owing to their several advantages such as reducing CO_2 emission, being weather independent in contrast to other renewable energy technologies and finally availability in most lands [47]. In such systems, the most prominent feature of ground loop heat exchanger is the backfill grout , which allows the heat-exchange between the heat-carrier fluid in pipes and the surrounding formations [48]. Therefore, the thermal conductivity of the backfill grout should be as close as possible to the thermal conductivity of the surrounding formations to successfully exchange the heat with minimum heat loss [11]. More specifically, as the thermal conductivity of the grout increases, the more heat can be transferred through the borehole

and the length of the pipe to be constructed under the ground can be shortened, thus the installation costs are reduced [49].

According to the literature, several attempts have been carried out over the years to develop thermally enhanced grouts by using carbon nanotubes as nano-scaled additives. Lee *et al.* incorporated different concentrations of multi-walled carbon nanotubes (MWCNT) into a grout consisting of cement, sand and a surfactant resulting in the improvement of electrical resistance of 1.0% MWCNT based grout with the filling rates of 100%, 75%, 50% and 25% as 0.449 kΩ, 0.575 kΩ, 0.846 kΩ, and 0.934 kΩ, respectively [50]. In another study, Zhang and Li produced a cement-based composite for a thermally conductive layer in a deicing road system by integrating 3 wt% MWCNT and obtained thermal conductivity of 2.83 W/mK [51]. However, there are still challenges in the utilization of CNT in grouting mixtures especially in mass production due to their rigid surface, the requirement of an additional surface treatment and high cost [52, 53]. Therefore, the trend has so far been mainly gone through ease available materials to overcome the needs in the backfill grouts used in the borehole heat exchangers.

In previous studies carried out to improve thermal conductivity of the backfill grouts, various types of graphitic materials and treatment techniques have been tested to meet the defined requirements. For instance, Delaleux *et al*. studied on the dispersion of different graphite loadings between 0 to 25 wt% with different intrinsic densities changing from 20 to 150 kg/m^3 in bentonite mortars indicating an attainment of highest thermal conductivity of 5 W/mK by the addition of 5 wt% graphite with the internal density of about 100 kg/m^3 [54]. In another work, Lee *et al.* compared the effect of graphite and silica sand in thermal conductivity of bentonite grout and stated that use of 20% graphite increased the thermal conductivity of bentonite grout close to that in the geologic formation (1.7–2.1 W/mK), whereas silica sand did not change thermal conductivity even by 60% loading [5]. Following that, Jobmann *et al.* investigated the influence of temperature, water content and density on thermal conductivity, using graphite as an admixture and achieved the thermal conductivity of 3 W/mK with the water content of 14% and the graphite content of 15% [19]. In addition to the thermal conductivity characteristic of grouts, it is possible to enhance the mechanical properties of cementitious grouts by polymer coating and the attachment of -COOH groups on graphite nanomaterials to improve their dispersion behaviors [55]. Therefore, the structural properties of the graphitic materials should be also taken into consideration to allow

improvement of the interfacial interactions with the cement matrix and the other components of the grout by tailoring surface chemistry.

Among the graphitic materials, expanded graphite (EG) with high carbon content has a beneficial of improving thermal conductivity of grout mixtures due to its remarkable thermal properties, low density, high porosity, planar geometry and low price [56, 57]. In one of the works, Bao *et al.* conducted infrared thermal image analysis to compare the performance of 20 wt% EG- Paraffin and 10 wt% graphene nanoplatelets (GNP)-Paraffin used as the phase change materials in the developed cement-based composites, resulting in better thermal-regulatory with GNP due its high thermal conductivity coefficient [58]. Furthermore, Zhang *et al.* fabricated EG/paraffin gypsum-based composite with 1 wt% carbon fiber and increased the thermal conductivity by 36.0% and 28.6% with the addition of 10% and 20% EG, respectively [59]. Accordingly, the recent investigations clearly show the potential of EG to use as a phase change material and its direct use in grout mixes without any required surface modification, especially in paraffin systems.

Another important criterion in grout mixtures is to obtain uniform dispersion of the used additives. The incorporation of carbon-based materials into the cement mixture increases the viscosity and decrease the fluidity. Therefore, surface treatments on carbon-based materials gains high importance to enhance their dispersion in cementitious matrix by providing an efficient heat transfer. Luping *et al.* enhanced the interactions between graphene oxide (GO) and calcium silicate hydrate in cement matrix by applying silane functionalization to form covalent bonds and provide better dispersion [60]. Moreover, Wang *et al.* improved the fluidity and rheological properties of cement paste and prevent the aggregation of particles by applying copolymerization on silane modified GO [24]. These studies stated that the working performance of cement mixtures can be raised by the silanization of the selected additive. Silica has also gained considerable attention due to its ease distribution, high modulus, electrical insulation, hardness as well as extreme temperature sustainability [61]. Furthermore, the incorporation of silica into the cementitious mixture/mortar can improve the interfacial bonding of cement hydrates with modified carbon-based materials during the hydration reaction and more compact structure can be obtained by filling the remaining voids in hydrated cement paste [55, 62–64]. Especially the development of silica-based hybrid additives by using graphitic structures can noticeably influence the performance of grout used in Shallow Geothermal Energy Systems. There are numerous attempts for the attachment of silica particles on the surface of graphite and graphene based structures to pose high thermal conductivity in

the field of improving the properties of latex and electronic industry as high-performance thermal interface materials [65, 66].

To the best of our knowledge, the performance of EG and silica in combined structures has not yet been sufficiently evaluated in the grout mixes and there are very limited studies about utilization of the hybrid additives for development of thermally enhanced grout composites. In order to maintain an effective interfacial bonding between EG and the cementitious grout composites, the dispersibility of the graphitic materials added to the grout mix should be enhanced by surface treatment [67]. To overcome the low dispersibility of EG in cementitious grout composite, new approach has been carried out by modifying the surface of EG with silane coupling agents in order to increase the surface hydrophilicity and interfacial interactions between EG and the cement matrix. Surface functionalization by organo-silanes is one of the efficient ways to improve the chemical adhesion between two materials [68]. Several studies have been conducted to improve the rheological properties and/or strength of cement mortars by addition of carbon-based materials[15].

In the present study, silanization process is employed to develop new forms of EG-based hybrid additives by changing the amounts of functionalized silica and EG for the fabrication of thermally enhanced grout composites to enhance interfacial interactions between the developed additives, bentonite and the other grout components. In order to understand the extent of influence of carbon content on the performance of the developed cementitious grout composites, chemical compositions of hybrid additives were tailored by changing silica and EG contents. Detailed spectroscopic and macroscopic studies were carried out to confirm the structural formation of EG-based hybrid additives. Then, the performances of the produced EG-based hybrid additives were tested in the grout mixes formulated to obtain the highest possible thermal conductivity with the proper rheological properties.

3.2. Materials and Methods

3.2.1. Materials

In this investigation, 3-Aminopropyl triethoxysilane (APTES >98%), acetic acid and Tetrahydrofuran (THF) were provided from Sigma-Aldrich, USA. Amorphous silica (SiO_2) was provided from Merck, Germany. Expanded graphite-GFG5 with 5 μm particle size was obtained from SGL Carbon, Germany. Portland Cement CEM I 42.5 R from

Cimsa, Turkey, Silica Sand (AFS 30-35 and AFS 60-70) from Kumsan Co, Turkey, superplasticizer (SMRC-310S) from Sika, Turkey and bentonite from Canbensan Bentonite, Turkey were used in preparation of the grout composites. Malvern 3000, laser diffraction particle size analyzer was used to analyze the particle size distribution of constituents. Table 7 summarizes the particle size distributions of cement, bentonite, silica sands AFS 30-35 and AFS 60-70 regarding D10, D50, and D90 which are the intercepts for 10%, 50%, and 90% of the cumulative mass of analysis results. The product of Silica Sand AFS 30-35 with D90 = 912 μm has the largest particle size among the samples, whereas cement with D90 = 46.4 μm has the smallest one.

Table 7. Particle size distributions (D10, D50 and D90) of cement, bentonite, two types of silica sands according to 10%, 50%, and 90%.

Constituent names	D10 (μm)	D50 (μm)	D90 (μm)
Cement	3.72	17.8	46.4
Bentonite	9.21	40.6	131
Silica Sand 30-35 AFS	401	621	912
Silica Sand 60-70 AFS	134	250	454

3.2.2. Synthesis of Functionalized Silica

Silane coupling agents have considerable influence on the dispersion of fillers and the improvement of interfacial interactions between fillers and the constituents in cement matrix. The dispersion quality of the selected fillers directly enhances the thermal, mechanical and physical properties of nanocomposites since silane coupling agents acting as bridge between silica and EG by increasing the compatibility with the component of grout mixes. APTES is one of the most commonly used silane coupling agents that connects chemically reactive functional amino groups to silica and hydrolyzable groups on EG by silanization process. In order to provide effective functionalization, the optimum APTES to silica ratio was determined as 1:2 by adjusting weight to weight ratio of silica and silane amounts. In more details, 1 g of silica was first mixed into 50 mL distilled water. Then, 2 mL APTES was dissolved into the mixture and the pH level of the solution was adjusted to 5.5 by adding acetic acid. Afterwards, the mixture was stirred

at 80 °C for 24 h to ensure completion of the silanization reaction. At the end of the reaction, the mixture was filtered by washing with water and ethanol twice in order to remove the remaining silane coupling agent. The filtrate was then dried in an oven at 70 °C for 24 h. The detailed production process of APTES functionalized silica particles with an average diameter of 130 nm can be found in our previous publication [8].

3.2.3. Hybridization of EG with Functionalized Silica

In this study, hybrid EG/silica additives modified by silane coupling agents were developed by tailoring surface functional groups. To produce a homogeneously dispersed EG solution, THF was selected as a reaction medium [69]. Accordingly, approximately 240 g EG was added to 7.5 liter of THF. The solution was then subjected to ultrasonic dispersion process by Handheld Ultrasonic Homogenizer from Hielscher Ultrasonics at room temperature for 30 min. Afterwards, a previously prepared APTES functionalized silica aqueous solution (Silica:APTES=1:2, encoded as fSi) was slowly added into EG-based suspension. The reaction was carried out through refluxing at 60 °C overnight. After the reaction, the resultant material was obtained by centrifugation and then separated by decantation and dried at 70 °C overnight in vacuum oven. While the silica to silane ratio in functionalized silica was kept as 1:2 in hybrid additives, as summarized in Table 8, the ratios of functionalized silica and EG were adjusted as 1:1 and 1:5 encoded as H-EG-1 and H-EG-2 (also called as fSi/EG based hybrid additive), respectively, to monitor the effect of carbon content on the performance of hybridized additives in grout mixes.

Table 8. Summary of synthesis conditions of EG based hybrid additives.

Samples	Silica:APTES=1:2 (fSi), (g)	EG Amount (g)	Reaction Medium	Reaction Time (h)
H-EG- 1 (fSi:EG=1:1)	1	1	THF	24
H-EG-2 (fSi:EG=1:5)	1	5	THF	24

3.2.4. Preparation of grout samples by using hybrid additives

Since addition of EG-based materials affects the properties of neat grout composites, optimization process is crucial to obtain the best possible properties. As shown in Table 9, the neat grout composition consists of 65.69 wt% of silica sands having different

particle sizes named as 30-35 AFS and 60-65 AFS, 33.94 wt% of cement, 0.37 wt% of bentonite and superplasticizer and then EG based hybrid additives were added with two different concentrations of 3 wt% and 5 wt% by tailoring the amount of bentonite and water uptake. The grout composites were mixed using a high-share dispersion system from VMA-Getzmann. While part of the prepared grout mix was separated each time for Marsh-cone and flow-table tests, rest of the material was poured into disk-shaped molds (20 mm in height × 60 mm in diameter) and kept in climate chamber under 100% relative humidity and 20 °C for curing. The curing stages of the samples were examined on 7th, 14th and 28th days. Conductivity measurements were carried out on the mentioned days after the cement sample was poured into the mold and placed in a 100% moist environment at 20 °C. Since no significant change was observed on these days, thermal conductivity tests were carried out for the samples cured on the 7th day. The samples were then used to determine the thermal conductivity of the EG-based hybrid additive enhanced cementitious grout composites. Thermal conductivity tests were performed under 23°C and 50% ± 2% humidity. Further details about mixing regime, sample preparation and the tests conducted for the thermal and rheological characterizations of the grout mixes can be found in the previous article [8].

Table 9. Reference grout formulation.

Component	wt%
Cement	33.94
Silica Sand (30-35 AFS)	32.845
Silica Sand (60-65 AFS)	32.845
Bentonite	0.37

3.2.5. Characterization

The morphologies of neat EG, silica and fSi:EG=1:1 and fSi:EG=1:5 hybrid additives were examined by Scanning Electron Microscope (SEM, Leo Supra 35VP Field Emission). The thermal properties of the prepared samples were conducted by using thermal gravimetric analyzer over the temperature range of 25 °C to 1000 °C at a heating rate of 10 °C/ min under flow of nitrogen (TGA, Mettler Toledo TGA/DSC 3+). The crystallinity of the samples was analyzed by X-ray diffraction with a CuKα radiation

source (XRD, Bruker D2 PHASER Desktop). X-ray Photoelectron Spectroscopy System (XPS, Thermo Scientific K-Alpha) was also used to examine the elemental composition of EG and its hybrid additives. The thermal conductivity of silica/EG-based cementitious grout composites was investigated using a thermal conductivity analyzer (Hot Disk Thermal Constants Analyser, TPS 2500 S). The thermal conductivity tests were repeated with three different combinations of identical samples to obtain more accurate results and the reported values were the average of the three repetitions. Surface areas of the samples were measured by Brunauer-Emmett-Teller technique using Micromeritics 3Flex surface analyzer equipment. The structural changes in carbon-based materials were characterized by Raman spectroscopy with the laser wavelength of 532 nm in the range of 100-3500 cm^{-1} (RAMAN, Renishaw inVia Reflex Raman Microscopy System).

3.3. Results and Discussion

3.3.1. Structural Properties of Functionalized Silica and Silica Modified Hybrid EG Additives

Although the addition of EG as an additive improves the rheological, mechanical and thermal properties of cementitious grout composites, homogenous dispersion of EG is one of main requirements to get uniform composition. Therefore, the coverage of EG surface with silanized silica might be an effective method to provide proper interaction between EG and other grout constituents. In the initial part of functionalization, silane coupling agents of APTES were attached covalently to the surface of silica with their hydrolyzed groups in water medium with adjusted pH as seen in Figure 12a. In other words, the formation of a network between three hydrolyzable groups of silanes and OH groups of silica cause covalent interactions to preserve the uniformity in the structure. In the second part, amine functional groups were linked to the EG sheets and formed the hybrid additive as shown in Figure 12b.

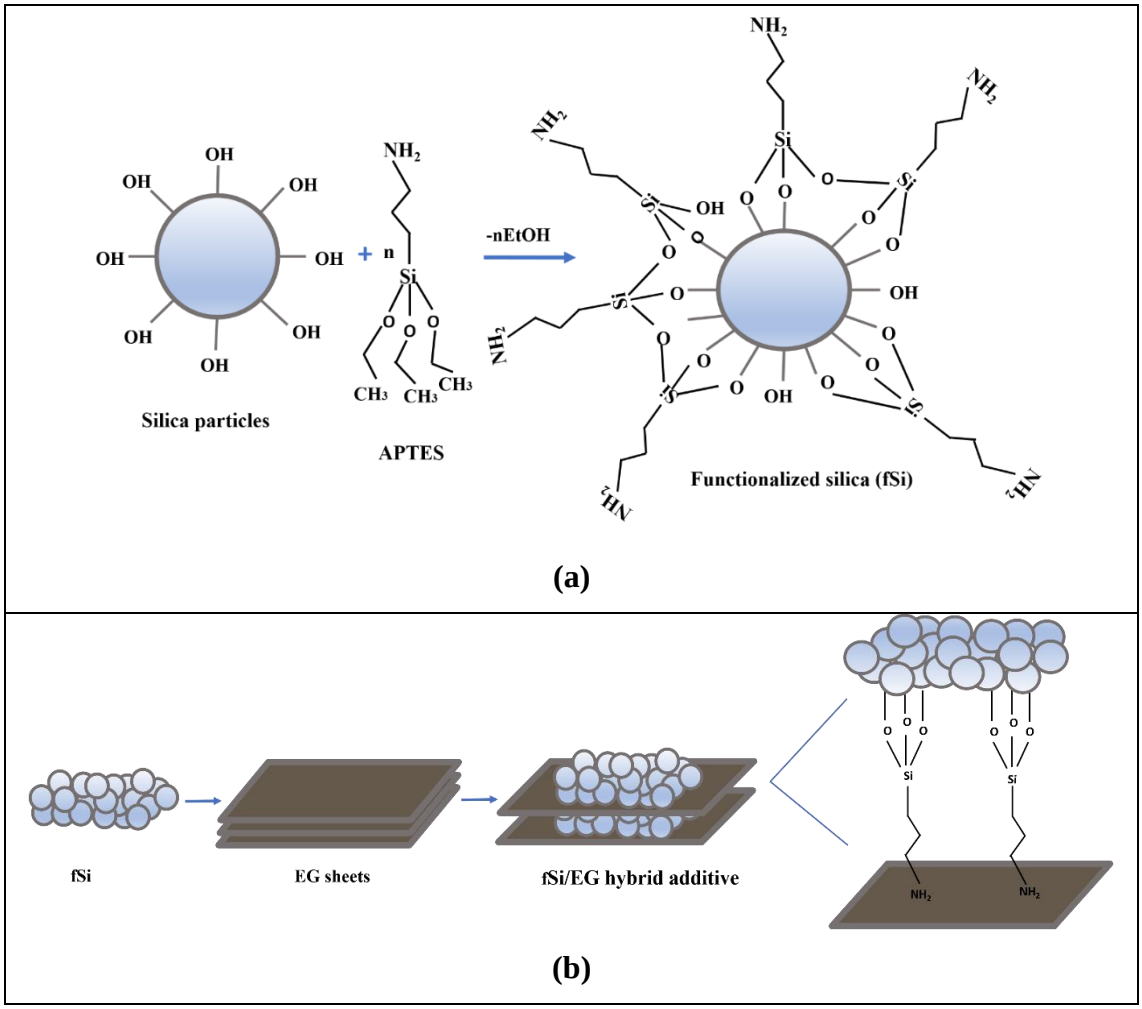

Figure 12. Schematic representation of (a) APTES functionalized silica (fSi) and (b) fSi/EG based hybrid additive.

In order to observe the influence of fSi/EG ratio on thermal conductivity of the developed cementitious grouts, two different hybrid additives were produced and tested by changing the amounts of silica and EG as 1:1 and 1:5, while keeping the ratio of silica to APTES constant. The results showed that by changing the carbon content in the structure of the hybrid additive, the specific surface area of the hybrid is noticeably changed. In case of H-EG-1, BET surface area was measured as 74 m^2/g compared to that of neat EG, which was evaluated as 30 m^2/g. In case of H-EG-2, as the carbon content in the hybrid structure was increased, the BET surface area was decreased down to 12 m^2/g. That is mainly due to the very high surface area of neat silica (473.8 m^2/g) compared to that of EG (30 m^2/g). Herein, as carbon content was increased, the surface area of hybrid was decreased.

Amino groups coming from APTES that are attached on the silica surface play a significant role to obtain an ideal hybridization with the EG particles. Therefore, chemical

composition analysis was carried out by XPS to monitor the changes in the chemical composition on the surface of the hybrid EG additives compared to neat silica and EG. Survey scans of EG, represented in Figure 13a, show two main peaks of C1s and O1s at 286 eV and at 534 eV, respectively, indicating the presence of carbon and oxygen content [70]. According to the XPS results tabulated in Table 10, EG contains 98% of carbon and 2% of oxygen in its structure, which makes it an excellent candidate to enhance higher thermal conductivity than other carbon-based materials [71]. As seen in XPS scans in Figure 13a and Table 10, while neat silica consists of 60% oxygen, 3.3% carbon, and 36.7% silicon, there is a decrease in the oxygen and the silicon contents, and an increase in the carbon and the nitrogen contents in Si:APTES=1:2, indicating successful silanization. Furthermore, after functionalization of silica surface with APTES (fSi), nitrogen appeared at around 399 eV in the survey scan of Si:APTES=1:2. This was a clear evidence of bonding between silica and APTES. Considering the scans of the hybrid additives, the increase in carbon content and the decrease in nitrogen content clarify the formation of the hybrid structures. Herein, the increased carbon content is an indication of modification of APTES functionalized silica with EG. The results also showed that H-EG-2 had higher carbon content and lower Si content compared to H-EG-1. This shows that it is feasible to control the surface composition using proper chemical approach. Moreover, the deconvolution of C1s, O1s and N1s spectra for EG, silica, H-EG-1 and H-EG-2 were carried out to investigate formation of interfacial interaction between the components. In C1s deconvolution shown in Figure 13b, the peaks at around 284.5 eV belong to C-C, indicating highly ordered sp^2 graphitic network [72, 73]. Figure 13c shows the deconvolution of O1s spectra of neat and hybrid structures which showed the peaks at around 532.8 eV attributing to the presence of O–Si in the structures [74]. Figure 13d represents the deconvolution of N1s spectra of functionalized silica and hybrid additives. The sharp N1s peak of functionalized silica at around 398.8 eV indicates the presence of NH_3 groups. After modifying the surface of EG with APTES functionalized silica, the N1s peak became broader. Moreover, they were shifted to higher values and appeared at around 400 eV and 399.4 eV for H-EG-1 and H-EG-2, respectively, indicating nitridation of EG surface. In addition, there are alterations in the intensities of N1s peaks of H-EG-2 (fSi:EG=1:5) and H-EG-1 (fSi:EG=1:1), coming from the formation of amine and charged amine moieties, respectively, in the hybrid structures [75].

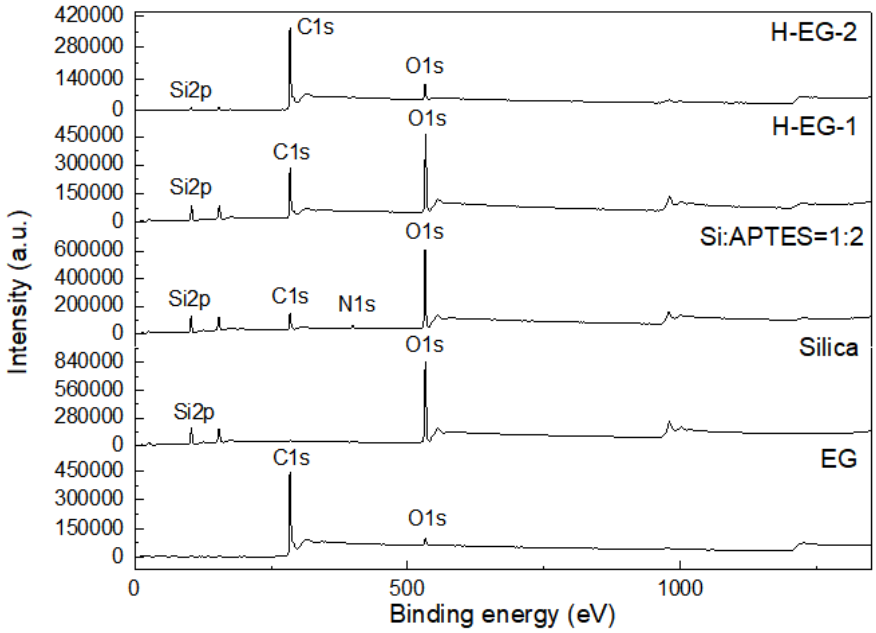
Intensity (a.u.)
Binding energy (eV)
H-EG-2
H-EG-1
Si:APTES=1:2
Silica
EG
C1s
O1s
Si2p
N1s

(a)

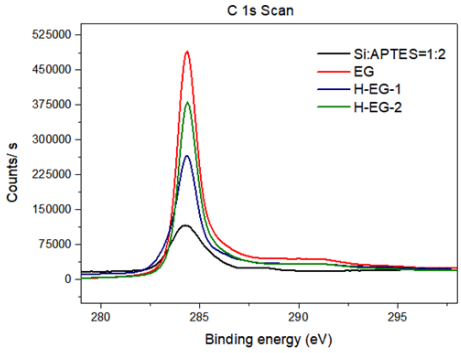
C 1s Scan
Counts/ s
Binding energy (eV)
Si:APTES=1:2
EG
H-EG-1
H-EG-2

(b)

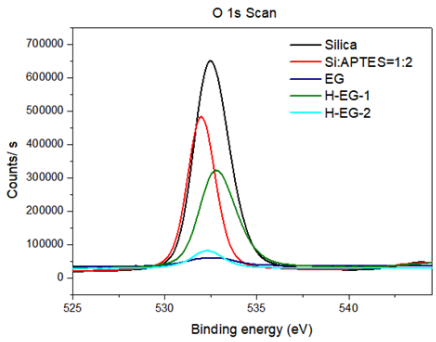
O 1s Scan
Counts/ s
Binding energy (eV)
Silica
Si:APTES=1:2
EG
H-EG-1
H-EG-2

(c)

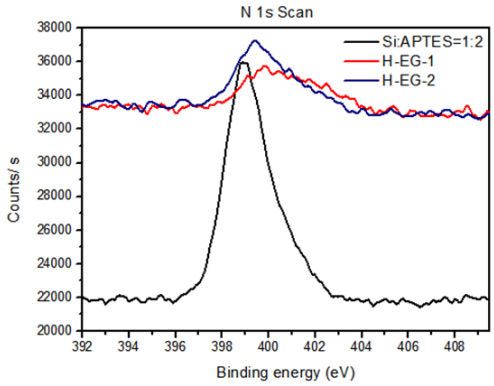
N 1s Scan
Counts/ s
Binding energy (eV)
Si:APTES=1:2
H-EG-1
H-EG-2

(d)

Figure 13. (a) XPS survey scan spectra, (b) C1s spectra, (c) O1s spectra and (d) N1s spectra of silica, Silica:APTES=1:2, EG, H-EG-1 and H-EG-2.

Table 10. XPS results of silica, Silica: APTES=1:2, EG and its hybrid additives with different carbon contents.

Sample Name	**Carbon (at%)**	**Oxygen (at%)**	**Silicon (at%)**	**Nitrogen (at%)**
Silica	3.3	60	36.7	-
Silica: APTES=1:2	26	43	27	3.1
EG	98	2	-	-
H-EG-1	50.5	30.3	18.2	1
H-EG-2	88.2	6.7	3.2	1.7

XRD analysis was performed to monitor the changes in the crystallinity of hybrid additives. Figure 14 exhibits XRD spectra of silica, EG, H-EG-1 and H-EG-2. The broad XRD peak on pattern of silica appeared at around 2θ=21° belonging to (101) planes revealing the amorphous structure of the silica [76] and the peak appeared at around 2θ= 43.6° belongs to the metallic holder. EG shows a sharp peak at around 2θ= 26.5° belonging to the diffraction of (002) planes and a smoother peak at around 2θ=54.6° belonging to the diffraction of (004) planes, indicating a crystalline structure [70]. As seen in Table 11, after attachment of the silica particles on EG surface, the crystallinity degree of EG decreases from 89% down to 70.6% and 68.7% in H-EG-1 and H-EG-2, respectively. This phenomenon can be observed in the XRD spectra showing the decrease in the intensity of (002) peak due to the amorphous structure of the silica that affects the crystallinity of the hybrids.

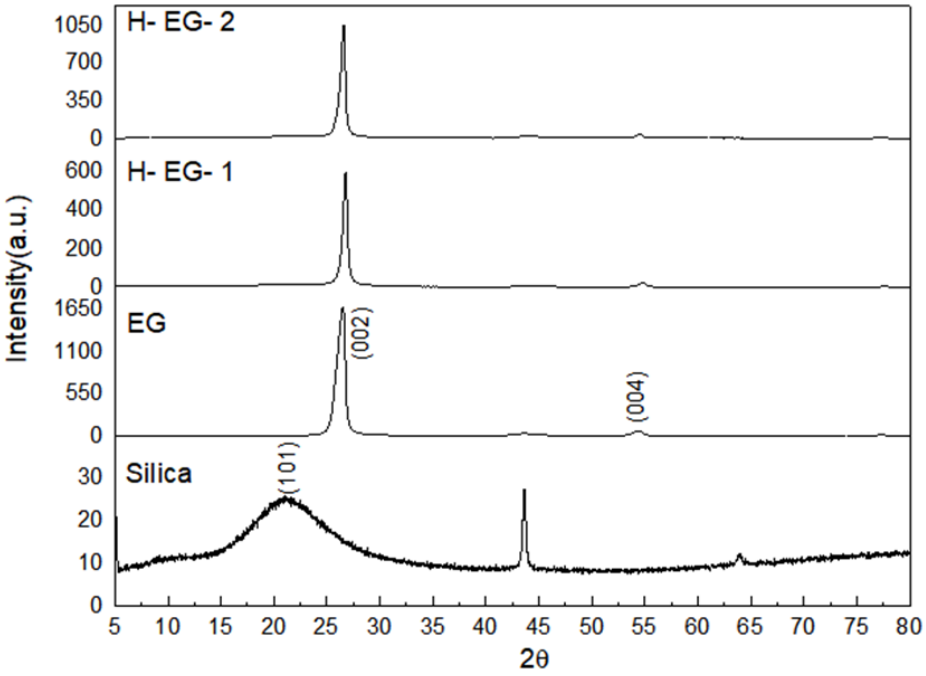

Figure 14. XRD spectra of silica, EG, H-EG-1 and H-EG-2.

Table 11. Crystallinity results received from XRD characterization.

Sample name	Crystallinity (%)	Amorphous (%)
Silica	58.7	41.3
Silica: APTES=1:2	38.2	61.8
EG	89	11
H-EG-1	70.6	29.4
H-EG-2	68.7	31.3

Figure 15 exhibits Raman spectra of silica, EG, H-EG-1 and H-EG-2. Three diffraction peaks were appeared in the Raman spectrum of EG. The sharp and strong G-peak seen at around 1579 cm^{-1}, the weak D-peak at 1350 cm^{-1} and the 2D band (the overtone of the D band) at 2700 cm^{-1} are indications of the graphitic carbon nature of EG. All three characteristic peaks known as D, G and 2D belonging to EG are also seen in the Raman spectra of H-EG-1 and H-EG-2 with slight up-shifts compared to the peak positions of EG due to the impregnation of the silica particles and chemical doping on the surface of EG [77]. There is no Raman peak attributed to silica. As carbon content of the hybrid additives increased (from H-EG-1 to H-EG-2), the intensity of D peak decreased indicating the reduction of disorderness in the lattice [78]. Furthermore, as shown in Table 12, the relative intensity (I_D/I_G) of H-EG-2 is calculated as 0.52 which is less than the

I_D/I_G ratios of H-EG-1 with 0.68 and neat EG with 0.61. This can be an indication of an increase in the order of the structure [72].

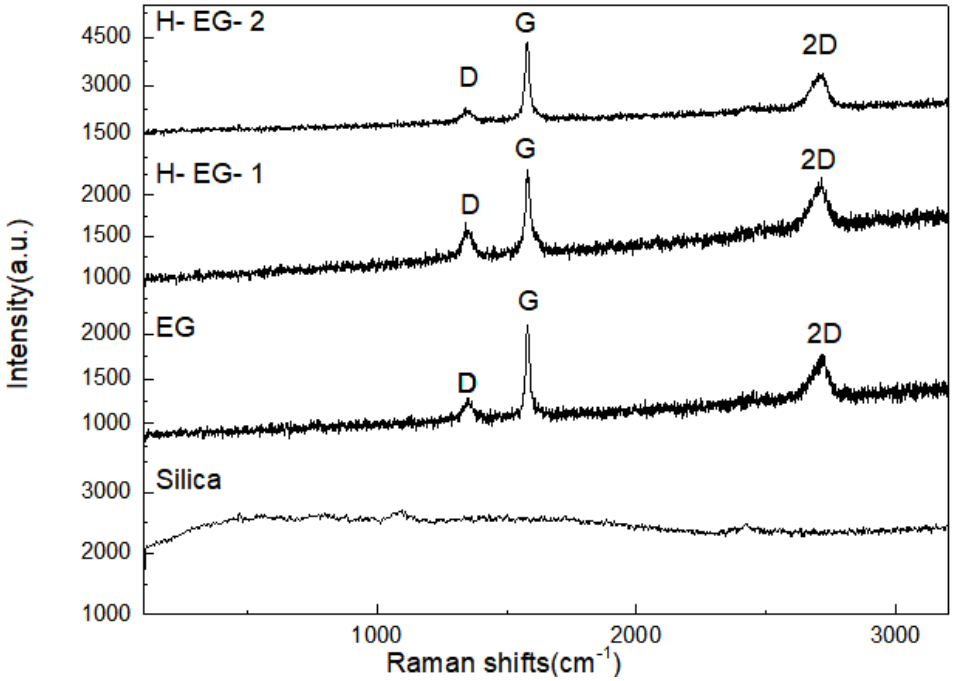

Figure 15. Raman spectra of silica, EG, H-EG-1 and H-EG- 2.

Table 12. Raman peak intensities and I_D/I_G ratios of EG, H-EG-1 and H-EG-2.

Sample Names	**D peak Intensity (a.u.)**	**G peak Intensity (a.u.)**	**2D Peak Intensity (a.u.)**	**I_D/I_G**
EG	1291.6	2108	1779	0.61
H-EG-1	1585.8	2309.4	2222.6	0.68
H-EG-2	2291.5	4364.1	3383.5	0.52

3.3.2. Thermal degradation behaviors of neat and silica modified EG hybrid additives

TGA was conducted in order to investigate the thermal stability and evaluate the functional groups of the developed EG-based hybrid additives. Figure 16 shows the TGA curves of silica, Silica:APTES=1,2, EG, H-EG-1 and H-EG-2. As seen in TGA curves, there is enormous decrease in the degradation profile with the functionalization of silica with APTES. After grafting the surface of EG with functionalized silica, degradation profiles of both hybrid additives become more thermally stable compared to functionalized silica, showing the successful bonding. Hybrid additives of H-EG-1 and

H-EG-2 have approximately 3% and 5% weight loss, respectively, at 1000°C. This alteration in weight loss comes from the differences in carbon and silica ratio since H-EG-1 contains high silica amount and thus shows better thermal stability than H-EG-2.

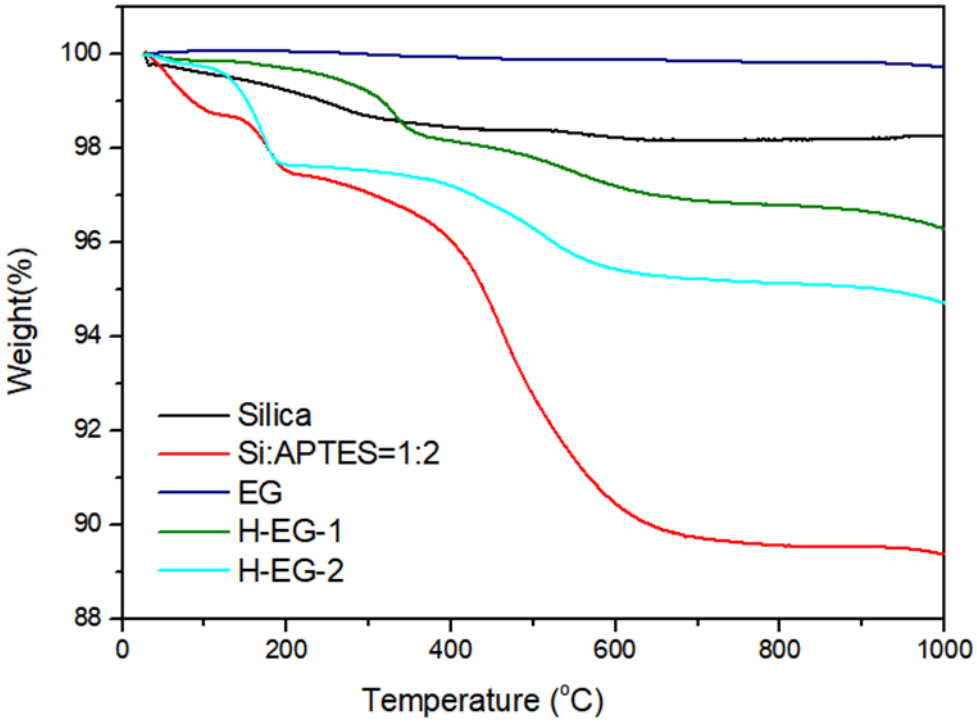

Figure 16. TGA curves of silica, Silica:APTES=1:2, EG, H-EG-1 and H-EG- 2.

3.3.3. Morphological Properties of Neat and Hybrid Additives

Figure 17 represents SEM images of neat EG, neat silica, H-EG-1 (low carbon content) and H-EG-2 (high carbon content). SEM image of neat EG in Figure 17a has sharp, rigid and stacked layers. SEM image in Figure 17b shows the randomly distributed of amorphous SiO_2 particles. After the hybridization of EG with functionalized silica with the ratios of fSi:EG=1:1 and fSi:EG=1:5 as seen in in Figure 17c and 17d, both silica particles and rigid EG structures are observed clearly. Especially, high moiety of silica particles is seen in Figure 17c due to the presence of high amount of fSi. To conclude, the morphological studies revealed that the silica particles were attached to the surface of EG with the help of silane-based coupling agents.

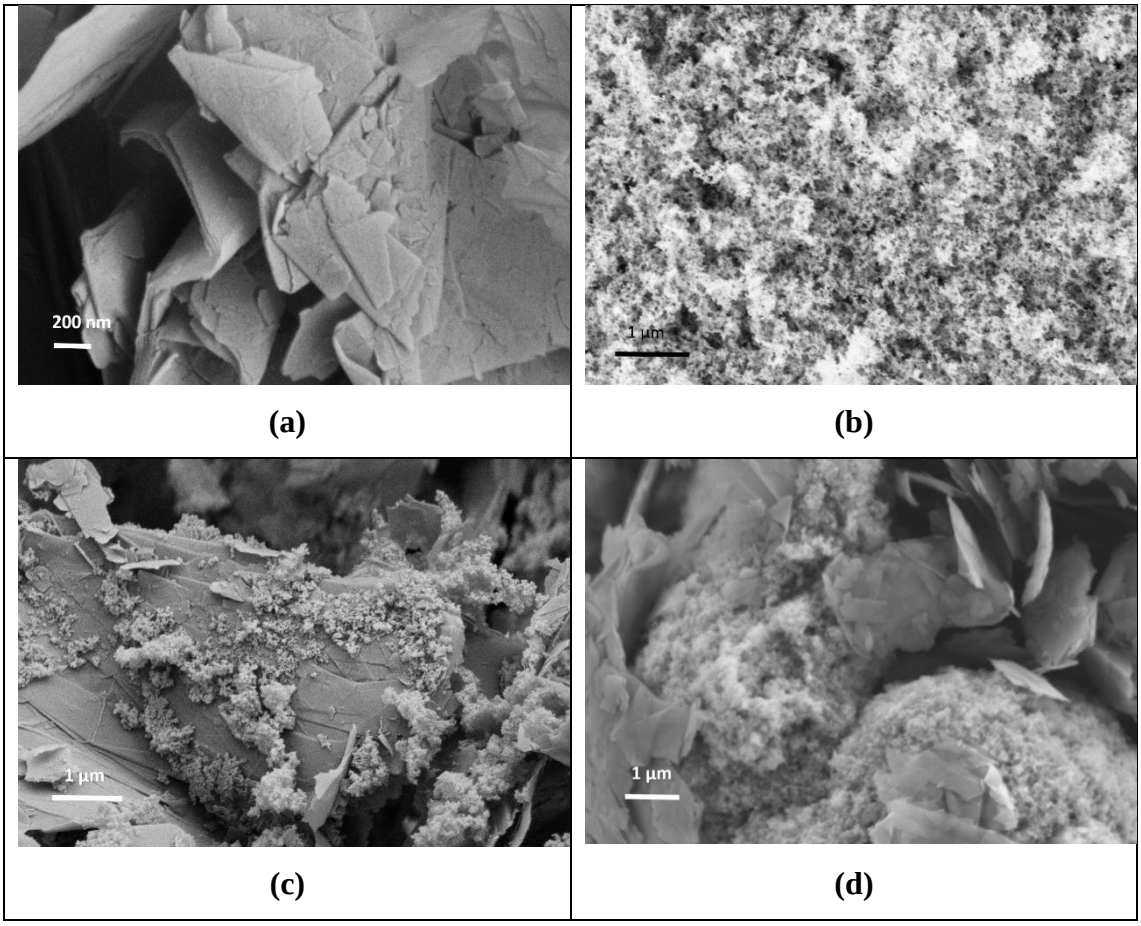

Figure 17. SEM images of (a) neat EG (b) neat silica (c) fSi:EG=1:1 and (d) fSi:EG=1:5 hybrid additives.

3.3.4. Thermal Conductivity and Rheological Behaviors of Silica-EG hybrid Additive Grout Composites

The results of thermal conductivity measurements of neat and grout samples having silica-EG hybrid additives with the loadings of 3 wt% and 5 wt% are presented in Table 13. The flowability tests, the bleeding tests and the density measurements of neat and grout samples conducted in fresh condition are also given in the same table. The developed thermally enhanced grouts consist of cement, two silica sands with different particle size distribution curves, bentonite, superplasticizer and two newly developed hybrid additives. The thermal conductivity of a cementitious grout produced with the same materials but with no additive (the reference grout) was measured as 2.373 W/mK (Test 1). Addition of 3 wt% of H-EG-1 into the reference grout mix increased the water demand from 650 g to 750 g and as a result decreased the thermal conductivity from 2.373 W/mK to 2.175 W/mK. To examine the effect of water content on thermal conductivity, in Test 3, the amount of water was reduced from 750 to 730 g, while contents of the other

components kept constant. The result of thermal conductivity measurement showed slightly higher value (2.429 W/mK) compared to the result of test 2 (2.175 W/mK). In comparison of Test 2 and Test 3, as the water content was decreased by 2.66%, the result of thermal conductivity showed an increase by 9.34%. This implies that in cementitious grout composite, increasing the water content decreases the thermal conductivity. To solve the issue and improve the thermal conductivity effectively, the fSi/EG ratio in the hybrid additive structure was changed from 1:1 in H-EG-1 to 1:5 in H-EG-2, respectively, with the aim to increase the carbon content. In addition, in test 4, the content of the hybrid additive in the grout composition was increased from 3 w% to 5 w%. Even though the result of test 4 showed slightly higher water demand, the resulting thermal conductivity of the re-formulated grout increased to 2.656 W/mK with rheological properties in the accepted ranges. This improvement is attributed to the low water demand but of high EG content in the grout composition produced with H-EG-2.

Table 13. Thermal conductivity results of reference grout and with the addition of H-EG-1 and H-EG-2 in different loading percentages.

Test no	**Cement (g)**	**Silica Sand 30–35 AFS (g)**	**Silica Sand 60–70 AFS (g)**	**Bentonite (g)**	**Additive (g)**	**SP (g)**	**Water (g)**	**Marshcone (sec)**	**Flowtable (cm)**	**Bleeding (%)**	**Density (g/cm^3)**	**Thermal Conductivity (W/mK)**
1	930	900	900	10	0 Reference	18.6	650	77	26	0.49	2.1	2.373
2	930	900	900	10	27.9 (fSi:EG=1:1) H-EG-1 (3 wt%)	18.6	750	90	25	0.22	2.01	2.175
3	930	900	900	10	27.9 (fSi:EG=1:1) H-EG- 1 (3 wt%)	18.6	730	109	24	0.10	2.02	2.429
4	930	900	900	25	46.5 (fSi:EG=1:5) H-EG- 2 (5 wt%)	18.6	735	103	30.3	1.7	1.95	2.656

3.4. Conclusions

In the present study, the enhancement of the thermal conductivity of the cement-based grouts used in shallow geothermal energy systems was carried out by the development of surface chemistry controlled expanded graphite (EG) based hybrid additives. For functionalization process, APTES as a silane coupling agent with amino functional groups was attached to silica surface in order to make suitable bridges with EG surface. Then, hybridization study was carried out to develop two kinds of EG based additives by controlling fSi ratio in order to monitor the influence of carbon content on the formulated grout mixtures and facilitate their dispersion in aqueous media. XPS characterization confirmed the changes in Si and C ratios on the surface of hybrid structures. C atomic percentages of H-EG-1 and H-EG-2 were measured as 50.5 and 88.2, respectively. In addition, crystallinity degree of EG based hybrids was decreased by the addition of amorphous silica. Afterwards, the incorporation of the silica/EG hybrid additives in the grout mix with optimized water demand enhanced the thermal conductivity noticeably compared to that in the reference grout. The result of thermal conductivity measurement of the grout mix developed with addition of 5 wt% silica/EG hybrid additive (H-EG-2) showed the highest thermal conductivity value of 2.656 W/mK. The effect of water content was also assessed for highlighting the strong influence on thermal conductivity of the grout composites. In other words, by changing the fSi/EG ratio in the hybrid additive structure from 1:1 to 1:5, the water demand decreased to such extent that by increasing the additive loading in the grout mix from 3% to 5%, the water demand was increased only by less than 1%. Consequently, the thermal conductivity showed a noticeable increase of approximately 12%. The increase in the thermal conductivity was attributed to the increase in the EG content in the hybrid additive structure as well as the increase in the additive loading in the grout composition but without considerable increase in the water demand. Consequently, the modification of EG provides carries significant importance on the performance enhancement of bentonite-based grout mixtures and functionalization improves the interfacial interactions between grout constituents and thus resulting in the fabrication of high performance cement composites.

CHAPTER 4: Controlling the surface chemistry of SiO_2 decorated carbon nanosheets from waste rice husk ash by silanization and its effect on heat flow and hydration of cement-bentonite based grouts

RHA having porous structure having high amount of amorphous silica nanoparticles (4 nm) decorated on the surface of carbon nanosheets is a suitable and cheap candidate to be used as a grout additive. In this study, neat RHA and functionalized RHA (f-RHA) with three different loadings were successfully integrated into the cement-bentonite based grouts by adjusting water to cement ratio. Workability of grouts having RHA based additives was analyzed in terms of bleeding, density, flow spread and Marsh cone time. Also, this study showed the thermal and prolongation of hydration performances of the cementitious grout were enriched by successful attachment of amino-silane functional groups on RHA surface. Heat of hydration performance of RHA and functionalized RHA introduced cementitious grout composite was assessed by isothermal calorimetry tests and especially kinetics of hydration was increased by adding RHA. The presence of amino silane groups in f-RHA intensified the adsorption and resulted in the retardation and reduction in the heat flow. Therefore, using amino-silane coupling agent increased the induction period and hindered the heat of hydration compared to reference grout. On the other hand, incorporation of RHA and f-RHA into cement matrix did not affect thermal conductivity of the grouts.

4.1. Introduction

In the last decades, global demand for renewable energy technology is growing owing to the high population and economic growth. At this point, geothermal energy can make great contribution since it is a type of clean renewable energy which generates electricity by adjusting heating and cooling processes by using heat retained in the Earth [79]. Geothermal energy has numerous advantages unlike other renewable sources such as wind turbines and solar systems since it does not depend on the climatic changes and can be installed in small lands. In shallow geothermal energy systems, thermal conductivity is an important criterion to get high efficiency from the oil surrounding the borehole field. Especially cementitious grout surrounding the borehole plays an essential role for the preservation of the heat flow from ground to the pipes. However, variation in some of the properties of cementitious grout such as workability, flowability and thermal conductivity can decrease the performance of the system due to temperature loss during heat transfer. Therefore, many studies have been focused on the performance enhancement of

cementitious composites by the incorporation of carbon based additive materials obtained from virgin and recycled sources [80, 81].

Rice husk as a raw biomass has also taken great attention of the researchers due to its being one of the major wastes of the world [82], and having high concentration of silica and organic components and this makes it suitable source to convert into value-added carbonaceous products [83]. With the proper heat treatment/calcination, rice husk can be recycled into rice husk ash (RHA) which is a highly porous material containing high amount of amorphous silica and also carries a significant potential for the fabrication of carbon based nanomaterials [84, 85]. For instance, Wang et al. produced large scale and controllable graphene quantum dot (GQD) by first synthesizing sp^2 carbon flakes from rice husk by applying bottom-up technique and then subsequently converting carbon flakes to GQDs through hydrothermal reaction [86]. Moreover, Ismail et al. synthesized graphene from RHA in a cost-effective and ease manner by using potassium hydroxide and applied heat treatment at 800^{o}C [87]. On the other hand, RHA acting as an additive or an adsorbent and catalyst carrier can be utilized in various composites structures consisting of rubbery, plastics and cements, and also in the concrete due to the presence of phases such as SiO_2, Al_2O_3 and others [88–90].

RHA contains significant amount of SiO_2 (≥90%) that enhances the mechanical property of cement mixture by improving the rate of hydration [91, 92]. In one of the work, Hamzeh *et al.* used white rice husk ash (WRHA) as an reinforcing agent in cement composites and showed that water absorption and bulk density of the prepared composites were significantly reduced [93]. Gastaldini et al. focused on the performance of electrical resistivity and compressive strength of concrete mixes by partially replacing RHA with cement and found that high amount of RHA addition led to the reduction in the electrical conductivity and compressive strength of concrete mixes [94, 95]. Up to now, the previous studies are mostly on the replacement of RHA with cement in order to decrease the content of cement used in the grout composition to minimize the environmental impact and provide economic advantage [96]. In addition to the mechanical effect of RHA in the cementitious composites, providing homogeneous dispersion of RHA in the matrix has been considered to optimize the proper grout with the desired properties such as viscosity, flowability and pumpability. High quality distribution also affects water to cement ratio and thus thermal properties of grout mix.

The integration of RHA considerably increases the viscosity of the grout composition, thus affects the flowability and pumpability of the grout in a negative manner. In order to

control these properties, additional superplasticizer is required to reformulate the grout and get similar workability compared to grout without RHA but this results in the increase in the total cost of operation [95]. Therefore, surface treatment of RHA is needed to overcome high-water demand and adjust the hydrophilicity. Herein, silane coupling agents are widely used as a surface treatment modifier since they are able to connect organic and inorganic compounds to each other by making bridges with their hydrolyzable and functional groups. Silane coupling agents are highly active chemicals especially under alkaline aqueous conditions which is general environment in cementitious material such as of concrete, mortar, and grout [97]. In one of the studies, Minet et al. intercalated organic groups in calcium silicate hydrates (C–S–H) layers by coprecipitation of organotrialkoxysilanes and tetra-ethoxysilane (TEOS) mixtures with $CaCl_2$ in alkali media [98]. In another work, Franceschini et al. prepared covalently bonded polymer- C-S-H composite with the formation of covalent linkages between polymer and C–S–H phases by grafting trialkoxysilane and/or methyldialkoxysilane to the polymer chains [99]. To the best of our knowledge, there is no study to activate RHA surface by silanization. It is known that the adjustment of surface composition of RHA based additives used in the preparation of grout mixes can change the water demand and it is possible to attain high performance grouts. Furthermore, there is no detailed work for understanding the interfacial interactions of SiO_2 particles inside RHA structure with the cement matrix since this type of resource is getting importance in terms of sustainability and circular economy.

In our previous studies, thermal conductivity properties of cementitious grout were improved by the incorporation of graphene nanoplatelet/silica and expanded graphite/silica additives in which carbon materials were connected to silica in the presence of silane coupling agents [8, 9]. In the present study, a different understanding was provided by the utilization of SiO_2 decorated carbon sheets that was directly obtained by the calcination of rice husk to be used as an additive in cement compositions, and surface silanization was applied and the surface of amino functional groups were attached on the surface of RHA to activate silica particles. The covalent attachment of RHA to inorganic C–S–H via APTES can enhance the stability of particles during grout mixing and thus prevent the aggregation by monitoring the rheological properties and fluidity of grouts [37, 100]. Comprehensive characterization was carried out to investigate the chemical composition and structural changes of these functionalized RHA samples. Then,

these developed additives were integrated into cement-bentonite based grouts with different loadings and the effect of amino surface functional groups and w/c on workability and the heat of hydration was studied systematically.

4.2. Materials and Methods

4.2.1. Materials

Rice husk ash with the average particle size of 174 nm and bulk density of 0.1-0.3 g/cc in the form of black powder was collected from Valencia, Spain. 3-Aminopropyl triethoxysilane (APTES, 50825) was purchased by Momentive, Germany. Acetic acid (100% Anhydrous) was purchased from Isolab, Germany. For grout composites, Portland cement: CEM I 42.5 R was obtained from Cimsa, Turkey and as aggregates, two types of silica sands (B55 and B20) were selected based on the particle size distribution and purchased from Baskarp Co., Sweden. Superplasticizer was purchased from Sika, Turkey and bentonite was obtained from Canbensan Bentonite, Turkey.

4.2.2. Functionalization of rice husk ash by silane coupling agent

In order to tailor the surface composition of RHA, silanization was performed to increase the interactions between carbon additive and constituents in grout mixes. Surface functionalization with APTES at ratio of 1:1 was performed by dispersing 1g of RHA in 50 ml distilled water via Handheld Ultrasonic Homogenizer from Hielscher Ultrasonics at room temperature. Then, 1 ml APTES as a silane coupling agent was added into the mixture to functionalize the surface of RHA. The pH level of solution was adjusted to 5.5 by the addition of acetic acid. The solution was poured into the round bottom flask and refluxed overnight at 80°C. After 24 h, filtration was performed by washing with water twice and dried 24 h in oven.

As shown in Figure 18, APTES as silane coupling agent possesses hydrolysis processes under alkaline condition and turns into “-OH” hydroxyl groups, which attach at the end and in the middle of calcium silicate hydrate (C–S–H) chains [98]. Remaining organofunctional NH_2 group is then forms a covalent bond with the surface of RHA.

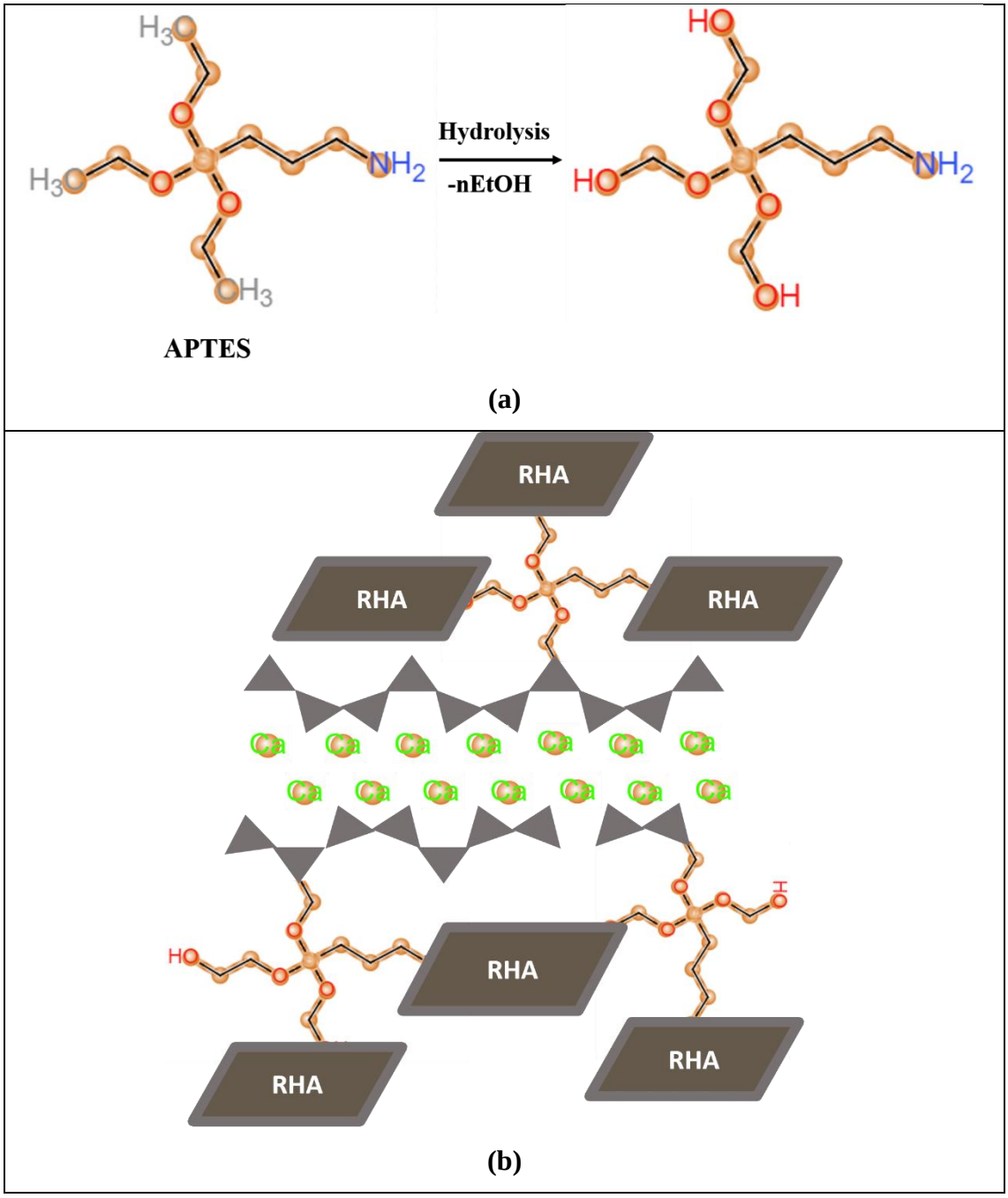

Figure 18. Schematic representations of (a) the hydrolysis of APTES and (b) the connection of APTES functionalized RHA to the chains of C–S–H via condensation reaction.

4.2.3. Cementitious grout composition and mixing procedure

The cementitious grout samples were prepared by mixing Portland cement, aggregate, superplasticizer, vegetal silica (RHA) or functionalized vegetal silica (f-RHA) and water. The ratio of cement: aggregate was selected as 1:2 by weight to weight and 1 wt% of superplasticizer was added into cement mixture. Then, RHA or f-RHA was added by 3

wt%, 5 wt% and 10 wt% into the mix. Table 14 summarizes composition of cementitious grout with neat RHA and f-RHA.

Table 14. Composition of cement-bentonite based grouts with neat RHA and f-RHA.

	Control	**Neat RHA**			**f-RHA**		
Sample Name	**C0**	**RHA3**	**RHA5**	**RHA10**	**f-RHA3**	**f-RHA5**	**f-RHA10**
RHA (wt%)	0	3	5	10	3	5	10
Cement (g)	930	930	930	930	930	930	930
Silica Sand 1 (g) B20	900	900	900	900	900	900	900
Silica Sand 2 (g) B55	900	900	900	900	900	900	900
Bentonite (g)	10	10	10	10	10	10	10
RHA (g)	-	27.9	46.5	93	-	-	-
f-RHA (g)	-	-	-	-	27.9	46.5	93
Superplasticizer (g)	18.6	18.6	18.6	18.6	18.6	18.6	18.6
Water (g)	650	680	700	730	670	690	720

The cementitious grout samples were mixed by high shear VMA mixer with 60 mm dispersion disk (Dissolver Dispermat® LC). For mixing, the dry constituents of the grout (cement, RHA or f-RHA and sands) were pre-blended in a bag for 1 min. The required quantity of water and superplasticizer (refer Table 13) were added into the mixing bowl and then pre-blended grout mixture was added in the mixing bowl. Initially, grout was mixed for 1 min at 2000 rpm then increased the mixing speed up to 6000 rpm and performed the mixing for 3 min at this stage. The resultant material was casted and cured at 100% relative humidity and 20 °C for 7 days until thermal conductivity testing. Furthermore, the other properties of grouts such as rheology, density of grout mixes were evaluated using marsh cone test, flow spread testing and mud balance testing, respectively. Further details regarding the preparation and testing for cementitious grout composites can be found in our previous studies [8, 9].

4.2.4. Characterization

Thermogravimetric analysis (TGA) was carried out on Mettler Toledo thermal analyzer (TGA/DSC 3+) over the temperature range of 25 °C to 1000 °C at a heating rate of 10K/min under nitrogen. Raman spectra of neat and functionalized RHA samples were monitored using Renishaw inVia Raman Microscope to investigate the structural properties of carbonaceous materials in RHA. Chemical composition of the produced samples was investigated by X-ray Photoelectron Spectroscopy (XPS). Particle size measurement was performed by Anton Paar Litesizer 500. In order to determine the crystallinity of various RHA samples, X-ray diffraction (XRD) tests were carried out from 2θ= 5° to 80° by Bruker D2 PHASER Desktop with a CuKα radiation source. The morphology and composition of the samples were examined using a Leo Supra 35VP field emission scanning electron microscope (SEM) and JEOL JEM-ARM200CFEG UHR- transmission electron microscopy (TEM).

Thermal conductivity performance of unmodified and modified RHA included cementitious grout composites were measured by using hot disk thermal constants analyzer, TPS 2500 S. Specimens with the diameter of 40 mm and the height of 20 mm were molded and cured at 100% relative humidity and 20 °C for evaluation of thermal conductivity.

The heat flow and cumulative heat evolved due to the hydration of each sample were determined under isothermal conditions at 20 ± 1 °C by an eight-channel conduction calorimeter (Tam Air TA Instruments, New Castle-USA) in accordance with SS-EN 196-11 : 2019 [101]. Prior to mixing, all materials were maintained at 20 ± 1 °C for 24 h. The samples for RHA and f-RHA were prepared by adding 3 wt%, 5 wt% and 10 wt% RHA or f-RHA in the neat cement. The process of mixing was performed manually in a glass beaker, with the aid of a glass rod at 0.7 w/c. Ampoules were filled with 7 g of paste and they were instantaneously placed into the isothermal calorimeter channel for measuring the heat of hydration at the relative temperature. The entire process took less than 5 min and data were recorded for a total of 45 h.

4.3. Results and Discussion

4.3.1. Structural, thermal and morphological properties of neat and functionalized rice husk ash

In order to increase the quality and estimate the potential of RHA in the cement industry, comprehensive characterization analyses were conducted to understand the structural properties of RHA, and silanization was applied to change the surface composition of RHA and increase its interactions with the cement components. At the first stage, neat RHA was functionalized by APTES used as a silane coupling agent by following hydrolysis and condenstation reactions. In order to monitor the differences before and after silanization on the morphological properties of RHA, microscopic studies were performed. Figure 19 shows SEM images of neat and functionalized RHA samples at different magnifications. As seen in SEM images, both samples have porous structures and the presence of silica particles are seen clearly. After funtionalization, there was no significant change on the surface properties of RHA but more porous structure was detected in some regions. Therefore, TEM characterization was conducted for neat RHA to observe silica particle distribution and estimate the particle size. Figure 20 represents TEM images of neat RHA. The results indicated that silica particles with the average particle size of 4 nm were homogeneously placed on the surface of carbon sheets with the average length of 36 nm.

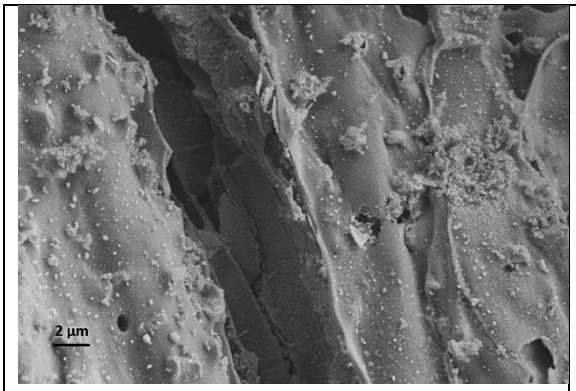

(a)

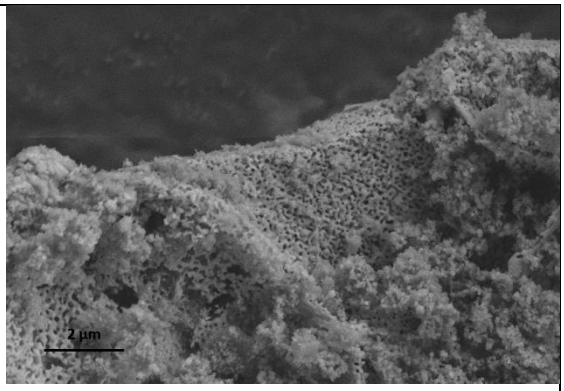

(b)

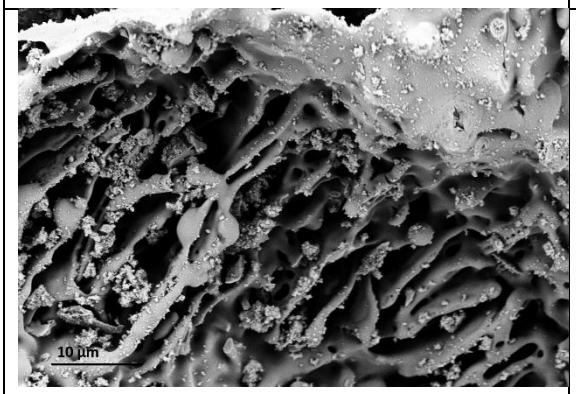

(c)

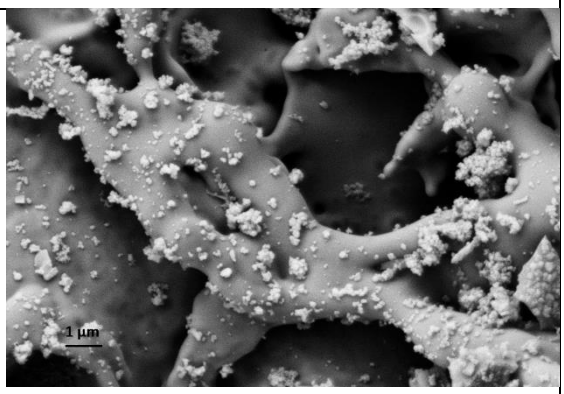

(d)

Figure 19. SEM images of (a) and (b) RHA, and (c) and (b) f-RHA at different magnifications.

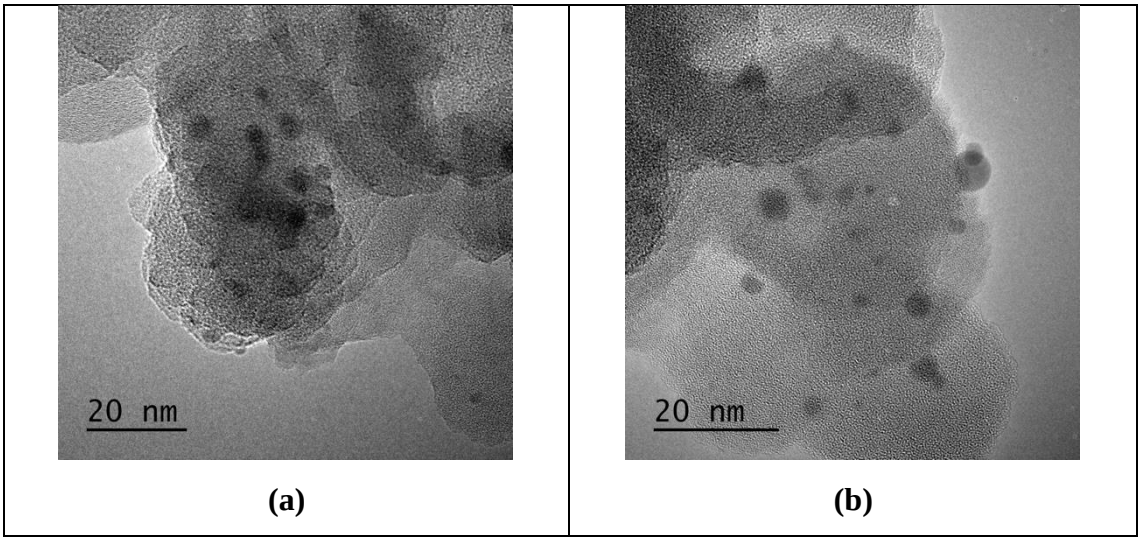

Figure 20. (a) and (b) TEM images of neat RHA.

In order to identify the functional groups of RHA and functionalized RHA samples, XPS characterization was conducted and C1s, O1s, and N1s signals were measured and the related groups were defined regarding their binding energy of carbon atoms [102]. The XPS peaks of C1s, O1s, and N1s for neat RHA and f-RHA were provided in the XPS survey scan spectra, Figure 21. C1s spectra of RHA and f-RHA in Figure 21b shows a peak at around 284 eV that can be attributed to the C-C bond, while O1s spectra in Figure 21c shows a peak at around 532 eV that can be allocated to the ethoxy group bond O-C [84]. In case of amine- functionalized RHA, both peaks show a slight decrease in the intensity. The C/O ratios of neat RHA and f-RHA were 0.80 and 0.67, respectively.

Table 15 summarizes XPS results of neat and f-RHA samples. As seen in the table, 1.53 at% of nitrogen was measured in f-RHA due to the attachment of amino groups from APTES. Also, oxygen content was increased from 25.48 at% to 30.44 at% after functionalization. There is a decrease in carbon content due to an increase in oxygen moiety. On the other hand, silicon amount increased from 5.88 at% to 8.15 at% and this increase in silicon amount was expected due to the attachement of silane groups during functionalization. Therefore, XPS analysis confirmed the successful incorporation of amino groups on the surface of RHA.

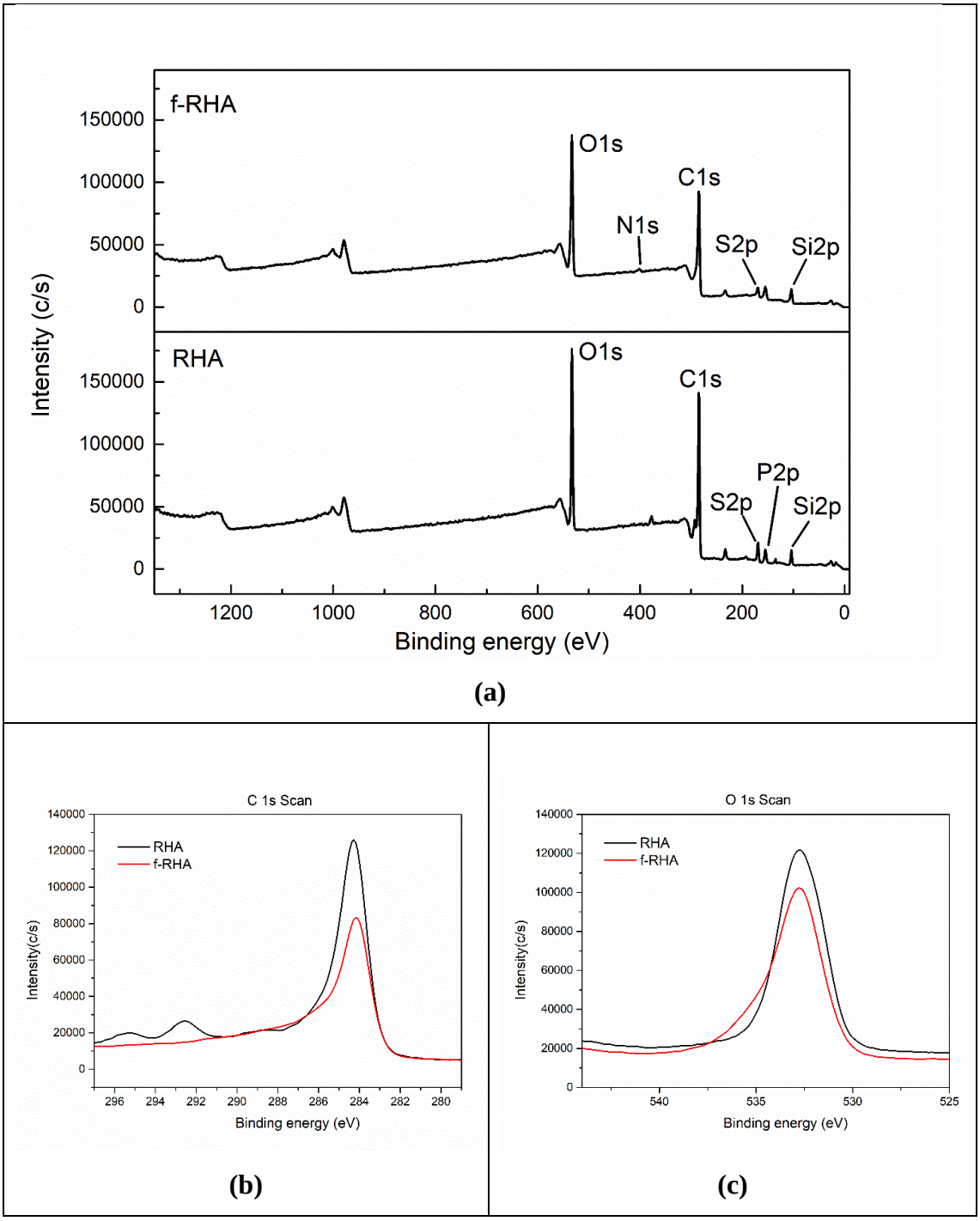

Figure 21. (a) XPS survey scan spectra, (b) C1s spectra and (c) O1s spectra of RHA and f-RHA.

Table 15. XPS results of RHA and f-RHA samples in terms of atomic percentages.

Sample Name	**Carbon (at%)**	**Oxygen (at%)**	**Silicon (at%)**	**Nitrogen (at%)**	**Sulphur (at%)**	**Others (at%)**
RHA	62.81	25.48	5.88	-	3.52	2.31
f-RHA	57.46	30.44	8.15	1.53	2.42	-

In order to examine the structural changes in functionalized RHA, Raman spectroscopy was used to investigate the properties of carbonaceous structure in RHA and Raman spectra of the samples are given in Figure 22. There are two main peaks appeared at around 1343 cm^{-1} and 1586 cm^{-1} attributed to D and G peaks, respectively. D peak attributes the degree of defects in the structure while G peak indicates the vibrational mode of sp^2 in carboneceous materials [8]. The structural changes were compared by taking into consideration the intensity ratios of the D and G bands (I_D/I_G). As shown in Table 16, I_D/I_G values of neat and f-RHA were calculated as 0.92 and 0.93, respectively. This change stems from an increase in surface amino functional groups due to chemical treatment and thus the successful functionalization is verified by structural characterization.

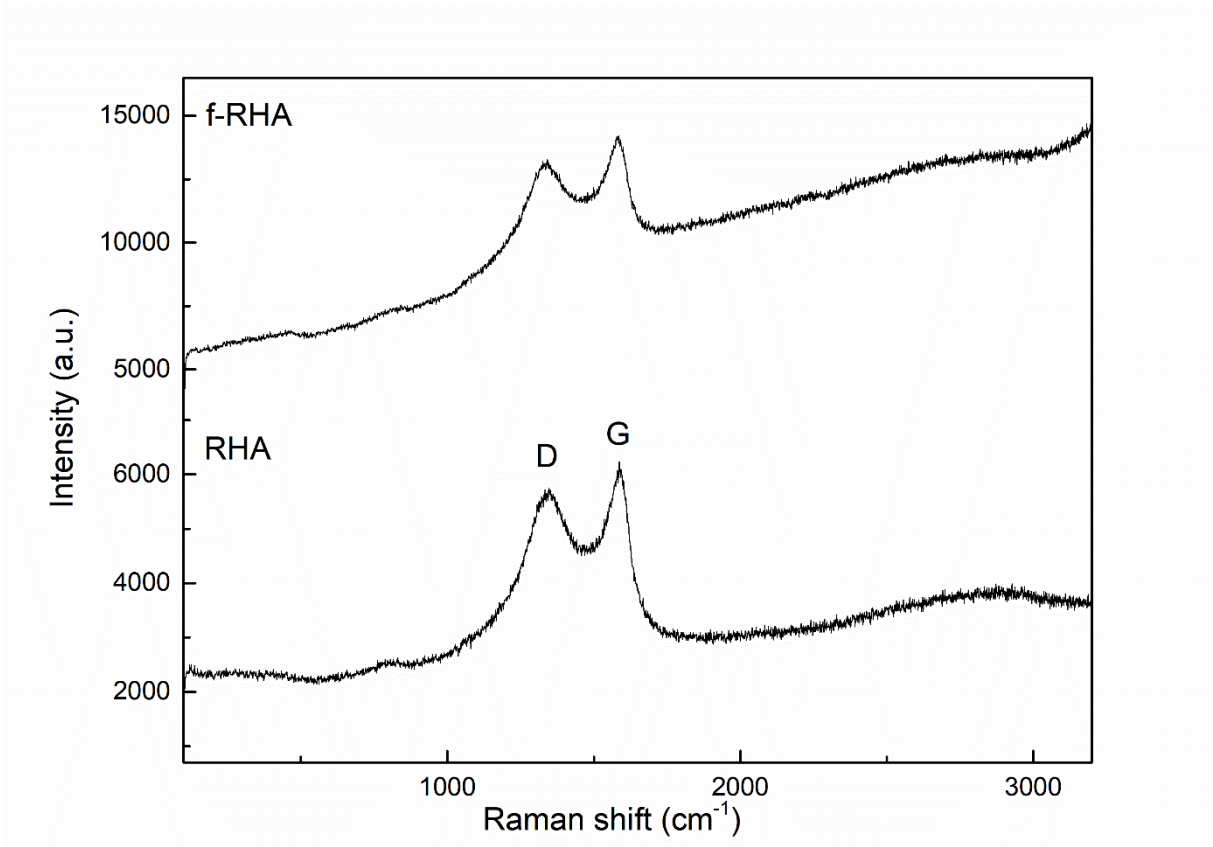

Figure 22. Raman spectra of RHA and f-RHA.

Table 16. Summary of Raman peak intensities and I_D/I_G ratios of RHA and f-RHA.

	D intensity (a.u.)	**G intensity (a.u.)**	**I_D/I_G**
RHA	5746.9	6233.9	0.92

f-RHA	13273.4	14206.3	0.93

Figure 23 shows XRD patterns of RHA and functionalized RHA. Unmodified RHA shows high crystalline cristobalite (Cr) peak at 2θ=22° hkl (004) and 2θ= 36.3° hkl (040) and a small Quartz's (Q) peak at 2θ= 21.1° hkl (220) [15]. Also, there is a broad peak between 2θ=20-30º overlapped with Cr peak indicating the presence of carbon and silica in the structure. After the modification by APTES, the peak at around 2θ= 28.62º belonging to Q was disappeared and the intensity of Cr peak increased in XRD pattern of f-RHA and thus crystallinity of RHA was slightly increased.

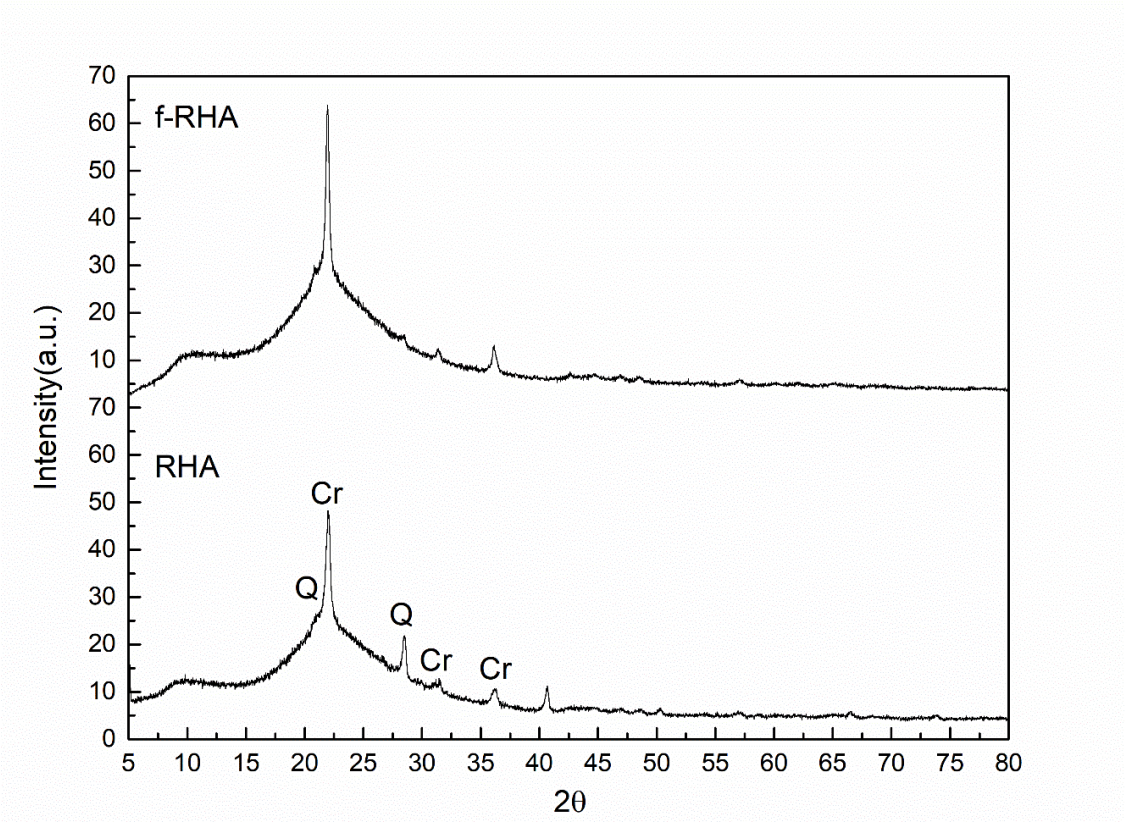

Figure 23. XRD patterns of RHA and f-RHA (Cr and Q signs in the XRD spectra of RHA represent cristobalite and Quartz peaks respectively [103–105]).

In addition, thermal degradation behaviors of neat and functionalized RHA samples were investigated by TGA. Figure 24 depicts neat RHA and f-RHA samples. Neat RHA showed higher thermal stability until 1000 °C and there was only 4.58% weight loss in the structure. After functionalization, the weight loss is around 3.73%. There is a slight difference in the degradation curves of neat and functionalized RHA samples. To conclude, the surface of RHA was treated by silane-based agents successfully and the

presence of functional groups were confirmed by spectroscopic and gravimetric techniques.

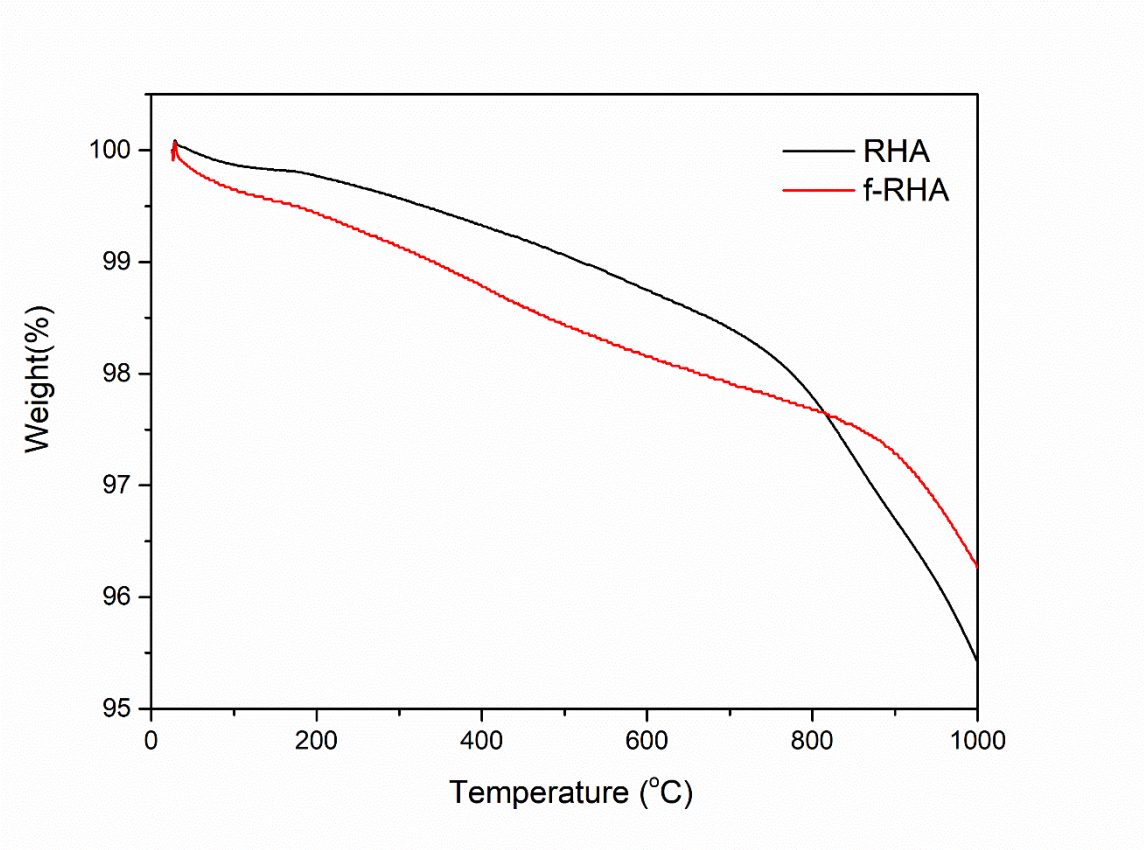

Figure 24. TGA curves of neat RHA and f-RHA samples

4.3.2. The characteristic properties of grout mixtures

After the preparation of f-RHA samples, grouts having neat RHA and f-RHA were produced at the loadings of 3 wt%, 5 wt% and 10 wt%. Marsh cone flow time, mini slump flow diameter, density, bleeding of grout samples and their thermal conductivity results are shown in Table 17. The properties of grouts were characterized by comparing workability, thermal conductivity and heat of hydration results.

Table 17. Benchmark and experimental properties of grouts containing RHA and f-RHA.

	Benchmark	Control	Neat RHA			f-RHA		
Sample Name		**C0**	**RHA3**	**RHA5**	**RHA10**	**f-RHA3**	**f-RHA5**	**f-RHA10**
Vegetal silica (wt%)		0	3	5	10	3	5	10
Water to cement ratio		0.70	0.73	0.75	0.78	0.72	0.74	0.77
Marsh cone time (sec)	100-120	98	83	83	96	113	99	106
Flow spread (cm)	23-28 cm	24	26	28	27	25	25	25
Bleeding (%)	<2%	0.5	0.6	0.6	0.6	0.3	0.3	0.2
Density (g/cc)	>1.3	2.10	2.09	2.07	2.05	2.11	2.08	2.04
Thermal conductivity (W/mK)		1.80	1.85	1.88	1.52	1.78	1.75	1.55

4.3.3. The workability properties of grout mixtures

The workability properties such as marsh cone time and flow were maintained in the benchmark range by adjusting water to cement ratio. It was found that f-RHA grout samples require less water to achieve similar workability of RHA grout samples. This comes from the functionalization with APTES leading to the enhancement of the wettability of RHA by water and thus an increase in the workability of the grout [106].

Deformability and fluidity (workability properties) of the grout mixtures are examined and Figure 25a and 25b represents the curves of Mini slum flow and marsh cone flow as a function of RHA amount. According to Figure 25a, for moderate addition of RHA (3 wt% and 5 wt%), slump flow was increased with the amount of RHA in the grout. However, slump flow was reduced at 10 wt% RHA addition. On the other hand, for f-RHA, slump flow was stayed constant at all the dosages. Similar behavior was monitored in the marsh cone testing. As shown in Figure 25b, for moderate addition of RHA, marsh cone flow time was reduced and at the addition of 10 wt% RHA, marsh cone time was increased. Moreover, at the lower additions (3 wt% and 5 wt%), marsh cone time for RHA grout is lower when compared to f-RHA grout samples but at higher additions (10 wt%), both samples showed rise the marsh cone time. These results showed that at the addition of 10 wt%, both RHA and f-RHA have impacted on the viscosity and yield point of the grout in a similar magnitude. Including high percentage of RHA or f-RHA have reduced the fluidity of grout samples due to high water absorption capacity of RHA and f-RHA compared to Portland cement. Voids and channels in amorphous structure of RHA can cause more water uptake [107]. In addition, the density and total weight of cementitious materials were kept constant, and then the volume of the grout mixture was increased by the incorporation of RHA. An increase in volume of paste leads to an increase in plasticity and cohesiveness of grout mix that reduces overall fluidity of grout mix [108]. Therefore, high water to cement ratio was required to optimize the grout workability in the acceptable range.

The density values of each grout sample at different additions for RHA and f-RHA are given in Table 17. The density of grout samples was slightly decreased as RHA or f-RHA content increased in the grout mix. Both RHA and f-RHA have no significant effect on the wet density of cementitious grout. Finally, the dimensional stability of grout mixes is described by bleeding test, in which shrinkage of grout after 24 h is evaluated. It was found that all samples showed negligible shrinkage according to the defined technical

specs provided in benchmarking study (< 2%). Furthermore, f-RHA grout showed less shrinkage in comparison of RHA grout samples, which can be attributed to high water retention capacity of f-RHA due to the presence of amino-silane functional groups [106].

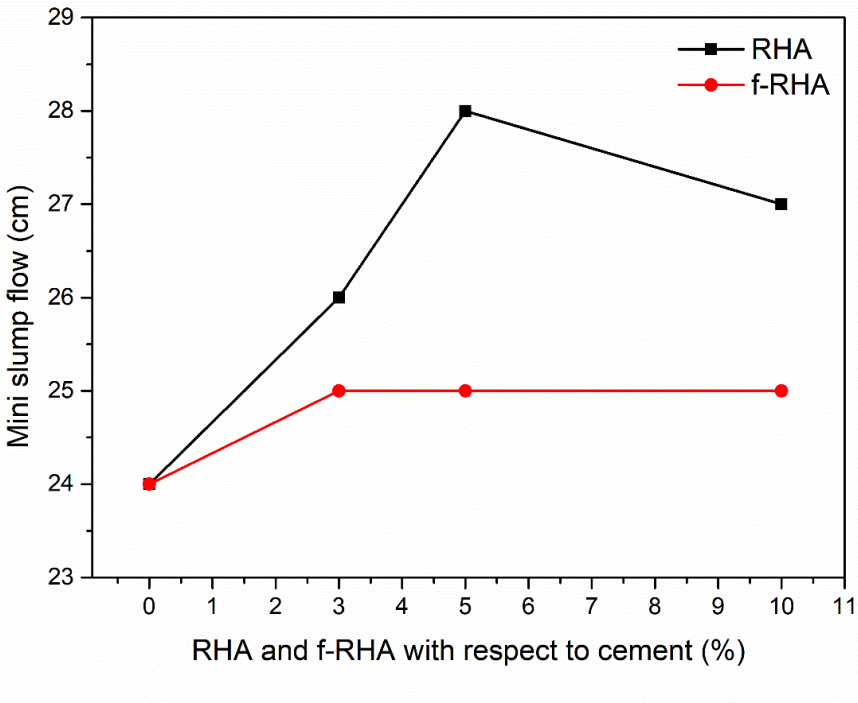

(a)

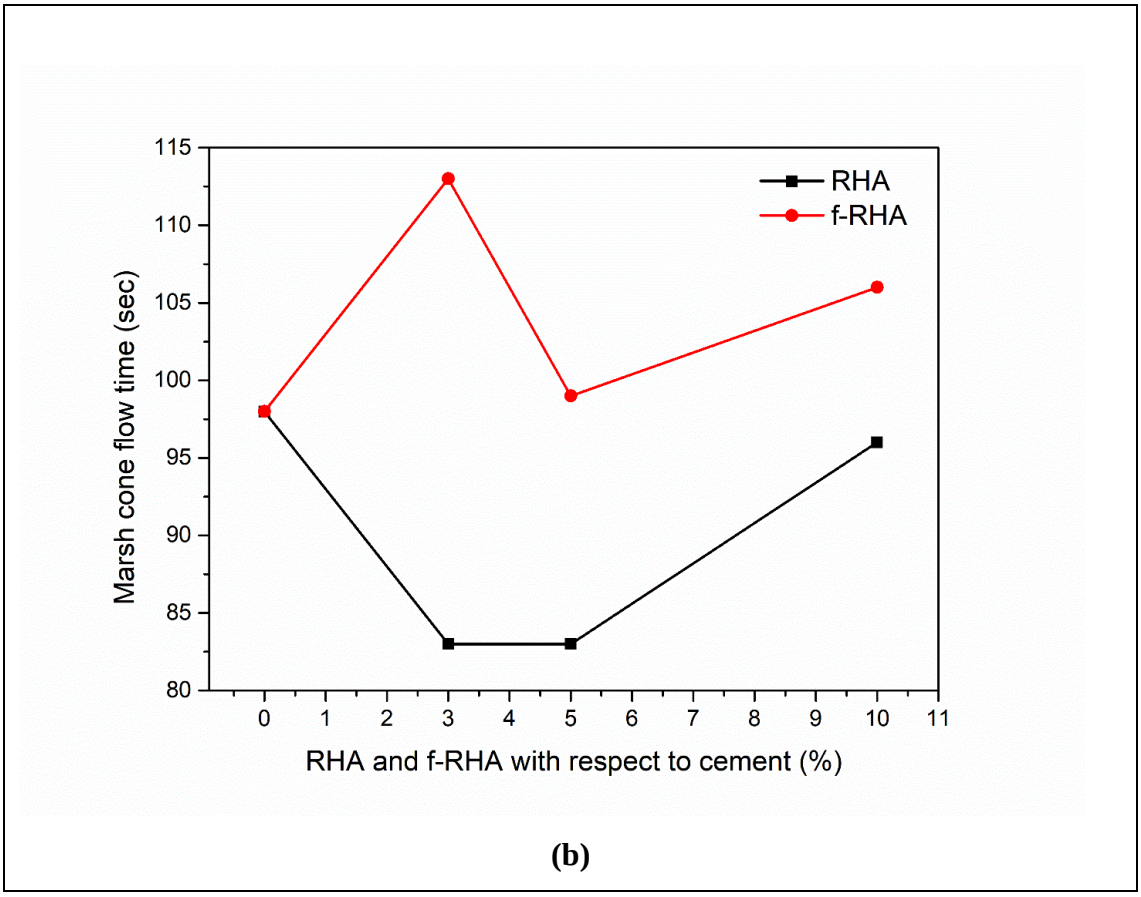

Figure 25. (a) Mini slum flow vs RHA and f-RHA amounts with respect to cement curves, and (b) Marsh cone flow time vs RHA and f-RHA amounts with respect to cement curves.

4.3.4. Thermal conductivity of rice husk ash-based grouts

The thermal conductivity results of grout composites having RHA and f-RHA with three different loadings are presented in Figure 26. The thermal conductivity of reference grout was measured as 1.80 W/mK. After the integration of 3 wt% and 5 wt% RHA, there was a slight increase in thermal conductivity. However, as RHA amount reached to 10 wt%, thermal conductivity has started to decrease. This showed that 5% is the optimum loading of RHA to achieve maximum thermal conductivity of the grout. On the other hand, there is a decrease trend in thermal conductivity of grouts having f-RHA. At the loading of 10 wt% f-RHA, a sharp loss in thermal conductivity was detected which was consistent with 10 wt% RHA based grout. This also supports that there is a direct relation between thermal conductivity and the amount of water uptake in the grout [8, 9]. Furthermore, f-RHA becomes more hydrophilic after the functionalization by APTES and retains more water during the hydration of grout. In other words, since available water content has

adverse effect on the thermal conductivity, the integration of RHA, which has tendency to retain the water in the grout, leads to lower thermal conductivity [109]. In case of neat RHA, extra water was required during grout mixing which was retain during hydration of grout. Furthermore, the thermal conductivity can be reduced due to accessible porosities and lower density microstructure of grout caused by the addition of RHA or f-RHA [110]. Consequently, both neat RHA and f-RHA do not cause significant improvement in thermal conductivity of bentonite-cement based grouts but change the viscosity profiles of grouts due to the differences in water uptake.

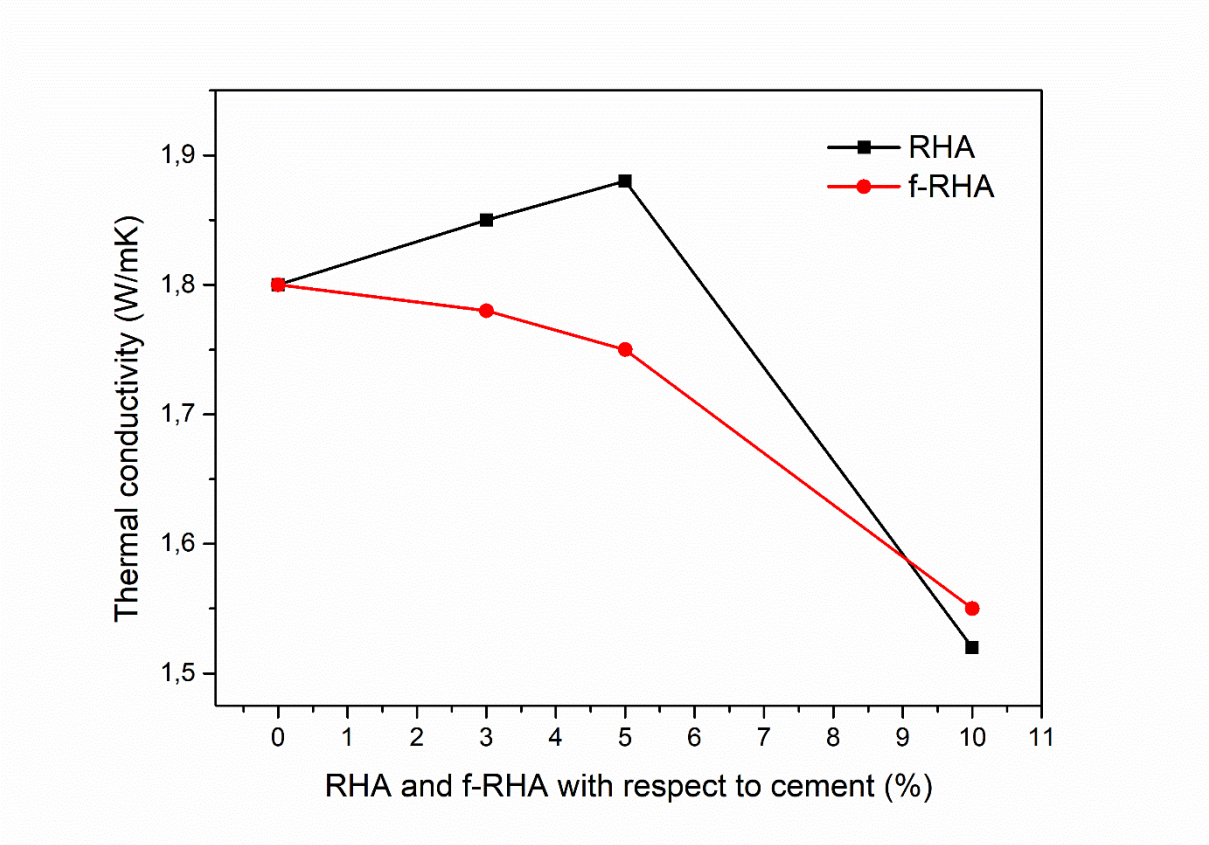

Figure 26. Thermal conductivity of grout containing RHA and f-RHA samples at different loadings.

4.3.5. The effects of RHA on heat of hydration

When water is mixed with the constituents of grouts, an exothermic reaction occurs between cement and water and thus resulting in heat release [111]. The reaction proceeds in the different phases and depends on the cement type, composition, w/c and additives, the magnitude of heat release varies as a function of time. Measurement of the rate of heat evolution provides understanding on the rate of hydration of grout in the presence of RHA and f-RHA. Hydration heat release of each grout sample was estimated by using an

isothermal conduction calorimeter. To examine the effect of only RHA and f-RHA, other workability enhancing additives (superplasticizer and bentonite) were excluded from grout mix, and w/c = 0.7 was considered as an adjustable parameter. When water is mixed with the constituents of grouts, an exothermic reaction occurs that causes heat release [110]. In the beginning of the reaction, the rate of heat release can be as much as higher and then start to decrease in a gradual manner. Figure 27 and Figure 28 represent the heat flow and cumulative heat release of paste containing cement with RHA and f-RHA, respectively. In the heat flow curves (Figure 27a and Figure 28a), enlarged plots were displayed in the first 6 h of hydration in detail. The heat flow and heat for all the samples were normalized by using weight of cement. In heat flow curves, the first heat flow peak (Peak 1) is due to cement wetting (which was out of the scale in the graph), shows an induction period of low heat flow and an acceleration period and then the second peak called Peak 2 associates with the hydration of Ca_3SiO_5 (C_3S) [33]. In addition, the weak shoulder of Peak 2 is directly related to sulfate depletion and the reaction of $Ca_3Al_2O_6$ (C_3A) for the formation of ettringite due to the nucleation [112, 113].

Figure 27a indicates the heat flow evaluation of paste containing 3 wt%, 5 wt% and 10 wt% RHA compared to reference (0 wt% RHA). The calorimetric results indicated that the use of RHA in cement increase the kinetics of hydration compare to reference paste. In addition, the kinetic of hydration was enhanced by increase RHA content. Moreover, the heat flow peak values for the samples having 3 wt%, 5 wt% and 10 wt% were 3.71 mW/g, 3.87 mW/g, and 4.18 mW/g, respectively. Herein, the porous structure of RHA leads to the absorption of more water during the grout mixing [114]. The absorbed water in RHA have reduced the degree of hydration of the cement at an early stage since amount of available water is less to react with the cement particles resulting in the prolong induction period as shown in Figure 27a. However, the absorbed water in the RHA structure can act as an additional water reservoir during the hydration process. As the hydration proceeded, initially captured water in cement hydration reaction reduced stoichiometric amount of water in order to keep the rate of hydration constant, and thus the water captured in the pores of RHA was released. This additional water can accelerate the hydration of cement at later stages [115]. Similarly, as shown in Figure 27b, cumulative heat released during the hydration process is enhanced by the addition of RHA and this trend is similar to the heat flow analysis in Figure 27a.

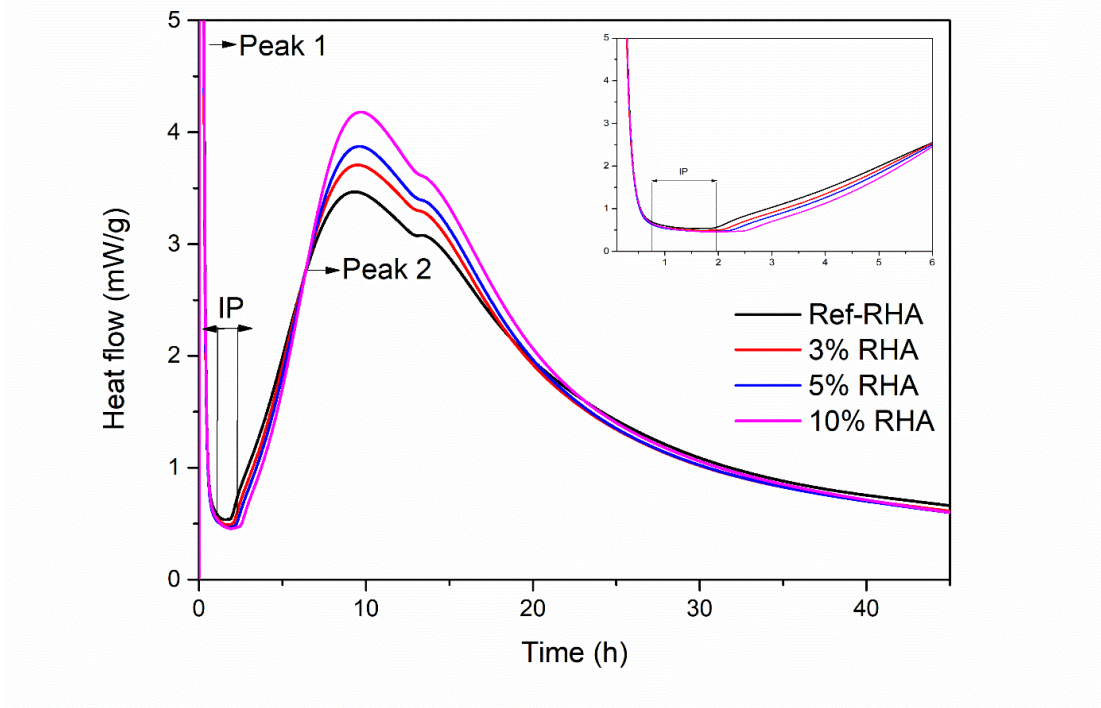
Peak 1
Peak 2
IP
Heat flow (mW/g)
Time (h)
Ref-RHA
3% RHA
5% RHA
10% RHA

(a)

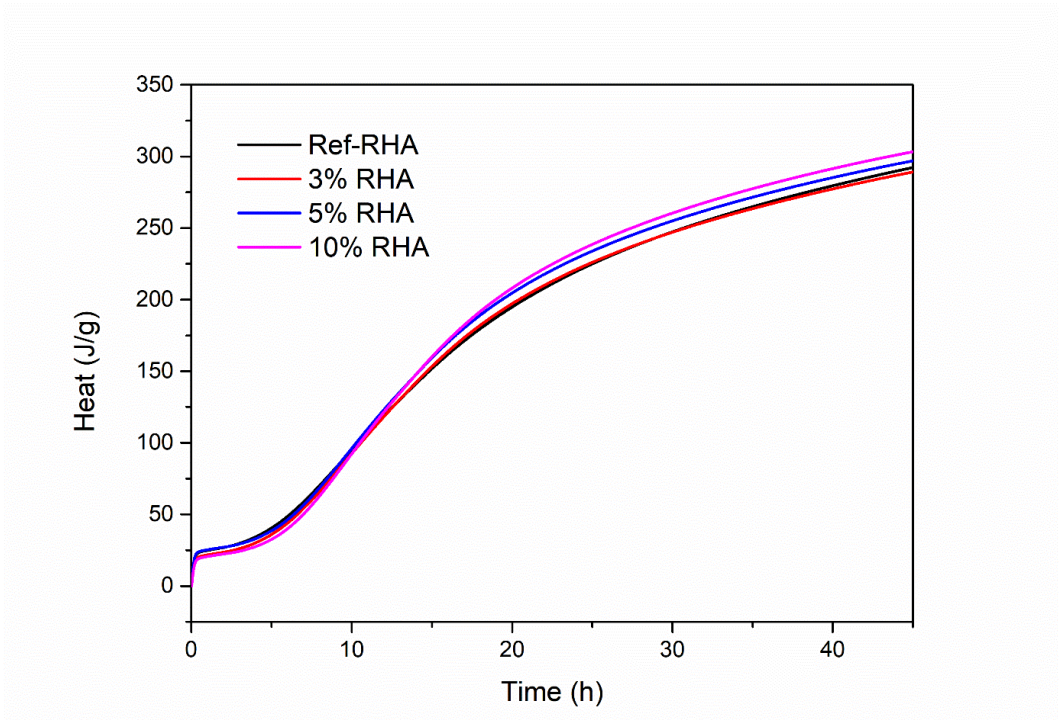
Heat (J/g)
Time (h)
Ref-RHA
3% RHA
5% RHA
10% RHA

(b)

Figure 27. Hydration heat curves of RHA based grouts: (a) heat flow and (b) cumulative heat release.

Figure 28a showed the heat flow evaluation of paste containing 3 wt%, 5 wt% and 10 wt% f-RHA compared to reference (0 wt% RHA). After APTES functionalization, the heat flow values for the grouts containing 3 wt%, 5 wt% and 10 wt% were measured as 3.29 mW/g, 3.25 mW/g, and 3.16 mW/g, respectively. The addition of f-RHA in paste was altered the hydration curve significantly, extended the induction period and reduced the magnitude of the second peak. The incorporation of 3 wt% and 5 wt% f-RHA increased 15- and 30-min induction period, whereas 10 wt% f-RHA increased the induction period by 60 min in comparison to reference. Furthermore, the heat generation in the paste was significantly reduced by addition of f-RHA (Figure 28b). The prolong induction period and reduction in heat flow can be attributed to the influence of chemical nature of functional groups in f-RHA. The retarding effect of f-RHA may be caused by silane based functional groups. The silane has tendency to adsorb and react on the surface of the cement hydration products which hinders the cement hydration reaction. As f-RHA dosage increases, APTES in f-RHA may further intensify the adsorption and result in the retardation and reduction in the heat flow [97].

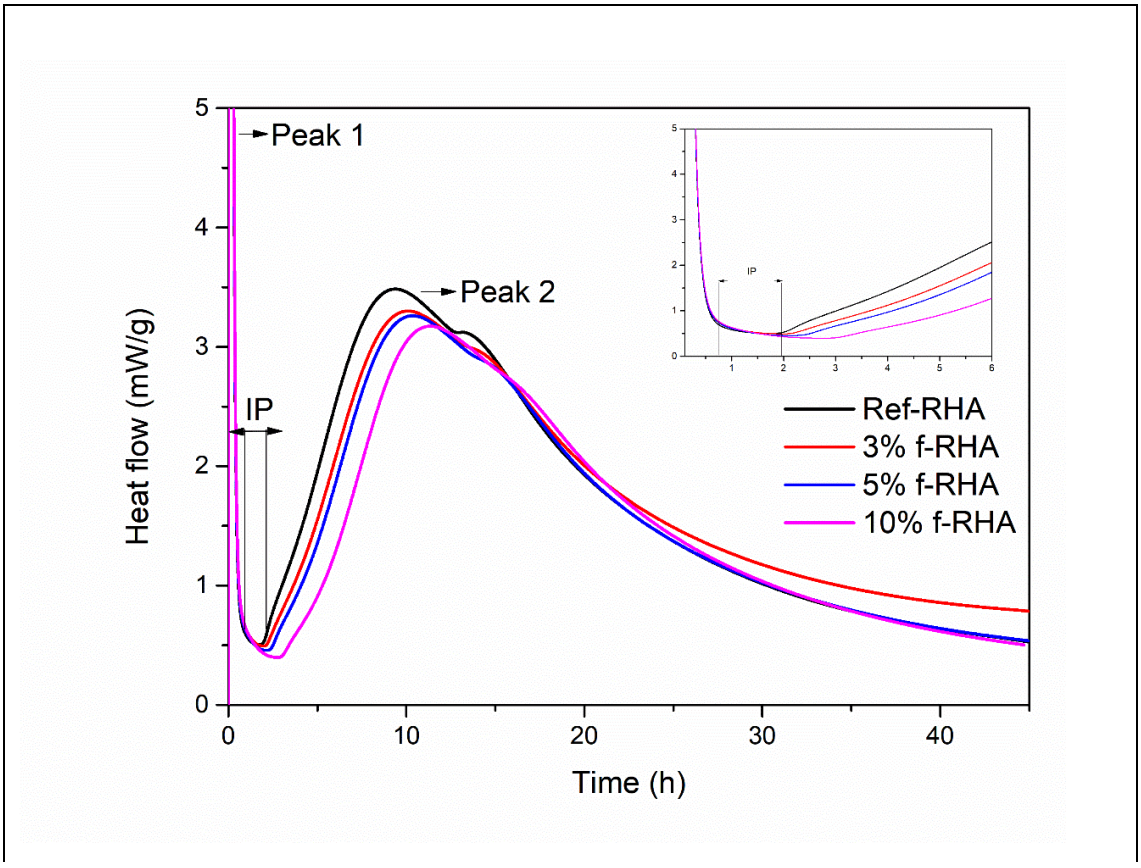

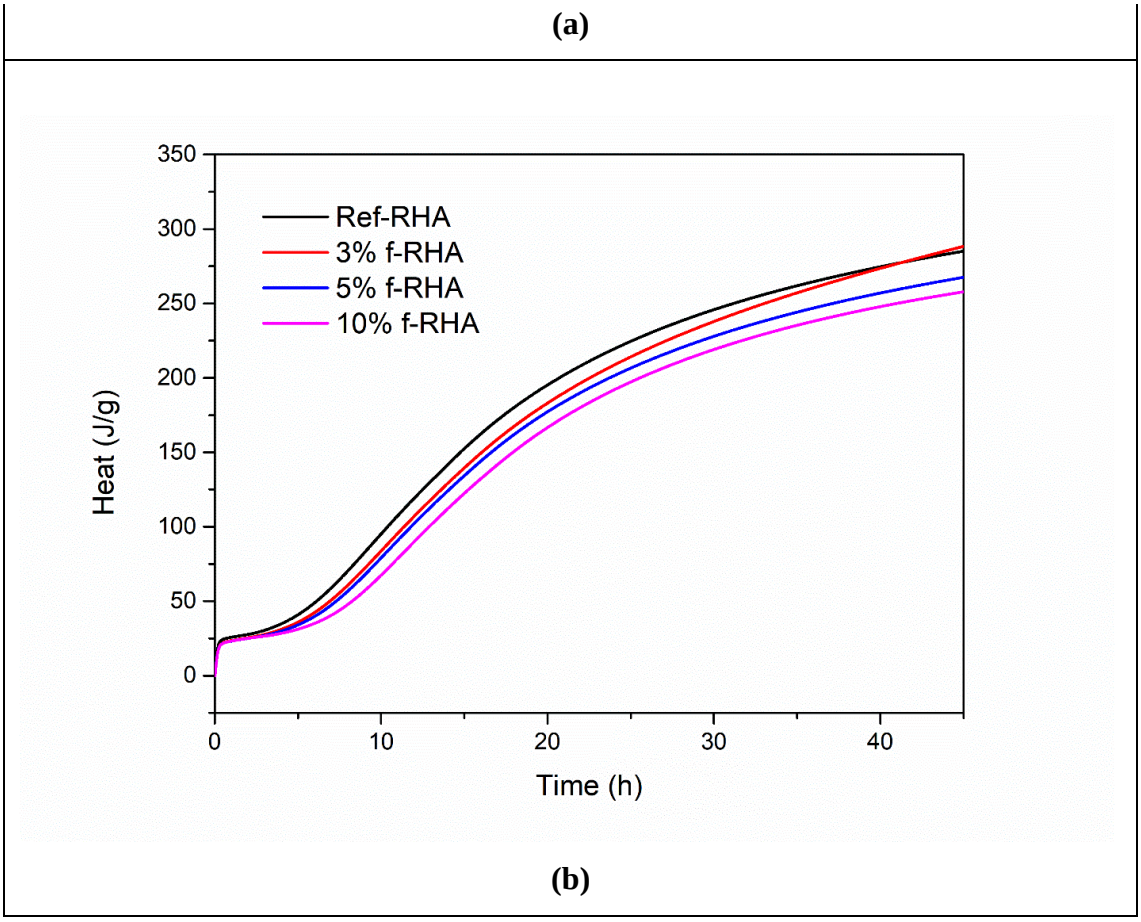

Figure 28. Hydration heat curves of f-RHA based grouts: (a) heat flow and (b) cumulative heat release.

4.4. Conclusion

In the present study, a different approach was brought about the utilization of biomass of rice husk and its conversion into an additive in cement composites to monitor the changes in thermal conductivity and grout properties. Therefore, a detailed characterization was carried out to understand the physical, chemical, thermal and morphological characteristics of RHA by using spectroscopic and microscopic techniques. In order to increase the interfacial interactions of RHA with the constituents of cement such as bentonite, silica sand and superplasticizers, APTES functionalization was applied to the surface of RHA by hydrolysis process to form covalent bonds by taking into consideration our previous studies conducted by using expanded graphite and graphene nanoplatelet. The surface chemical composites confirmed an increase in nitrogen content meaning the attachment of amino functional groups. Then, grout formulation was developed successfully by getting an ideal water to cement ratio and RHA based additive amount. Benchmarking studies and experimental properties of grouts containing RHA and f-RHA

showed that there was a slight increase in thermal conductivity of RHA based grout up to 5 wt% loading, and then at higher additive loadings, thermal conductivity was decreased. According to workability analysis, f-RHA grout samples got less water to obtain similar workability of RHA based grout since the functionalization with APTES leading to the enhancement of the wettability of RHA by water increased the workability of the grout. In addition, APTES functionalized RHA showed the tendency to adsorb and react with the surfaces of cement components and thus resulting in inhibiting the cement hydration reaction and increasing the induction time regarding the calorimetry analysis.

This study indicated that surface treatment by APTES as a silane coupling agent can easily activate RHA, and as the hydrophilicity of the additive surface affects the viscosity of grout directly by altering marsh cone time. Also, the thermal conductivity of grouts has started to decrease slightly by increasing additive amount of both RHA and functionalized RHA due to an increase in water uptake. To conclude, this study shows the potential of RHA as an additive which is a highly desirable and cheap source for cements owing to its high concentration of pure amorphous silica and the presence of nanometer sized carbon sheets.

CHAPTER 5: CONCLUSION

Among renewable energy types, geothermal energy, which uses the heat energy reserved at the shallow of Earth's surface, provides green, low-combustion energy with abundant reserves. Thus, SGES has attracted enormous research interest owing to its several advantages such as reducing CO_2 emission, being weather independent despite of other renewable energy technologies and availability in most of fields. Basically, once the ground is buried up to a certain length, a borehole is placed in the ground. As a following step, a pair of tubes are placed into the borehole. Next, the gap between the borehole and pipes are filled with the grout which is responsible of ensuring the stability and providing heat transfer between pipes and ground. As the thermal conductivity of the grout used in SGES is enhanced, the system loses less heat during transfer of heat, thus the efficiency of overall system would be much higher.

To increase the thermal conductivity of cement, CBMs can be introduced into the cementitious grouts, however the added CBMs may agglomerate and since they are not dispersing homogeneously through the matrix, desired properties such as thermal conductivity or workability may not be achieved. In other words, the main problem behind this is the less functional groups on the surface of CBMs and high water demand of grout composites may lead to agglomeration, low dispersion in grout formulation and low thermal conductivity in grouts, respectively. Therefore, a new methodology should be developed to overcome the problem of aggregation, cost and environmental impact. The performance of grout can be enhanced by controlling the grout chemistry and water demand by developing new formulation and modification of carbon surface with silane functionalized silica particles. Within this perspectives, three different hybrid additives were synthesized for cement-based composites in which CBMs were utilized as additives. In the hybrid additive synthesis, APTES as silane coupling agent was used as an interface modifier between CBMs and silica particles. By linking silica particles to the surface of CBMs with the help of APTES, the dispersion of new hybrid additive become much better since silica particles are compatible with the chemistry of cement.

This study consists of four major sections and the findings for each chapter can be summarized as follows:

1. Facile synthesis of graphene from waste tire/silica hybrid additives and optimization study for the fabrication of thermally enhanced cement grouts.

In this part of study, modification of APTES functionalized silica on the surface of near prime graphene nanoplatelet recycled with the pyrolysis of waste tire has been performed since GNP has extraordinary properties such as high thermal and electrical properties and it reduces the cost due to being a recycled material. As a first step, the functionalization of silica particles with APTES were optimized to fabricate an ideal bridge structure with the CBMs. After optimizing the silica to APTES ratio as 1:2, GNP- based hybrid additives were produced in two different ratios which are 1:5 and 1:10 weight ratio of functionalized silica to GNP. The structural formation of hybrid additive was confirmed by characterization techniques such as TEM images showing the attachment of silica nanoparticles on GNP sheets and XPS analysis showing the presence of nitrogen in the atomic percentage of 1 and 1.15 in the chemical composition of H-GNP-1 and H-GNP-2 respectively. The thermal conductivity effect of the integration of two GNP- based hybrid additives into cementitious grout composite showed that, as the amount of hybrid additive increases, the water demand increases as well which leads to decrease in thermal conductivity. Addition of 1 wt% H-GNP-1 in the reference grout and keeping the water content unchanged, thermal conductivity increased to 2.427 W/mK from 2.373 w/mK. However, adding 3 wt% and 5 wt% of H-GNP-1 increased the water demand of grout composition and higher water content decreased the thermal conductivity value. On the other hand, increasing the ratio of GNP in hybrid additive from 5 to 10 led to an increase in thermal conductivity by 29% by keeping the GNP loading ratio of 5 wt%.

2. Synergistic Effect of Expanded Graphite-Silane Functionalized Silica as a Hybrid Additive in Improving Thermal Conductivity of Cementitious Grouts with Controllable Water Uptake.

In this section, EG- based hybrid additives were produced in two different ratios which are 1:1 and 1:5 weight ratio of functionalized silica to EG. Higher atomic percentage of carbon was found in the XPS result of 2nd hybrid additive since it has more carbon content and less silica content in the structure. When the effect of incorporation of EG-based hybrid additives in cementitious grouts was investigated, the thermal conductivity

outcomes are similar to the ones observed within GNP-based hybrid additives. With the addition of 3 wt% of 1st hybrid additive with respect to cement, the thermal conductivity decreased to 2.175 W/mK from 2.373 W/mK with respect increasing water demand to 750 from 650 when it was compared to reference cement grout. However, with keeping the ratio of EG-based hybrid additive addition stable and decreasing the water amount, increasement in thermal conductivity was observed to 2.429 W/mK from 2.175 W/mK. Highest thermal conductivity which was 2.656 W/mK, was observed with the addition of 5 wt% of 2nd hybrid additive having high content of EG.

3. Controlling the surface chemistry of SiO_2 decorated carbon nanosheets from waste rice husk ash by silanization and its effect on heat flow and hydration of cement-bentonite based grouts.

In this part of the study, RHA, which is also a recycled material produced by the calcination of rice husk, was functionalized with APTES at ratio of 1:1 for enhancing the interfacial bonding between RHA and cementitious grout. Several analyses such as marsh cone flow time, mini slump flow diameter, density, bleeding, thermal conductivity and heat of hydration have been conducted to examine the influence of RHA on the properties of grout composite. While all of the properties were within the desired limits, similar behavior of high water content in low thermal conductivity was also observed in the analyses of RHA and f-RHA introduced cementitious grout samples. The cementitious samples having 3 wt%, 5 wt% and 10 wt% of RHA showed 3.71 mW/g, 3.87 mW/g, and 4.18 mW/g of heat flow peak values, respectively. The reason behind this is the porosity in the structure of RHA which causing the absorption of water during hydration. While absorbed water reduces the degree of hydration at early stages, the water absorbed in the pores diffuses out as the water outside is consumed during the process. This water, which is included in the system later, can accelerate the hydration of cement at later stages. On the other hand, retardation and reduction in heat flow have been observed with the addition of higher f-RHA which may attributed to the presence of APTES in f-RHA.

Regarding the laboratory-scale studies, borehole heat exchanger installation of the developed grout has been conducted by using EG as an additive in the grout mixture that was tested in Zwenkau, Germany in pilot scale. The highest thermal conductivity was

achieved by the addition of EG which was about 2.67 w/mK. The values of grout composition were reported as in the range applicable for grouting in Germany and the mixing procedures were nearly similar to the mixing in laboratory, which has been proven that the conducted experiments in laboratory can be applied in field studies as well. Pilot tests was successfully carried out and good performance was obtained with EG based grout compared to conventional grouts. Consequently, thermally conductive cementitious grout composites by the integration of CBMs as additive will bring new direction in the SGES applications to develop and construct more reliable and efficient systems.

References

1. Michaelides EE, Michaelides DN (2020) Impact of nuclear energy on fossil fuel substitution. Nuclear Engineering and Design 366:110742. https://doi.org/10.1016/j.nucengdes.2020.110742
2. Zhang L, Chen S, Zhang C (2019) Geothermal power generation in China: Status and prospects. Energy Science and Engineering 7:1428–1450. https://doi.org/10.1002/ese3.365
3. Li M, Lai ACK (2015) Review of analytical models for heat transfer by vertical ground heat exchangers (GHEs): A perspective of time and space scales. Applied Energy 151:178–191
4. Xu YS, Wang XW, Shen SL, Zhou A (2020) Distribution characteristics and utilization of shallow geothermal energy in China. Energy and Buildings 229:110479. https://doi.org/10.1016/j.enbuild.2020.110479
5. Lee C, Lee K, Choi H, Choi HP (2010) Characteristics of thermally-enhanced bentonite grouts for geothermal heat exchanger in South Korea. Science China Technological Sciences 53:123–128. https://doi.org/10.1007/s11431-009-0413-9
6. Sani AK, Singh RM, Amis T, Cavarretta I (2019) A review on the performance of geothermal energy pile foundation, its design process and applications. Renewable and Sustainable Energy Reviews 106:54–78. https://doi.org/10.1016/j.rser.2019.02.008
7. Aresti L, Christodoulides P, Florides G (2018) A review of the design aspects of ground heat exchangers. Renewable and Sustainable Energy Reviews 92:757–773. https://doi.org/10.1016/j.rser.2018.04.053
8. Berktas I, Ghafar AN, Fontana P, et al (2020) Facile synthesis of graphene from waste tire/silica hybrid additives and optimization study for the fabrication of thermally enhanced cement grouts. Molecules 25:. https://doi.org/10.3390/molecules25040886
9. Berktas I, Ghafar AN, Fontana P, et al (2020) Synergistic effect of expanded graphite-silane functionalized silica as a hybrid additive in improving the thermal conductivity of cementitious grouts with controllable water uptake. Energies 13:. https://doi.org/10.3390/en13143561
10. Allan ML, Kavanaugh SP (1999) Thermal conductivity of cementitious grouts and impact on heat exchanger length design for ground source heat pumps. HVAC and

R Research 5:85–96. https://doi.org/10.1080/10789669.1999.10391226

11. Javadi H, Ajarostaghi SSM, Rosen MA, Pourfallah M (2018) A comprehensive review of backfill materials and their effects on ground heat exchanger performance. Sustainability (Switzerland) 10:4486. https://doi.org/10.3390/su10124486
12. Cracking T (2009) CIP 42-Thermal Cracking of Concrete. In: National Ready Mixed Concrete Association. www.icri.org
13. Sedaghat A, Ram MK, Zayed A, et al (2014) Investigation of Physical Properties of Graphene-Cement Composite for Structural Applications. Open Journal of Composite Materials 04:12–21. https://doi.org/10.4236/ojcm.2014.41002
14. Lu L, Ouyang D (2017) Properties of Cement Mortar and Ultra-High Strength Concrete Incorporating Graphene Oxide Nanosheets. Nanomaterials 7:187. https://doi.org/10.3390/nano7070187
15. Shang Y, Zhang D, Yang C, et al (2015) Effect of graphene oxide on the rheological properties of cement pastes. Construction and Building Materials 96:20–28. https://doi.org/10.1016/j.conbuildmat.2015.07.181
16. Ramakrishnan S, Wang X, Sanjayan J (2019) Effects of various carbon additives on the thermal storage performance of form-stable PCM integrated cementitious composites. Applied Thermal Engineering 148:491–501. https://doi.org/10.1016/j.applthermaleng.2018.11.025
17. Habsya C, Diharjo K, Setyono P, Satwiko P (2018) Physical, mechanical and thermal properties of lightweight foamed concrete with fly ash. IOP Conference Series: Materials Science and Engineering 420:. https://doi.org/10.1088/1757-899X/420/1/012062
18. Asadi I, Shafigh P, Abu Hassan ZF Bin, Mahyuddin NB (2018) Thermal conductivity of concrete – A review. Journal of Building Engineering 20:81–93. https://doi.org/10.1016/j.jobe.2018.07.002
19. Jobmann M, Buntebarth G (2009) Influence of graphite and quartz addition on the thermo – physical properties of bentonite for sealing heat-generating radioactive waste. Applied Clay Science 44:206–210. https://doi.org/10.1016/j.clay.2009.01.016
20. Al-Kheetan MJ, Rahman MM, Chamberlain DA (2019) Fundamental interaction of hydrophobic materials in concrete with different moisture contents in saline environment. Construction and Building Materials 207:122–135.

https://doi.org/10.1016/j.conbuildmat.2019.02.119

21. Hoffmann F, Cornelius M, Morell J, Fröba M (2006) Silica-based mesoporous organic-inorganic hybrid materials. Angewandte Chemie - International Edition 45:3216–3251. https://doi.org/10.1002/anie.200503075
22. Cestari AR, Vieira EFS, Nascimento AJP, et al (2001) New factorial designs to evaluate chemisorption of divalent metals on aminated silicas. Journal of Colloid and Interface Science 241:45–51. https://doi.org/10.1006/jcis.2001.7711
23. Vandenberg ET, Bertilsson L, Liedberg B, et al (1991) Structure of 3-aminopropyl triethoxy silane on silicon oxide. Journal of Colloid and Interface Science 147:103–118. https://doi.org/10.1016/0021-9797(91)90139-Y
24. Wang Q, Li SY, Pan S, Guo ZW (2018) Synthesis and properties of a silane and copolymer-modified graphene oxide for use as a water-reducing agent in cement pastes. New Carbon Materials 33:131–139. https://doi.org/10.1016/S1872-5805(18)60330-0
25. Zhao L, Guo X, Liu Y, et al (2017) Synergistic effects of silica nanoparticles/polycarboxylate superplasticizer modified graphene oxide on mechanical behavior and hydration process of cement composites. RSC Advances 7:16688–16702. https://doi.org/10.1039/c7ra01716b
26. Schaefer CE, Kupwade-Patil K, Ortega M, et al (2018) Irradiated recycled plastic as a concrete additive for improved chemo-mechanical properties and lower carbon footprint. Waste Management 71:426–439. https://doi.org/10.1016/j.wasman.2017.09.033
27. Norambuena-Contreras J, Thomas C, Borinaga-Treviño R, Lombillo I (2016) Influence of recycled carbon powder waste addition on the physical and mechanical properties of cement pastes. Materials and Structures/Materiaux et Constructions 49:5147–5159. https://doi.org/10.1617/s11527-016-0850-4
28. Zareei SA, Ameri F, Dorostkar F, Ahmadi M (2017) Rice husk ash as a partial replacement of cement in high strength concrete containing micro silica: Evaluating durability and mechanical properties. Case Studies in Construction Materials 7:73–81. https://doi.org/10.1016/j.cscm.2017.05.001
29. B.C. Brodie (1859) On the Atomic Weight of Graphite Author (s): B . C . Brodie Source : Philosophical Transactions of the Royal Society of London , Vol . 149 (1859), pp . 249- Published by : Royal Society Stable URL : http://www.jstor.org/stable/108699 Accessed : 27-04-. Philosophical Transactions

of the Royal Scociety of London 149:249–259

30. Staudenmaier L (1899) Verfahren zur Darstellung der Graphitsäure. Berichte der deutschen chemischen Gesellschaft 32:1394–1399. https://doi.org/10.1002/cber.18990320208
31. Kluth GJ, Sung MM, Maboudian R (1997) Thermal behavior of alkylsiloxane self-assembled monolayers on the oxidized Si(100) surface. Langmuir 13:3775–3780. https://doi.org/10.1021/la970135r
32. Zhang D, Hegab HE, Lvov Y, et al (2016) Immobilization of cellulase on a silica gel substrate modified using a 3 - APTES self - assembled monolayer. SpringerPlus. https://doi.org/10.1186/s40064-016-1682-y
33. Pasternack RM, Amy SR, Chabal YJ (2008) Attachment of 3-(aminopropyl)triethoxysilane on silicon oxide surfaces: Dependence on solution temperature. Langmuir 24:12963–12971. https://doi.org/10.1021/la8024827
34. Pena- Alonso R, Rubio F, Rubio J, Oteo JL (2007) Study of the hydrolysis and condensation of c -Aminopropyltriethoxysilane by FT-IR spectroscopy. Journal of Materials Science 42:595–603. https://doi.org/10.1007/s10853-006-1138-9
35. Majoul N, Aouida S, Bessaïs B (2015) Progress of porous silicon APTES-functionalization by FTIR investigations. Applied Surface Science 331:388–391. https://doi.org/10.1016/j.apsusc.2015.01.107
36. Sehlleier YH, Abdali A, Schnurre SM, et al (2014) Surface functionalization of microwave plasma-synthesized silica nanoparticles for enhancing the stability of dispersions. Journal of Nanoparticle Research 16:. https://doi.org/10.1007/s11051-014-2557-1
37. Rahman IA, Jafarzadeh M, Sipaut CS (2009) Synthesis of organo-functionalized nanosilica via a co-condensation modification using γ-aminopropyltriethoxysilane (APTES). Ceramics International 35:1883–1888. https://doi.org/10.1016/j.ceramint.2008.10.028
38. Kim DS, Dhand V, Rhee KY, Park SJ (2015) Study on the effect of silanization and improvement in the tensile behavior of graphene-chitosan-composite. Polymers 7:527–551. https://doi.org/10.3390/polym7030527
39. Estrade-Szwarckopf H (2004) XPS photoemission in carbonaceous materials: A “defect” peak beside the graphitic asymmetric peak. Carbon 42:1713–1721. https://doi.org/10.1016/j.carbon.2004.03.005
40. Williams EH, Schreifels JA, Davydov A, Oleshko VP (2013) Selective

streptavidin bioconjugation on silicon and silicon carbide nanowires for biosensor applications Selective streptavidin bioconjugation on silicon and silicon carbide nanowires for biosensor applications. https://doi.org/10.1557/jmr.2012.283

41. Dresselhaus MS, Jorio A, Hofmann M, et al (2010) Perspectives on carbon nanotubes and graphene Raman spectroscopy. Nano Letters 10:751–758. https://doi.org/10.1021/nl904286r
42. Haghighi Poudeh L, Cakiroglu D, Cebeci FÇ, et al (2018) Design of Pt-Supported 1D and 3D Multilayer Graphene-Based Structural Composite Electrodes with Controlled Morphology by Core-Shell Electrospinning/Electrospraying. ACS Omega 3:6400–6410. https://doi.org/10.1021/acsomega.8b00387
43. Gong J, Liu J, Wen X, et al (2014) Upcycling waste polypropylene into graphene flakes on organically modified montmorillonite. Industrial and Engineering Chemistry Research 53:4173–4181. https://doi.org/10.1021/ie4043246
44. Reuß M, Proell M, Koenigsdorff R (2009) Quality Control of Borehole Heat Exchanger Systems. Proceedings of the Effstock
45. Javed S, Spitler JD (2016) Calculation of borehole thermal resistance. In: Advances in Ground-Source Heat Pump Systems. pp 63–95
46. Chiasson AD (2016) Theory and practice. In: Geothermal Heatpump and heatengine systems. John Wiley & Sons, Ltd
47. Sarbu I, Sebarchievici C (2016) Using Ground-Source Heat Pump Systems for Heating/Cooling of Buildings. In: Basel II (ed) Advances in Geothermal Energy. InTech, Croatia
48. Yang H, Cui P, Fang Z (2010) Vertical-borehole ground-coupled heat pumps : A review of models and systems. Applied Energy 87:16–27. https://doi.org/10.1016/j.apenergy.2009.04.038
49. Zhang W, Yang H, Lu L, Fang Z (2015) Investigation on influential factors of engineering design of geothermal heat exchangers. Applied Thermal Engineering 84:310–319. https://doi.org/10.1016/j.applthermaleng.2015.03.023
50. Lee H, Park S, Park S, Chung W (2019) Enhanced Detection Systems of Filling Rates Using Carbon Nanotube Cement Grout. Nanomaterials 10:10. https://doi.org/10.3390/nano10010010
51. Zhang Q, Li H Experimental investigation on the ice/snow melting performance of CNFP & MWCNT/cement-based deicing system. In: 6th International Workshop on Advanced Smart Materials and Smart Structures Technology.

Dalian, China

52. Song YS, Youn J (2005) Influence of dispersion states of carbon nanotubes on physical properties of epoxy nanocomposites. Carbon 43:1378–1385
53. Ajayan, P.M.; Schadler, L.S.; Giannaris, C. & Rubio A (2000) Single-Walled Carbon Nanotube–Polymer Composites: Strength and Weakness. Advanced Materials 12:750–753
54. Delaleux F, Py X, Olives R, Dominguez A (2012) Enhancement of geothermal borehole heat exchangers performances by improvement of bentonite grouts conductivity. Applied Thermal Engineering 33–34:92–99. https://doi.org/10.1016/j.applthermaleng.2011.09.017
55. Peyvandi A, Soroushian P, Abdol N, Balachandra AM (2013) Surface-modified graphite nanomaterials for improved reinforcement efficiency in cementitious paste. Carbon 63:175–186. https://doi.org/10.1016/j.carbon.2013.06.069
56. Karaipekli A, Biçer A, Sarı A, Veer V (2017) Thermal characteristics of expanded perlite / paraffin composite phase change material with enhanced thermal conductivity using carbon nanotubes. Energy Conversion and Management 134:373–381. https://doi.org/10.1016/j.enconman.2016.12.053
57. Zhang Z, Fang X (2006) Study on paraffin/expanded graphite composite phase change thermal energy storage material. Energy Conversion and Management 47:303–310. https://doi.org/10.1016/j.enconman.2005.03.004
58. Bao X, Memon SA, Yang H, et al (2017) Thermal properties of cement-based composites for geothermal energy applications. Materials 10:11–13. https://doi.org/10.3390/ma10050462
59. Zhang B, Tian Y, Jin X, et al (2018) Thermal and Mechanical Properties of Expanded Graphite/Paraffin Gypsum-Based Composite Material Reinforced by Carbon Fiber. Materials 11:2205. https://doi.org/10.3390/ma11112205
60. Luping T, Liu J, Wang N, Ye L (2014) Pre-Study of Graphene-Enhanced Cementitious Materials
61. Sharma N, Nasimul S, Chandra B, et al (2018) Diamond & Related Materials Silica-graphene nanoplatelets and silica-MWCNT composites : Microstructure and mechanical properties. Diamond & Related Materials 87:186–201. https://doi.org/10.1016/j.diamond.2018.06.009
62. Aly, M., Hashmi, M. S. J., Olabi, A. G., Messeiry, M., & Hussain AI (2011) Effect of nano clay particles on mechanical, thermal and physical behaviours of waste-

glass cement mortars. Materials Science and Engineering: A 528:7991-7998.

63. Aly M, Hashmi MSJ, Olabi AG, et al (2012) Effect of colloidal nano-silica on the mechanical and physical behaviour of waste-glass cement mortar. Materials and Design 33:127–135. https://doi.org/10.1016/j.matdes.2011.07.008
64. Gopalakrishnan K, Birgisson B, Taylor P, Attoh Okine N (2011) Nanotechnology in civil infrastructure. Springer, Berlin, Heidelberg
65. Shen C, Wang H, Zhang T, Zeng Y (2018) Silica Coating onto Graphene for Improving Thermal Conductivity and Electrical Insulation of Graphene/polydimethylsiloxane Nanocomposites. Journal of Materials Science and Technology 35:36–43. https://doi.org/10.1016/j.jmst.2018.09.016
66. Liu K, Shang Y, Yang L, Du A (2019) Silica/GO hybrids reinforced NR: Better interface interaction and dynamic behavior. Journal of Elastomers & Plastics 009524431987767. https://doi.org/10.1177/0095244319877671
67. Sadiq MM (2013) REINFORCEMENT OF CEMENT-BASED MATRICES WITH GRAPHITE A DISSERTATION. Michigan State University
68. Cao L, Sinha TK, Tao L, et al (2019) Synergistic reinforcement of silanized silica-graphene oxide hybrid in natural rubber for tire-tread fabrication: A latex based facile approach. Composites Part B: Engineering 161:667–676. https://doi.org/10.1016/j.compositesb.2019.01.024
69. Mondal T, Bhowmick AK, Krishnamoorti R (2014) Conducting instant adhesives by grafting of silane polymer onto expanded graphite. ACS Applied Materials and Interfaces 6:16097–16105. https://doi.org/10.1021/am5040472
70. Jiao X, Zhang L, Qiu Y, Yuan Y (2017) A new adsorbent of Pb(II) ions from aqueous solution synthesized by mechanochemical preparation of sulfonated expanded graphite. RSC Advances 7:38350–38359. https://doi.org/10.1039/c7ra05864k
71. Desai S, Njuguna J (2012) Enhancement of thermal conductivity of materials using different forms of natural graphite. IOP Conference Series: Materials Science and Engineering 40:012017. https://doi.org/10.1088/1757-899X/40/1/012017
72. Mengal N, Arbab AA, Memon AA, et al (2018) A promising hybrid graphite counter electrode doped with fumed silica nano-spacers for efficient quasi-solid state dye sensitized solar cells. Electrochimica Acta 261:246–255. https://doi.org/10.1016/j.electacta.2017.12.109
73. Rao KS, Senthilnathan J, Liu Y-F, Yoshimura M (2014) Role of Peroxide Ions in

Formation of Graphene Nanosheets by Electrochemical Exfoliation of Graphite. Scientific Reports 4:1–6. https://doi.org/10.1038/srep04237

74. Shanmugharaj A, Kumar KT, Sundari GS, et al (2019) Study on the effect of silica–graphite filler on the rheometric, mechanical, and abrasion loss properties of styrene–butadiene rubber vulcanizates. Journal of Elastomers & Plastics 51:359–378. https://doi.org/10.1177/0095244318787560
75. Ederer J, Janoš P, Ecorchard P, et al (2017) Determination of amino groups on functionalized graphene oxide for polyurethane nanomaterials: XPS quantitation vs. functional speciation. RSC Advances 7:12464–12473. https://doi.org/10.1039/c6ra28745j
76. Vinoda B, Vinuth M, Bodke Y, Manjanna J (2015) Photocatalytic Degradation of Toxic Methyl Red Dye Using Silica Nanoparticles Synthesized from Rice Husk Ash. Journal of Environmental & Analytical Toxicology 5:2161--0525. https://doi.org/10.4172/2161-0525.1000336
77. Ferrari AC, Meyer JC, Scardaci V, et al (2006) Raman spectrum of graphene and graphene layers. Physical Review Letters 97:187401
78. Pavoski G, Maraschin T, Fim FDC, et al (2017) Few layer reduced graphene oxide: Evaluation of the best experimental conditions for easy production. Materials Research 20:53–61. https://doi.org/10.1590/1980-5373-MR-2015-0528
79. Barbier E (2002) Geothermal energy technology and current status: An overview. Renewable and Sustainable Energy Reviews 6:3–65. https://doi.org/10.1016/S1364-0321(02)00002-3
80. Borinaga-Treviño R, Pascual-Muñoz P, Castro-Fresno D, Del Coz-Díaz JJ (2013) Study of different grouting materials used in vertical geothermal closed-loop heat exchangers. Applied Thermal Engineering 50:159–167. https://doi.org/10.1016/j.applthermaleng.2012.05.029
81. Azadi MR, Taghichian A, Taheri A (2017) Optimization of cement-based grouts using chemical additives. Journal of Rock Mechanics and Geotechnical Engineering 9:623–637. https://doi.org/10.1016/j.jrmge.2016.11.013
82. Sun L, Gong K (2001) Silicon-based materials from rice husks and their applications. Industrial and Engineering Chemistry Research 40:5861–5877. https://doi.org/10.1021/ie010284b
83. Liu Y, Wang Z, Zeng H, et al (2015) Photoluminescent mesoporous carbon-doped silica from rice husks. Materials Letters 142:280–282.

https://doi.org/10.1016/J.MATLET.2014.12.034

84. Bakdash RS, Aljundi IH, Basheer C, Abdulazeez I (2020) Rice husk derived Aminated Silica for the efficient adsorption of different gases. Scientific Reports 10:1–13. https://doi.org/10.1038/s41598-020-76460-0
85. Narayanan DP, Sankaran S, Narayanan BN (2019) Novel rice husk ash - reduced graphene oxide nanocomposite catalysts for solvent free Biginelli reaction with a statistical approach for the optimization of reaction parameters. Materials Chemistry and Physics 222:63–74. https://doi.org/10.1016/j.matchemphys.2018.09.078
86. Wang Z, Yu J, Zhang X, et al (2016) Large-Scale and Controllable Synthesis of Graphene Quantum Dots from Rice Husk Biomass: A Comprehensive Utilization Strategy. ACS Applied Materials and Interfaces 8:1434–1439. https://doi.org/10.1021/acsami.5b10660
87. Ismail MS, Yusof N, Mohd Yusop MZ, et al (2019) Synthesis and characterization of graphene derived from rice husks. Malaysian Journal of Fundamental and Applied Sciences 15:516–521. https://doi.org/10.11113/mjfas.v15n4.1228
88. Turmanova S, Genieva S, Vlaev L (2012) Obtaining Some Polymer Composites Filled with Rice Husks Ash-A Review. International Journal of Chemistry 4:. https://doi.org/10.5539/ijc.v4n4p62
89. Battegazzore D, Bocchini S, Alongi J, Frache A (2014) Rice husk as bio-source of silica: Preparation and characterization of PLA-silica bio-composites. RSC Advances 4:54703–54712. https://doi.org/10.1039/c4ra05991c
90. Sandhu RK, Siddique R (2017) Influence of rice husk ash (RHA) on the properties of self-compacting concrete: A review. Construction and Building Materials 153:751–764. https://doi.org/10.1016/j.conbuildmat.2017.07.165
91. Van Tuan N, Ye G, Van Breugel K, et al (2011) The study of using rice husk ash to produce ultra high performance concrete. Construction and Building Materials 25:2030–2035. https://doi.org/10.1016/j.conbuildmat.2010.11.046
92. Fapohunda C, Akinbile B, Shittu A (2017) Structure and properties of mortar and concrete with rice husk ash as partial replacement of ordinary Portland cement – A review. International Journal of Sustainable Built Environment 6:675–692
93. Hamzeh Y, Ziabari KP, Torkaman J, et al (2013) Study on the effects of white rice husk ash and fibrous materials additions on some properties of fiber-cement composites. Journal of Environmental Management 117:263–267.

https://doi.org/10.1016/j.jenvman.2013.01.002

94. Mohseni E, Naseri F, Amjadi R, et al (2016) Microstructure and durability properties of cement mortars containing nano-TiO2 and rice husk ash. Construction and Building Materials 114:656–664. https://doi.org/10.1016/j.conbuildmat.2016.03.136
95. Gastaldini ALG, Isaia GC, Hoppe TF, et al (2009) Influence of the use of rice husk ash on the electrical resistivity of concrete: A technical and economic feasibility study. Construction and Building Materials 23:3411–3419. https://doi.org/10.1016/j.conbuildmat.2009.06.039
96. Mohseni E, Khotbehsara MM, Naseri F, et al (2016) Polypropylene fiber reinforced cement mortars containing rice husk ash and nano-alumina. Construction and Building Materials 111:429–439. https://doi.org/10.1016/j.conbuildmat.2016.02.124
97. Feng H, Thanh H, Le N, et al (2016) Effects of silanes and silane derivatives on cement hydration and mechanical properties of mortars. Construction and Building Materials 129:48–60. https://doi.org/10.1016/j.conbuildmat.2016.11.004
98. Minet J, Abramson S, Bresson B, et al (2006) Organic calcium silicate hydrate hybrids: A new approach to cement based nanocomposites. Journal of Materials Chemistry 16:1379–1383. https://doi.org/10.1039/b515947d
99. Franceschini A, Abramson S, Mancini V, et al (2007) New covalent bonded polymer-calcium silicate hydrate composites. Journal of Materials Chemistry 17:913–922. https://doi.org/10.1039/b613077a
100. Gomes MC, Cunha Â, Trindade T, Tomé JPC (2016) The role of surface functionalization of silica nanoparticles for bioimaging. Journal of Innovative Optical Health Sciences 09:1630005. https://doi.org/10.1142/S1793545816300056
101. Ics E (2020) Svensk standard ss-en 196-11:2019 Methods of testing cement – Part 11: Heat of hydration – Isothermal Conduction Calorimetry method SIS
102. Zhang L, Li Y, Zhang L, et al (2011) Electrocatalytic oxidation of NADH on graphene oxide and reduced graphene oxide modified screen-printed electrode. International Journal of Electrochemical Science 6:819–829
103. Foletto EL, Castoldi MM, Oliveira LH, et al (2009) Conversion of rice husk ash into zeolitic materials. Latin American Applied Research 39:75–78. https://doi.org/10.1590/S1516-14392006000300014

104. Zabihi SM, Tavakoli H, Mohseni E (2018) Engineering and Microstructural Properties of Fiber-Reinforced Rice Husk–Ash Based Geopolymer Concrete. Journal of Materials in Civil Engineering 30:04018183. https://doi.org/10.1061/(ASCE)MT.1943-5533.0002379
105. Serra MF, Conconi MS, Gauna MR, et al (2016) Mullite (3Al2O3·2SiO2) ceramics obtained by reaction sintering of rice husk ash and alumina, phase evolution, sintering and microstructure. Journal of Asian Ceramic Societies 4:61–67. https://doi.org/10.1016/j.jascer.2015.11.003
106. Xu Y, Chung DDL (1999) Improving the workability and strength of silica fume concrete by using silane-treated silica fume. Cement and Concrete Research 29:451–453. https://doi.org/10.1016/S0008-8846(98)00228-2
107. Celik F, Canakci H (2015) An investigation of rheological properties of cement-based grout mixed with rice husk ash (RHA). Construction and Building Materials 91:187–194. https://doi.org/10.1016/j.conbuildmat.2015.05.025
108. Çınar M, Çelik F, Çanakcı H, Nassani DE (2017) Fresh Properties of Cementitious Grout with Rice Husk Powder. Arabian Journal for Science and Engineering 42:3819–3827. https://doi.org/10.1007/s13369-017-2467-5
109. Qin L, Gao X, Chen T (2018) Recycling of raw rice husk to manufacture magnesium oxysulfate cement based lightweight building materials. Journal of Cleaner Production 191:220–232. https://doi.org/10.1016/j.jclepro.2018.04.238
110. Indacoechea-Vega I, Pascual-Muñoz P, Castro-Fresno D, Calzada-Pérez MA (2015) Experimental characterization and performance evaluation of geothermal grouting materials subjected to heating-cooling cycles. Construction and Building Materials 98:583–592. https://doi.org/10.1016/j.conbuildmat.2015.08.132
111. Bohloli B, Skjølsvold O, Justnes H, et al (2019) Cements for tunnel grouting – Rheology and flow properties tested at different temperatures. Tunnelling and Underground Space Technology 91:. https://doi.org/10.1016/j.tust.2019.103011
112. Taylor HFW (1997) Cement chemistry. Thomas Telford Publishing
113. Hargis CW, Telesca A, Monteiro PJM (2014) Calcium sulfoaluminate (Ye'elimite) hydration in the presence of gypsum, calcite, and vaterite. Cement and Concrete Research 65:15–20. https://doi.org/10.1016/j.cemconres.2014.07.004
114. Zunino F, Lopez M (2017) A methodology for assessing the chemical and physical potential of industrially sourced rice husk ash on strength development and early-age hydration of cement paste. Construction and Building Materials 149:869–881.

https://doi.org/10.1016/j.conbuildmat.2017.05.187

115. Park KB, Kwon SJ, Wang XY (2016) Analysis of the effects of rice husk ash on the hydration of cementitious materials. Construction and Building Materials 105:196–205. https://doi.org/10.1016/j.conbuildmat.2015.12.086